BALLISTICALLY TOLERANT ROTOR BLADE INVESTIGATION

Edward T. Keast

Boeing Vertol Company

Prepared for:

Army Air Mobility Research and Development Laboratory

April 1975

EUSTIS DIRECTORATE POSITION STATEMENT

Current Army helicopter rotor blades are relatively invulnerable to small-arms fire; however, the next-generation Army helicopters may have to operate in mid- and high-intensity warfare environments where higher ballistic threats may prevail.

Eight rotor blade designs were developed and evaluated against such factors as survivability, weight, producibility, cost, radar reflectivity, reliability, and maintainability. Based on this evaluation, three designs were selected for fabrication and tests against the effects of 23mm HEI.

The information herein will be used as an aid in advancing the state of the art of helicopter rotor blade survivability against mid- and high-intensity threats.

Mr. Harold Holland of the Military Operations Technology Division served as technical monitor for this effort.

UNCLASSIFIED

SECURITY CLASSIFICATION OF THIS PAGE (When Data Entered)

REPORT DOCUMENTATION PAGE		READ INSTRUCTIONS BEFORE COMPLETING FORM
1. REPORT NUMBER USAAMRDL-TR-75-4	2. GOVT ACCESSION NO.	3. RECIPIENT'S CATALOG NUMBER AD-A009 516
4. TITLE (and Subtitle) BALLISTICALLY TOLERANT ROTOR BLADE INVESTIGATION		5. TYPE OF REPORT & PERIOD COVERED Final Report 6. PERFORMING ORG. REPORT NUMBER D210-10866-1
7. AUTHOR(s) EDWARD T. KEAST		8. CONTRACT OR GRANT NUMBER(s) DAAJ02-73-C-0098
9. PERFORMING ORGANIZATION NAME AND ADDRESS Boeing Vertol Company P.O. Box 16858 Philadelphia, Pennsylvania 19142		10. PROGRAM ELEMENT, PROJECT, TASK AREA & WORK UNIT NUMBERS Project 1F163208DB52
11. CONTROLLING OFFICE NAME AND ADDRESS Eustis Directorate, U. S. Army Air Mobility R&D Laboratory Fort Eustis, Virginia 23604		12. REPORT DATE April 1975 13. NUMBER OF PAGES 117
14. MONITORING AGENCY NAME & ADDRESS (if different from Controlling Office)		15. SECURITY CLASS. (of this report) UNCLASSIFIED 15a. DECLASSIFICATION DOWNGRADING SCHEDULE

16. DISTRIBUTION STATEMENT (of this Report)

Approved for public release; distribution unlimited.

17. DISTRIBUTION STATEMENT (of the abstract entered in Block 20, if different from Report)

18. SUPPLEMENTARY NOTES

19. KEY WORDS (Continue on reverse side if necessary and identify by block number)

Blade vulnerability	Interlaminar shear
Survivable blade concepts	Ballistic tests
Unidirectional fiberglass	Tension/bending stresses
Fiberglass blades	Nonstructural material

20. ABSTRACT (Continue on reverse side if necessary and identify by block number)

The objective of this program was to design and test rotor blades that are more tolerant of ballistic damage than current blades. Eight blade design concepts were conceived and compared with a previously tested baseline blade. Three of these concepts were selected for fabrication and were ballistically tested. Analysis of all hits showed a significant increase in survivability, as well as a penalty in blade weight, for each of the three designs.

DD FORM 1 JAN 73 1473 EDITION OF 1 NOV 65 IS OBSOLETE

UNCLASSIFIED

SECURITY CLASSIFICATION OF THIS PAGE (When Data Entered)

SUMMARY

This report presents the results of a design, fabrication and test program to investigate the ballistic tolerance of rotor blades especially designed to be survivable. Eight survivable designs were conceived and evaluated. Three of these concepts, Designs 2, 3, and 6A, shown below, were selected for test against 23mm HEI rounds and compared with a baseline blade.

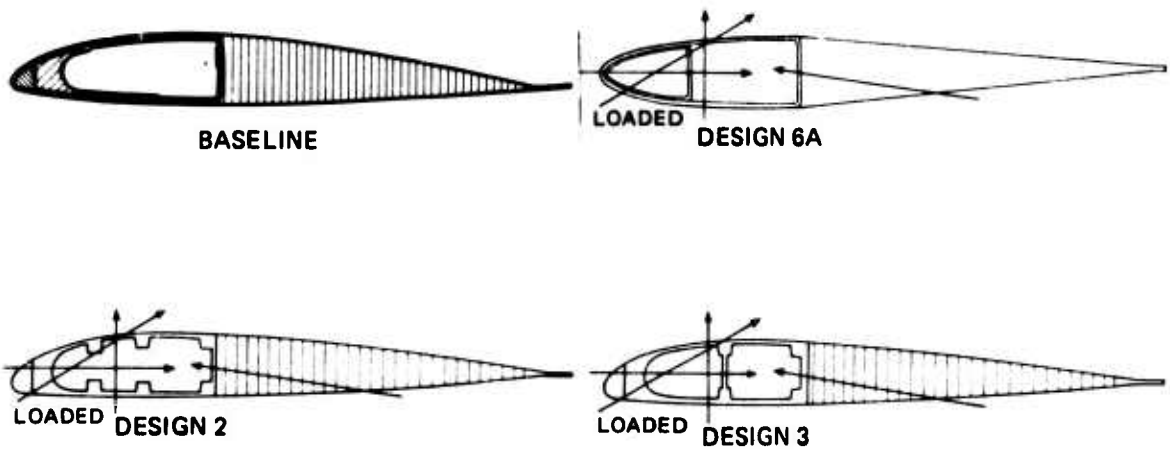

The baseline blade was a fiberglass "D" spar design which had proved to be highly survivable in prior tests, but whose design had not been penalized to provide survivability. The increased survivability was provided in the various test concepts by the addition of discretely placed survivable spanwise load paths. This permitted a realistic evaluation of the improved survivability of the new concepts versus the penalties for incorporating such survivability.

Each of the survivable designs was represented by three individual test sections. Two sections of each design were ballistically impacted while not under load. One section of each design was impacted while under simulated static flight loads. Four different most damaging hits, shown above, were made for each design on the unloaded sections. The hit from the front and 30 degrees below the chord line, shown above, was repeated on the loaded sections.

Two of the loaded blades, Designs 2 and 6A, separated on impact. The third specimen, Design 3, survived the impact test. It was then fatigue tested for the equivalent of eight flight hours at V_{max} and an additional 6 minutes at 1.50g maneuver loads without failure.

Designs 2 and 6A failed under static load in interlaminar shear. This may be a realistic failure mode for some grossly damaged fiberglass blades. However, the specimens were different from actual blades in subtle, but possibly significant, ways, including resins, curing pressures, span length, and lack of mechanical end connections of the unidirectional fiberglass.

The blades were cut chordwise through each of the 15 hits, and residual material was measured. Each hit was analyzed for residual strength to prevent separation, remaining fatigue life, possibility of flutter and degree of out-of-track. Based on these analyses, none of the hits would have caused flutter or excessive out-of-track. Also, by calculation of tension/bending stresses, only one hit would have caused separation in less than 30 minutes of flight at V_{max}. Thus, almost all of the hits are defined as survivable based on the analysis.

The designs showed a weight increase over the baseline blade of 13 percent for Design 2, 15 percent for Design 3, and 7 percent for Design 6A. In terms of amount of material remaining at the impact point (residual strength to prevent separation), Design 6A had the most, Design 3 was next, and Design 2 had the least. Design 6A gains its survivability mainly by utilizing unidirectional fiberglass as the nose balance weight. Designs 2 and 3 had nonstructural material in the nose. Designs 2 and 3 would benefit by having more structural material in the nose. Design 6A would be improved by having more structural material in the back of the spar.

PREFACE

This Ballistically Tolerant Rotor Blade Investigation was performed under Contract DAAJ02-73-C-0098 with the Eustis Directorate, U.S. Army Air Mobility Research and Development Laboratory, Fort Eustis, Virginia, under the general technical cognizance of Mr. Harold Holland of the Safety and Survivability technical area.

The ballistic testing was conducted at the Army Ballistic Research Laboratories at Aberdeen Proving Ground, Aberdeen,

Boeing Vertol's principal participants were Edward Keast, Robert Aiello, John Nicely, and James Morris.

TABLE OF CONTENTS

LIST OF ILLUSTRATIONS

LIST OF TABLES

INTRODUCTION

COMBAT EXPERIENCE

Combat experience in Southeast Asia has demonstrated that current production helicopter rotor blades are relatively invulnerable to small-arms fire. Hundreds of 7.62mm and 12.7mm combat blade hits on a variety of helicopter types have been survived. Vulnerability to small-caliber hits is probable only in critical areas of the smaller main- and tail-rotor blades.

ANTICIPATED COMBAT CONDITIONS

Next-generation Army helicopters, however, may have more to contend with than small-arms fire. They can be expected to operate in mid- and high-intensity warfare environments where higher threats prevail. Threats could include a variety of weapons, such as larger caliber and explosive ballistic rounds, surface-to-air missiles, and air-to-air missiles. Weapons may be visually directed, radar directed, or heat seeking. For each type of threat and aircraft subsystem, various means of defense are being explored by the Army. These defenses include such solutions as designing aircraft components for reduced vulnerability, armoring of the crew and critical parts, countermeasures to reduce detection, and tactical operation to avoid detection. The intent of this investigation is to provide guidance in reducing the vulnerability of rotor blades.

TECHNICAL DISCUSSION

BLADE VULNERABILITY

Rotor blades occupy a unique place in the aircraft vulnerability picture. Because of their high rotational speed, a blade hit is generally accidental in that it results from a miss of a shot fired at some other part of the helicopter. Nevertheless, the probability of taking a hit based on vulnerable area is just as great as if the blades were not rotating. Rotor blades cannot be armored as can some other critical aircraft components. In the event of a hit, the only practical solution for rotor blades is to design them for acceptable damage tolerance.

Selection of Threat

Based on consideration of the many factors involved, the 23mm high explosive incendiary (HEI) has been selected as the major threat for this investigation. These factors include the facts that Soviet 23mm quad antiaircraft guns exist in large numbers, are mobile, are extremely accurate, and have a high rate of fire and rapid all-weather aiming. Designing for invulnerability to 23mm HEI would also provide invulnerability or reduced vulnerability to hits by other weapons.

The 23mm HEI Threat

The specific round discussed and used in the tests is the Soviet 23mm fragmentation/high explosive incendiary tracer, model number OFZT. This round is fused in two ways: "delayed" and "superquick". The delayed fuse, MG-25, causes the round to detonate about 9 inches after impact. The superquick K20 and A23 fuses cause detonation immediately on impact. The rounds may be fired from a quad 23mm antiaircraft gun using either all superquick, all delayed, or a discrete mix of the two types. The delayed round is usually more damaging to the crew and to most critical aircraft components. However, a delayed round will generally pass through all but the heaviest sections of a blade, then detonate after exiting. For that reason, this round usually does no more blade damage than an armor piercing (AP) hit. An exception, however, is a hit in the chordwise direction on the aft section where detonation occurs inside the spar. The superquick round is generally the more devastating to most types of blade structure and has, therefore, been selected as the major threat for this program. Superquick 23mm HEI rounds were not available for these tests. Therefore, they were simulated by using delayed rounds and a function plate placed about 9 inches ahead of the blade. The delayed round has also been considered in respect to the possible, but unlikely, chordwise hit which detonates in the

spar, and was tested for this condition without a function plate. Figure 1 shows the 23mm HEI shrapnel pattern. The cone angle of the shrapnel is a function of the forward velocity of the round at impact and the radial velocity of the shrapnel due to the detonation.

At muzzle velocity, the cone angle is about 70 degrees. This angle increases as the round slows down. A small shrapnel angle provides a higher shrapnel density and higher shrapnel velocities. A larger shrapnel angle can be more damaging to extremely light structures, but, in most blade structures including those tested, the smaller angles are more damaging. Therefore, these blade tests were conducted at muzzle velocity.

Comparison of 20mm HEI With 23mm HEI

Because of limitations in availability of Soviet 23mm HEI rounds, American 20mm HEI is sometimes used to simulate their ballistic damage effects in preliminary testing. Twenty millimeter (20mm) HEI M56E2 rounds, with M505E3 PD fuses, were used in the preliminary tests of the baseline blade referred to in this program. It is, therefore, of interest to understand the differences between these two rounds as they affect the damage inflicted on blades.

The 20mm HEI round is smaller in length and diameter than the 23mm HEI (Figure 2). It contains less fragmentation mass and less explosive in the projectile. The shrapnel cone and the number of fragments is about the same, but the mass of the larger fragments is smaller than in the 23mm HEI. Blast is also reduced. The net result is that less damage is generally done by the 20mm HEI to a blade section which partially defeats the round. In cases where the target material is thin and weak enough for the 20mm HEI to make a complete hole the size of the shrapnel cone, the 23mm HEI may not do any more damage. The tests conducted in this program were all of sections which partially defeat the 20mm HEI round.

Importance of Blade Survivability

Vulnerability analyses of several of the larger current Army helicopters to a 23mm HEI threat indicate that blades, even when only the spar is vulnerable, represent approximately 30 percent of the total vulnerable area of the aircraft. Thus, regardless of what other steps may be taken to reduce aircraft vulnerability, the helicopter would remain relatively vulnerable unless the blades too were made invulnerable.

Test Experience

The Army has been conducting ballistic tests of production rotor blades for several years at the Ballistic Research

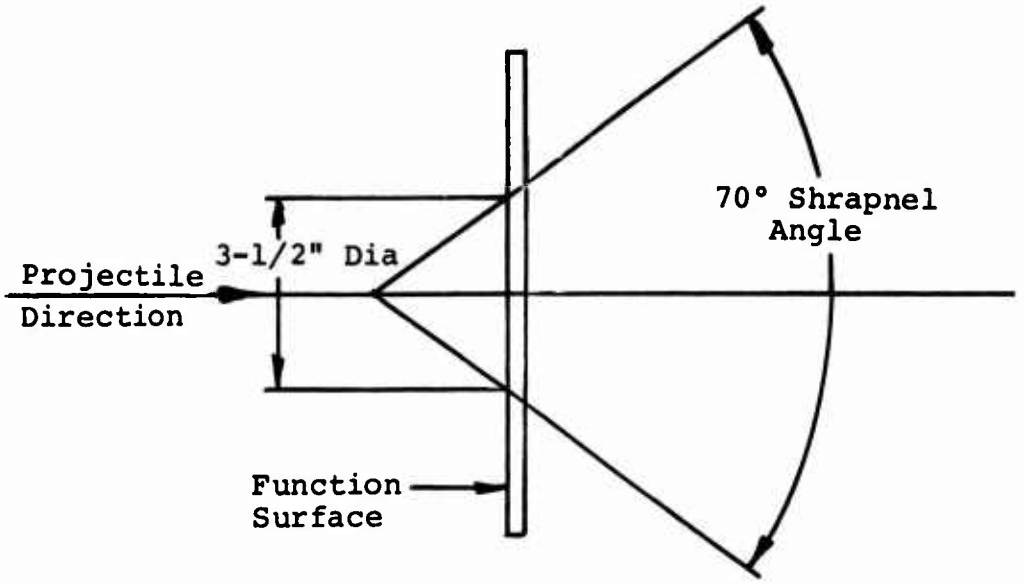

23mm HEI Superquick Detonation

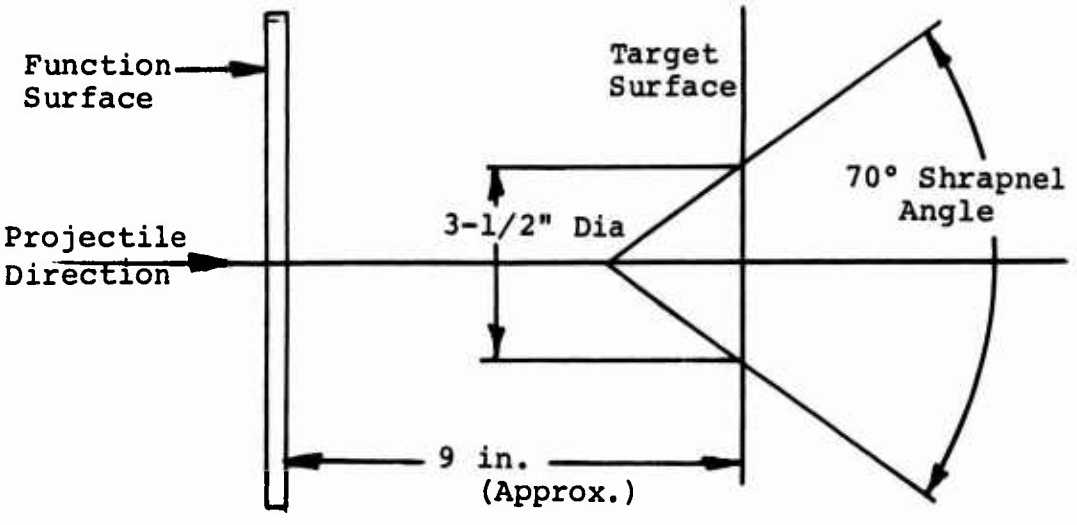

23mm HEI Delayed Detonation

Figure 1. 23mm HEI Shrapnel Pattern at Muzzle Velocity.

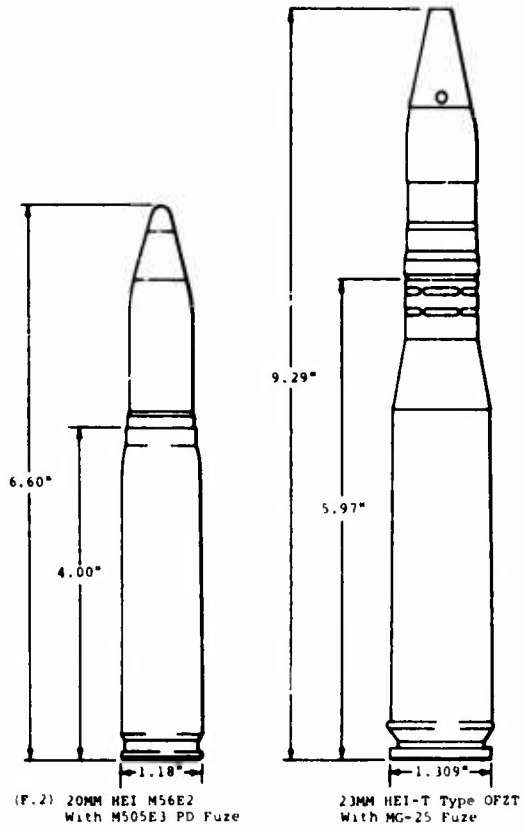

20mm and 23mm HEI PROJECTILE DATA		
	20mm HEI M56E2 with M505E3 PD Fuze	23mm HEI-T Type OFZT with MG-25 Fuze
Projectile Weight	1565 Grains	2347 Grains
Charge	165 Grains (65% RDX, 35% AL, 1% Graphite)	205 Grains (65% RDX, 35% AL)
Muzzle Velocity	3300 fps	3000 fps

Figure 2. Projectile Data.

Laboratories. These tests have covered most of the main rotor blades in the Army inventory. They have included hits by 7.62mm, 12.7mm AP and API, 20mm API, 20mm HEI, 23mm API-T and 23mm HEI-T. The test results have tended to confirm the survivability of blades against small-caliber rounds. They have shown varying degrees of survivability against 23mm HEI depending on blade chord and construction. However, most "worst" 23mm HEI hits on the various metal spars of production blades were not survivable. The probability indicated by these tests is that more than half of all hits on spars by 23mm HEI would be unsurvivable. Extensive ballistic testing has also been done on experimental fiberglass blades. These showed significant improvement in 23mm HEI survivability over an equivalent chord metal blade. The reasons for this improvement have to do with the physical characteristics of fiberglass. The major in-flight loads on a blade spar are spanwise, and most of the fibers of a composite blade are laid up in this direction. This, combined with the high ratio of tensile strength to fatigue allowable of glass (Table 1), gives a composite blade considerably more strength in that direction for a given weight than a metal blade. Residual tensile strength prevents the blade from separating after damage, while fatigue allowable determines the original design. Thus, a larger percentage of the cross-sectional area of a fiberglass blade can be shot away without losing sufficient strength to permit blade separation. Also, extensive testing has shown fiberglass to be less notch sensitive than metal. Fatigue tests on damaged blades have demonstrated that considerable fiberglass material can be lost before flight loads can cause rapid propagation of the damage. Tests to date indicate that fiberglass is the most ballistically tolerant material currently available for rotor blade construction.

Blade Safety Limits

Rotor blades operate at a delicate balance of weight, strength and stiffness to permit safe flight of the aircraft. When a blade is ballistically damaged, a number of factors may change which degrade the blade's operation:

- Rotor unbalance
- Blade instability
- Out-of-track
- Loss of lift

Rotor Unbalance

Probably the most critical consequence of ballistic damage is rotor unbalance due to the separation of a section of blade

TABLE 1. COMPARISON OF BLADE MATERIALS

Spar Material	Fatigue Allowable	Sharp Notch Fatigue Strength (psi)	Unnotched Ultimate Strength (psi)	Sharp* Notch Ultimate Strength (psi)	Unnotched Ultimate To Fatigue Ratio	Notched Ultimate to Unnotched Fatigue Ratio
4340 Steel	25,000	8,350	150,000	22,700	6:1	0.9:1
6061-T6 Aluminum	7,000	2,000	42,000	9,660	6:1	1.3:1
6AL-4V Titanium	17,200	6,680	130,000	22,300	7.5:1	1.3:1
XP250 1002/1014 Fiberglass	12,500	12,500	150,000	150,000	12:1	12:1

*Assuming 40 percent loss of area

outboard of the hit point. This loss of mass in one blade generates high alternating 1/rev in-plane hub forces. These forces could cause cockpit and control vibrations of sufficient magnitude that the pilot would lose control of the aircraft. In addition, large hub forces could do critical structural damage such as tearing the rotor transmission out of the fuselage.

Blade Instability

Blade instability can be a flight-critical factor even if the blade does not separate. A local reduction in blade stiffness due to a hit could result in either classical flutter or a divergent pitch oscillation. Either of these conditions could prove to be catastrophic.

Blade Out-of-Track

Blade out-of-track due to a local reduction in blade stiffness can also be critical if it becomes excessive. Blade out-of-track is probable when the reduction in stiffness is in the range caused by 23mm HEI hits on the spar. Excessive blade out-of-track produces high levels of 1/rev vibration. In the extreme, excessive blade out-of-track could also cause blade contact with the fuselage. This could occur either in flight or on the ground and is particularly likely after shutdown.

Loss of Lift

Loss of blade lift could be caused either by separation of part of the blade or by a locally reduced blade stiffness which could result in its operating at a lower angle of attack. Analysis and flight experience with failing blades confirm that loss of lift is not generally as critical a consequence of blade damage as other factors. Since the loss is generally small, except when operating under extreme conditions of overweight, altitude, or temperature, the lift loss sustained by one blade can be readily compensated for by increased pitch on all blades. Therefore, loss of lift has not been treated in this investigation.

DEVELOPMENT OF SURVIVABLE BLADE CONCEPTS

Principles of Blade Survivability

The prime consideration in blade survivability is to keep the blade intact, that is, to prevent it from separating so that an outboard section is lost. As previously described, the unbalance effect due to the separation of a spanwise blade section could be catastrophic. The secondary aim is to maintain sufficient stiffness about the flap, chord, and pitch axes to prevent instability or excessive out-of-track. In order to

achieve these two results, it is helpful to provide the blade with separated, survivable load paths (Figure 3). These load paths should run spanwise to carry the major centrifugal force, bending and torsional loads. They should be spaced chordwise so that a given hit will not eliminate enough of the load paths that blade separation will occur or that insufficient stiffness will remain. Also, their cross sections should be large enough to provide a good probability of surviving hits by shrapnel.

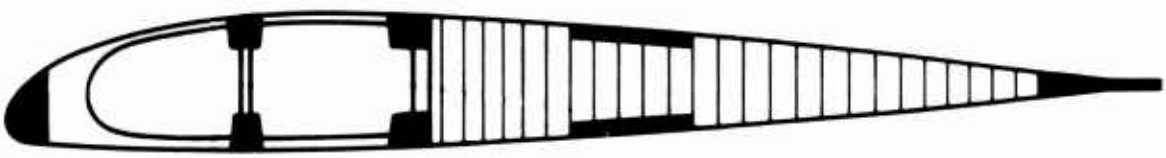

Figure 3. Blade With Separated, Survivable Load Paths.

Preliminary Testing of Load

Prior to this investigation, ballistic tests had been conducted jointly by Boeing and the Army Ballistic Research Laboratories to determine the probability of survival of fiberglass load paths. In these tests, the upper and lower surfaces of the rotor blade spars were simulated by plywood sheets. Strips of fiberglass sections 7/16 inch square were bonded to these sheets (Figures 4 and 5). They were impacted with 20mm HEI M56E2 rounds. The probability of such load paths surviving is dependent on the density of the shrapnel patterns, the mass of the individual fragments, and their velocities. The tests indicated about 50 percent chance of these 7/16-inch x 7/16-inch strips surviving 20mm HEI when in the shrapnel cone. Probability of survival against 23mm HEI is somewhat less due to the more potent shrapnel. Strips of larger cross sections would, of course, have a higher probability of survival. Strips of 1/2 inch by 1/2 inch may be expected to have a 50 percent chance of survival against 23mm HEI. This type and size strip was used in two of the concepts selected for these tests: Designs 2 and 3.

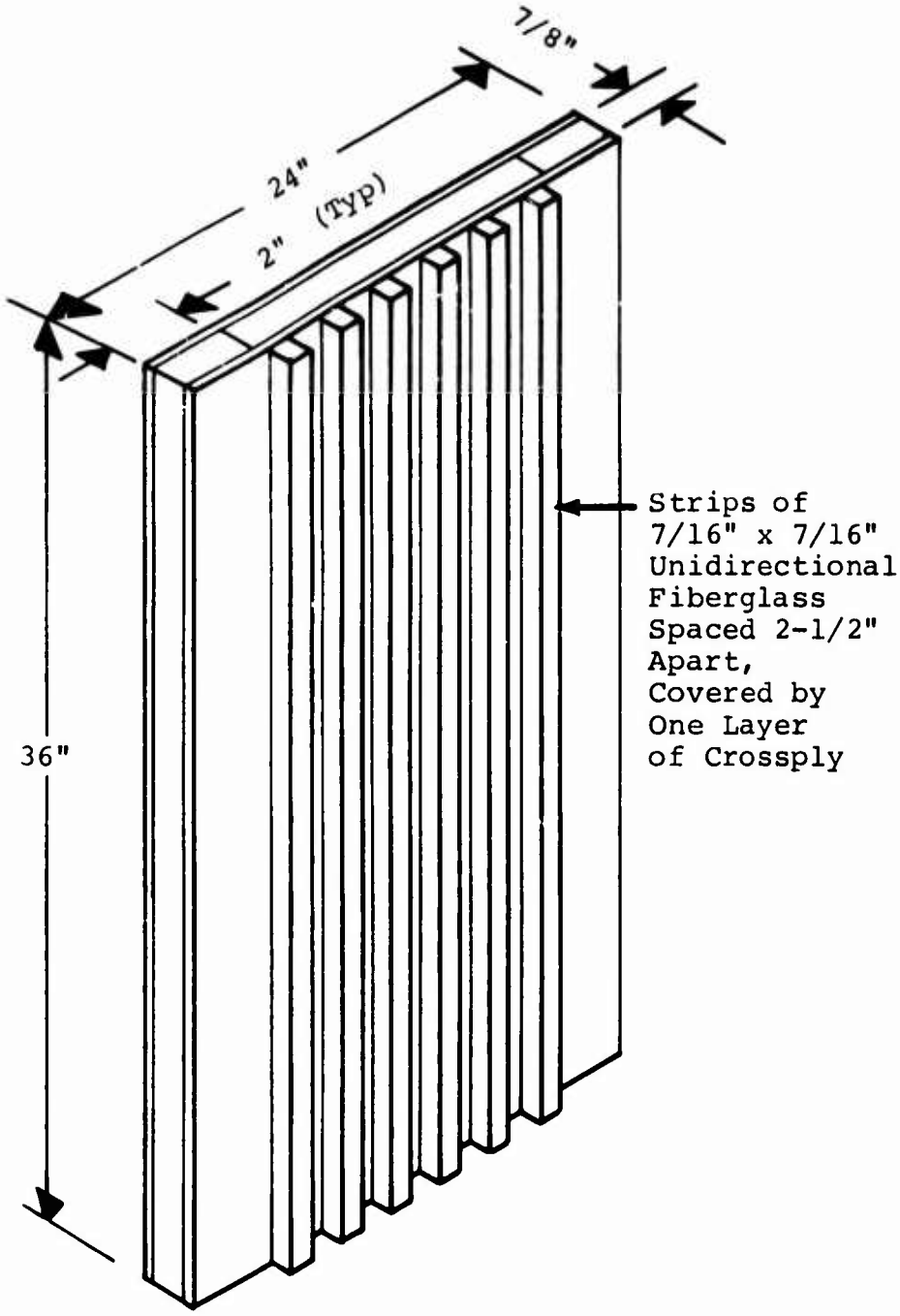

Figure 4. Test Panel To Simulate Separated Blade Load Paths.

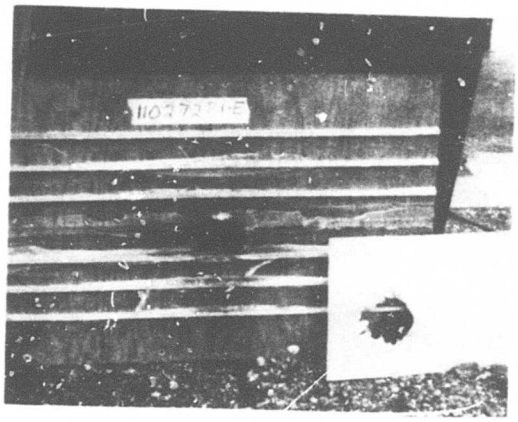

Entrance
and Detonation Plate

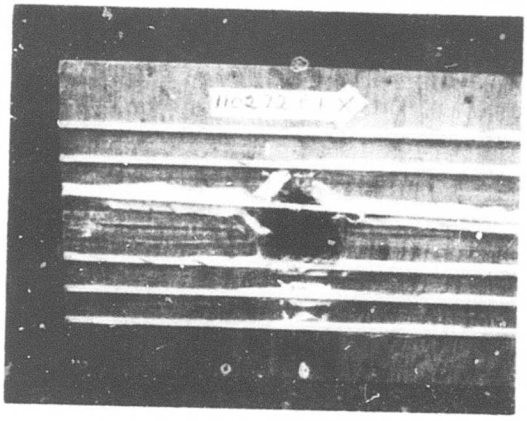

Exit

Entrance

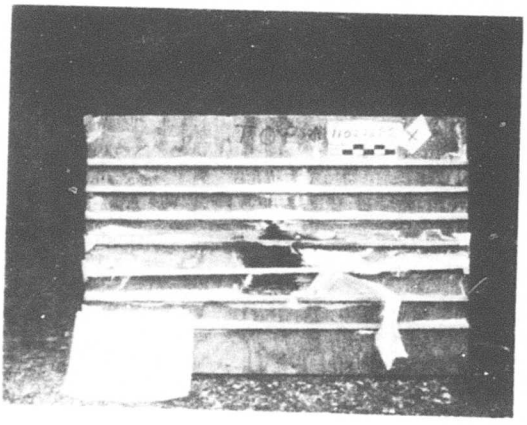

Exit

Figure 5. 20mm HEI Hits on Plywood Panel Reinforced With 7/16-Inch Square Fiberglass Load Paths.

Trades in Survivability Design

In designing blades for increased damage tolerance, certain basic factors of blade design must be considered. The steady spanwise load on the spar due to centrifugal force varies with the weight of the blade. Additional load paths add not only strength but also weight. Therefore, when load paths are added, the reduction in strains due to centrifugal force is less than directly proportional to the increase of strength.

Other major loads in the blade are flapwise and chordwise bending. These are steady and alternating loads resulting from aerodynamic lift and drag forces, relieved by centrifugal force and modulated by the dynamic characteristics of the rotor. When a blade is designed for discrete natural frequencies, its bending deflections tend to remain nearly the same even though the blade may be modified to be slightly stiffer and heavier by virtue of additional load paths. Since the bending deflections remain almost the same, the bending strains in the spar will remain almost the same. Thus, we do not get an appreciable reduction in the blade spar bending strains by adding cross-sectional area.

The most important gain to be derived from additional load paths is that an equal amount of damage to such a reinforced blade would leave more residual strength, and this strength would be strategically placed to provide maximum residual stiffness.

An additional design requirement is that the blade be balanced ahead of the aerodynamic center at 25-percent chord to avoid flutter. This means that load paths are most weight-efficient which are on or forward of this center of gravity location. Load paths placed aft of the 25-percent chord point must be counterbalanced by putting more weight in the nose. Thus, wide spacing of load paths in the chordwise direction, which results in an aft center of gravity, causes blade weight penalties higher than those of the load paths themselves.

Based on the above factors, it is considered logical to start improving damage tolerance by incorporating additional survivable load paths in the spar area. This was done in this program. The trailing edge, if continuous, may also be considered as a load path, but only if the spar also continues to carry some load. It is not advisable to make the trailing edge survivable to a direct hit by shrapnel, since this would require substantial nose weight to rebalance and since separation of the trailing edge alone would not be catastrophic.

Description of the Baseline Blade

The baseline blade design (Figures 6 and 7) was selected because it inherently provides a high degree of survivability for which no special penalty was paid. The increased survivability, in the various test concepts, was provided by the addition of discretely placed survivable spanwise load paths to the baseline blade. This permitted a realistic evaluation of the improved survivability of the new concepts versus the penalities for incorporating such survivability.

The baseline blade, as mounted on a rigid hub, has been designed and analyzed in sufficient detail to assure that it is a viable design. It is well defined in respect to all blade parameters including physical characteristics, loads, stresses, and natural frequencies. The inboard part of the blade is a thick-walled oval tube of fiberglass known as the "swan neck." This section permits controlled bending in the flapwise and chordwise axes. The airfoil section is of constant 12-percent thickness out to 75-percent span. Outboard of the 75-percent span it tapers to a 6-percent airfoil at the tip. The spar is of conventional "D" shape, and its wall thickness reduces as it goes outboard. The blade is balanced chordwise to 22.6 percent of chord by a nose weight. For purposes of natural frequency tuning, the nose weight does not extend over the entire span, but is concentrated near the blade mid-span. A typical section, for ballistic comparison, is the larger spanwise section which contains a low-density nose filler instead of the balance weight. The average weight of the 12-percent thick section is 0.739 pound per inch. The unbalanced portions are 0.566 pound per inch.

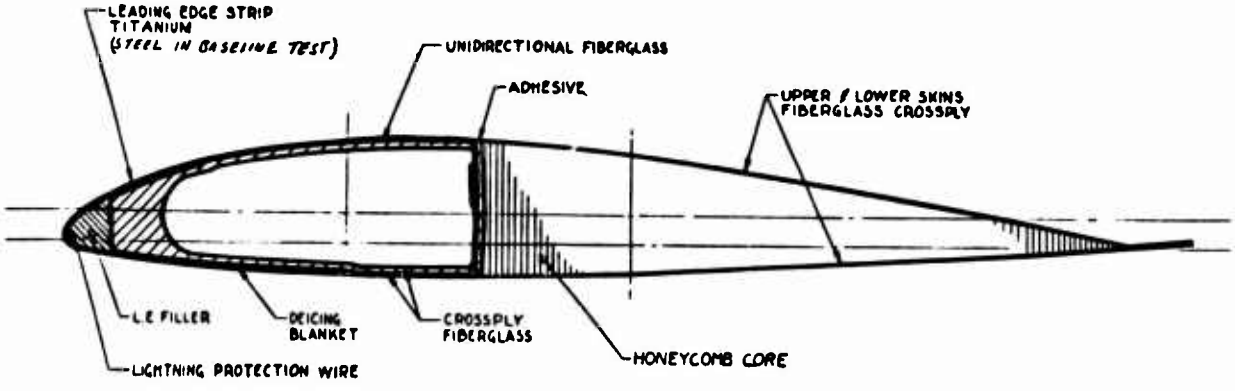

Figure 6. Baseline Design at 50 Percent of Span.

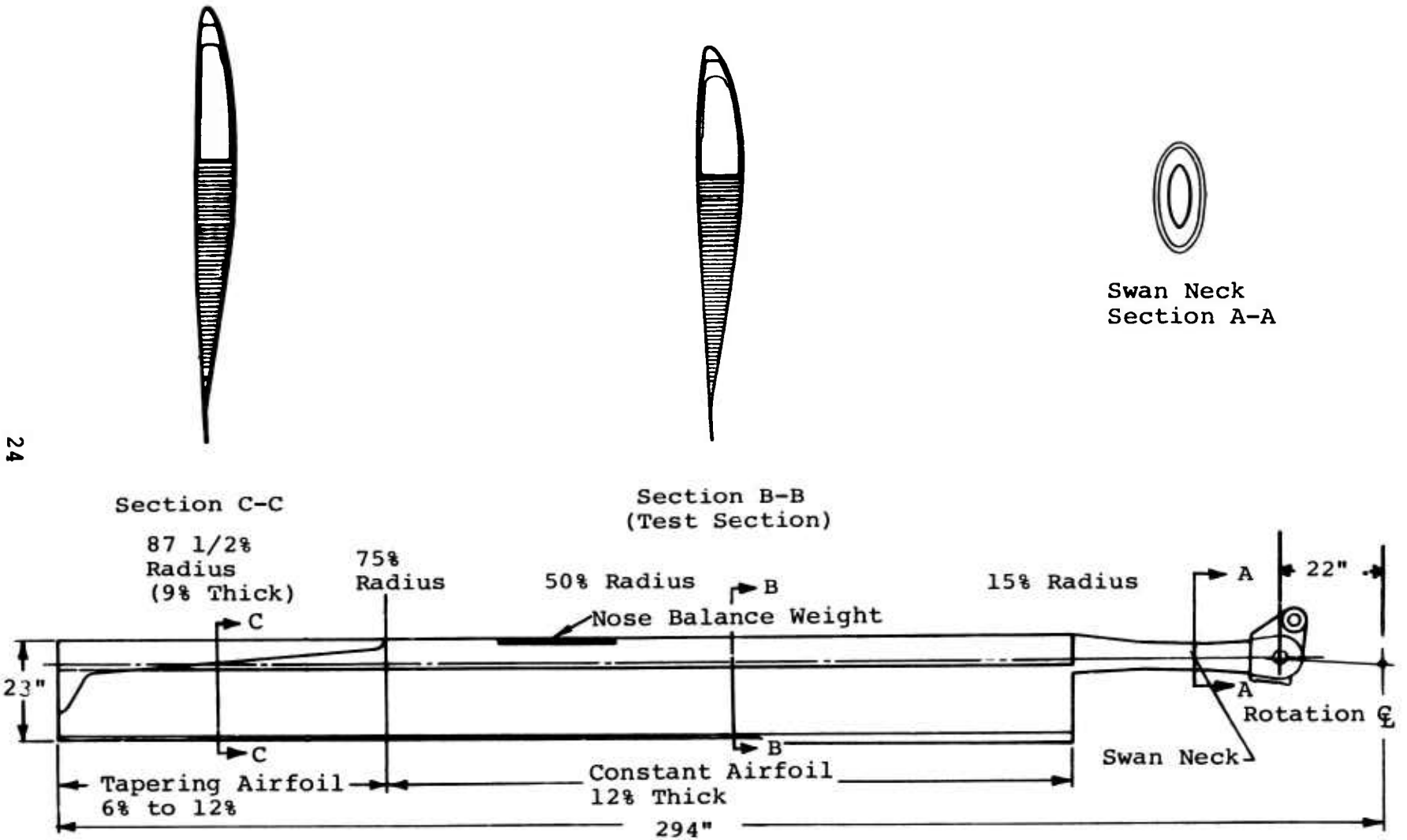

Figure 7. Baseline Blade.

SURVIVABLE BLADE CONCEPTS

Eight different survivable blades were conceived, defined, and compared to select the three which were ultimately tested. The following pages describe these eight concepts.* The average weight per inch was calculated for each, including sufficient nose weight to balance about 22.6 percent chord to be comparable with the baseline blade.

Survivable Concept 1 (Figure 8)

Survivable Concept 1 was modified from the baseline blade by the addition of an upper and lower load path at the back of the spar. The survivability theory is that loss of either the front or the back of the spar would permit continued flight. This design has a calculated weight of 7.0 percent higher than the baseline based on the addition of sufficient nose mass to retain the original 22.6-percent chord balance.

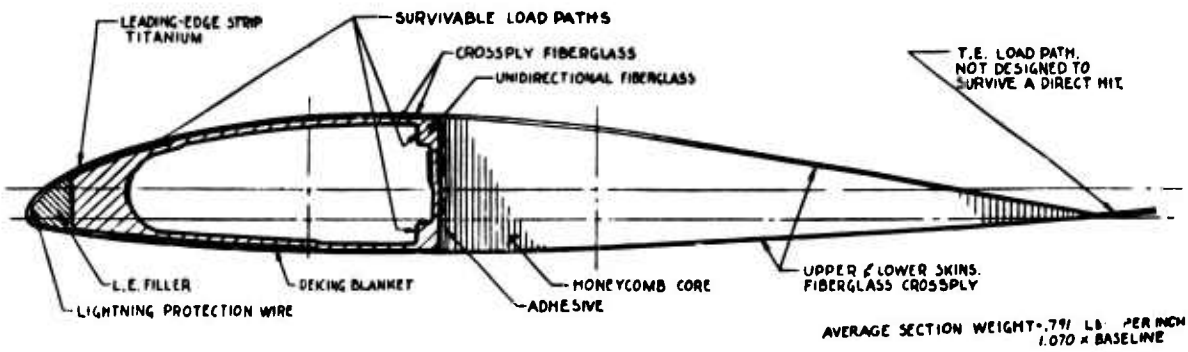

Figure 8. Concept 1 Ballistically Tolerant Blade.

*Survivable blades which were conceived for study purposes only are referred to in the text as concepts. Blade concepts which were selected for fabrication and testing are referred to as designs.

Survivable Concept 2 (Figure 9)

Survivable Concept 2 was modified from the baseline blade by the addition of three upper and lower load paths. This provides an increment of increased survivability over Concept 1 in that more load paths are likely to remain after a given hit. This would provide additional residual strength and stiffness. This concept has a calculated weight of 13 percent higher than the baseline based on the addition of sufficient nose mass to retain the original 22.6-percent chord balance.

Concept 2 was one of the three concepts selected for fabrication and test. Hereafter, it is referred to as Design 2.

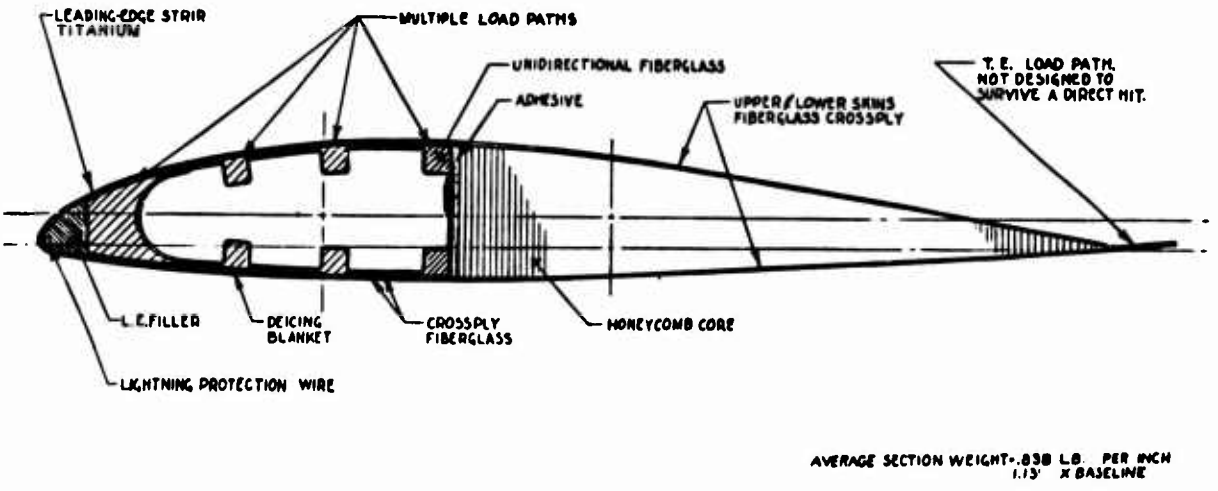

Figure 9. Concept 2 Ballistically Tolerant Blade.

Survivable Concept 3 (Figure 10)

Survivable Concept 3 was modified from the baseline blade by the addition of two upper and lower load paths and a centrally located web. This concept could provide a remaining torque box in the event of loss of either the front or back of the spar. This concept has a calculated weight of 15 percent higher than the baseline based on the addition of sufficient nose mass to retain the original 22.6-percent chord balance.

Concept 3 was one of the three concepts selected for fabrication and test. Hereafter, it is referred to as Design 3.

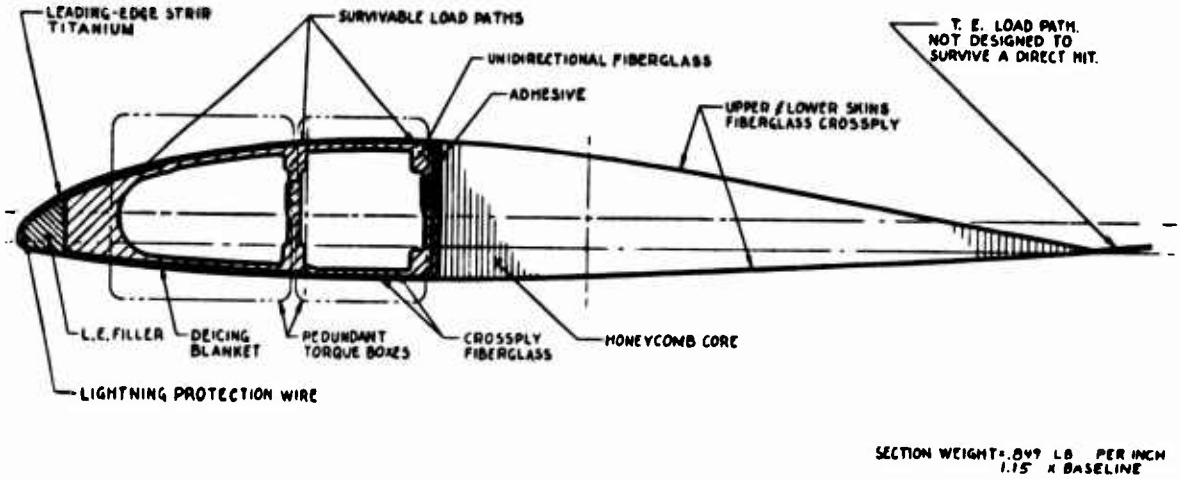

Figure 10. Concept 3 Ballistically Tolerant Blade.

Survivable Concept 4 (Figure 11)

Survivable Concept 4 was modified from the original baseline blade by extending the chord of the spar. This concept could survive the loss of a given hole size better than the baseline, since more spar strength would remain. This concept has a calculated weight of 13 percent higher than the baseline based on the addition of sufficient nose mass to retain the original 22.6-percent chord balance.

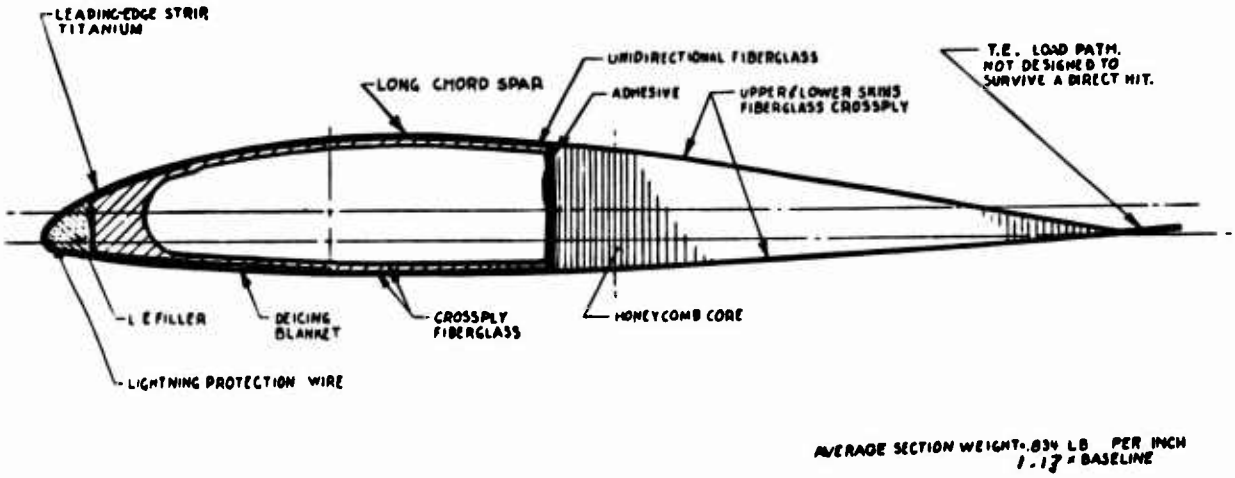

Figure 11. Concept 4 Ballistically Tolerant Blade.

Survivable Concept 5 (Figure 12)

Survivable Concept 5 was modified from the original baseline blade by the addition of two load paths at the back of the spar. In addition, the ability of the nose to carry spanwise load and to survive a hit is enhanced by a steel cable. This concept has a calculated weight of 7.0 percent higher than the baseline based on retention of the original 22.6-percent chord balance.

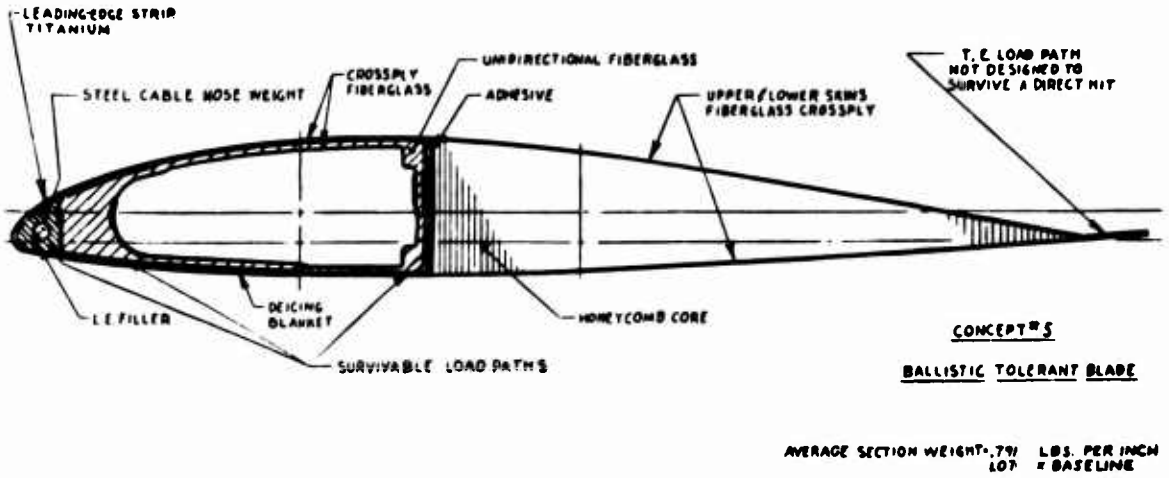

Figure 12. Concept 5 Ballistically Tolerant Blade.

Survivable Concept 6 (Figure 13)

Survivable Concept 6 was not considered a modification to the baseline blade. This concept was selected as a candidate because of its superior ballistic tolerance. The spar consists of unidirectional fiberglass containing several webs separated by hollow tubes. The blade is fabricated by using the filament winding process to a maximum practical degree. This concept has a calculated weight of 20 percent higher than the baseline blade based on retention of the original baseline balance at 22.6-percent chord.

A modification of Concept 6 was one of the three concepts selected for fabrication and test. Hereafter, it is referred to as Design 6A.

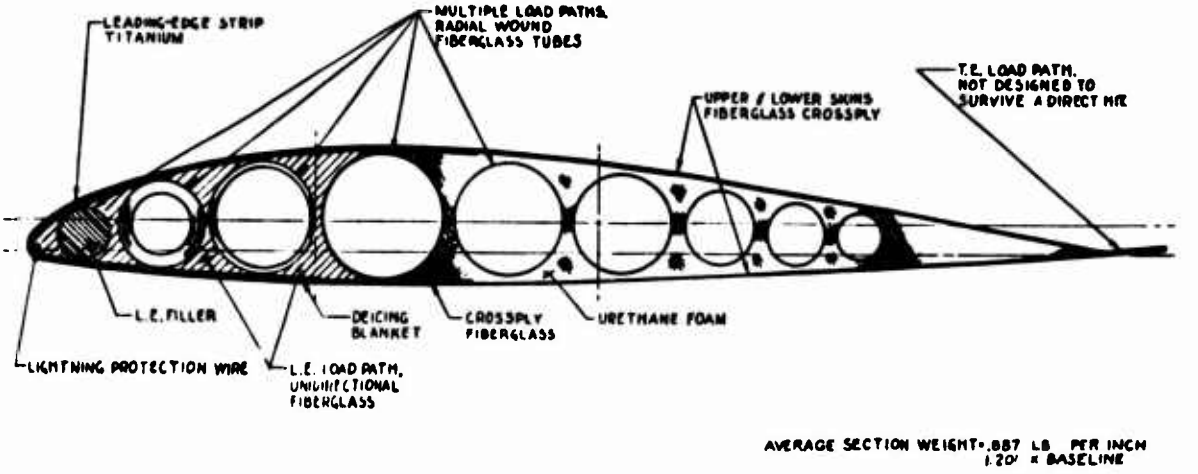

Figure 13. Concept 6 Ballistically Tolerant Blade.

Survivable Concept 7 (Figure 14)

Survivable Concept 7 was modified from the original baseline blade by the addition of multiple load paths spread out over the entire cross section of the spar. These load paths are each less survivable than the load paths in the previously described concepts; however, ballistic tolerance is gained by their increased number and by having their sections thin between the load paths to aid in venting the blast. This concept has a calculated weight of 15 percent higher than the baseline based on retention of the original 22.6-percent chord balance.

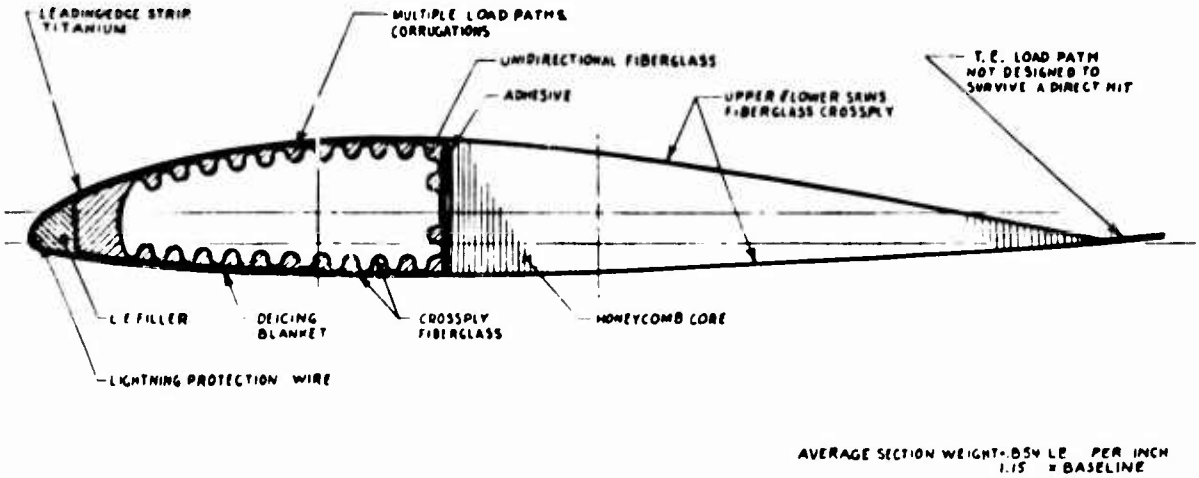

Figure 14. Concept 7 Ballistically Tolerant Blade.

Survivable Concept 8 (Figure 15)

Survivable Concept 8 was modified from the original baseline by the addition of multiple load paths spread out over the entire cross section of the spar. These load paths have a steel cable center surrounded by unidirectional fiberglass which is covered inside and out by crossply. In addition, the ability of the nose to carry spanwise load and to survive a hit is enhanced by a steel cable. This concept has a calculated weight of 24 percent higher than the baseline based on retention of the original 22.6-percent chord balance.

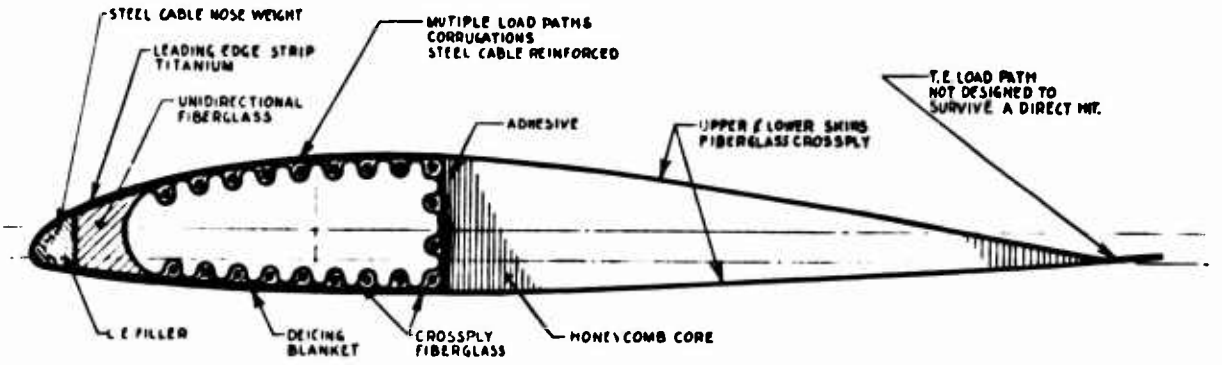

Figure 15. Concept 8 Ballistically Tolerant Blade.

SELECTION OF BLADE DESIGNS

Selection of the three preferred blade concepts to be tested was based on a rating system (Table 2) which considered all the major design parameters. A rating scale of 1 to 10 was used in which 10 is the best. The baseline blade was arbitrarily rated at 5 in all parameters.

In selecting the three test designs, only concepts rating high

TABLE 2. BLADE CONCEPT RATING

Design Concepts	Survivability	Weight	Producibility Experimental	Producibility Production	Cost	Crash Survivability	Radar Reflectivity	Reliability	Maintainability	Erosion Protection	Lighting Protection
Baseline	5	5	5	5	5	5	5	5	5	5	5
1	7	4	5	5	5	5	5	5	5	5	5
2	8	3	5	5	5	5	5	5	5	5	5
3	9	3	4	4	4	5	5	5	5	5	5
4	7	3	3	2	2	5	5	5	5	5	5
5	7	4	3	5	5	2	5	5	5	5	5
6	8	2	4	4	4	5	5	5	5	5	5
7	7	3	3	2	2	3	5	5	5	5	5
8	8	1	2	2	2	3	5	5	5	5	5

- Concepts are rated on a scale of 1 to 10 with 10 being the best
- Baseline blade is arbitrarily rated at 5 for each parameter

in survivability were considered. Weight was the next most important factor. Producibility, both in production and for this experimental program was also evaluated. Cost are primarily based on an evaluation of producibility. Crash survivability was related to the probability of the blade to shear off at the point of impact when striking an immovable object near the tip rather than failing at the root. No outstanding advantages were visualized for any concept with respect to the other parameters: radar reflectivity, reliability, maintainability, erosion protection and lightning protection. Therefore, all the concepts were rated equal to the baseline. Based on evaluation of the above considerations, Concepts 2, 3, and 6 were selected for test and are hereafter referred to as Design 2, Design 3, and Design 6A, respectively.

DESIGN OF TEST BLADES

Detail design and analysis were conducted on the three survivable designs selected for test. Survivable load paths were sized and located in the spar. Spar wall thicknesses and the proportion of unidirectional fiberglass to crossply were defined. Weight and centrifugal force distribution for each design were calculated (Figures 16 to 21). Dynamic analyses were conducted to determine blade chordwise, flapwise and torsional natural frequencies (Figures 22 to 24). These analyses provided a preliminary understanding of how the changes in blade weight and stiffness affected their natural frequencies in relation to rotor speed. Each figure compares the frequencies of a survivable design to those of the baseline blade.

The natural frequencies of the three designs are acceptable at normal operating rpm except for the following:

- Design 2; second chord is at 4.97/rev
- Design 6A; second flap is at 2.94/rev

Additional design refinements would be required on these two blades to drive the frequencies further away from an integer value. It is noted that all three survivable designs show a first torsional frequency crossing right on 5/rev at 296 rpm. With a little fine tuning, this is acceptable for a four-blade rotor and would, therefore, not require further major blade design changes.

Two types of test specimens were then designed. One test specimen (Figure 25) was designed to be ballistically impacted while not carrying any loads. On these test sections, all the different types of hits were made to provide analytical input data on damage incurred, residual strength, and residual stiffness. These unloaded test sections were made 6 feet in span.

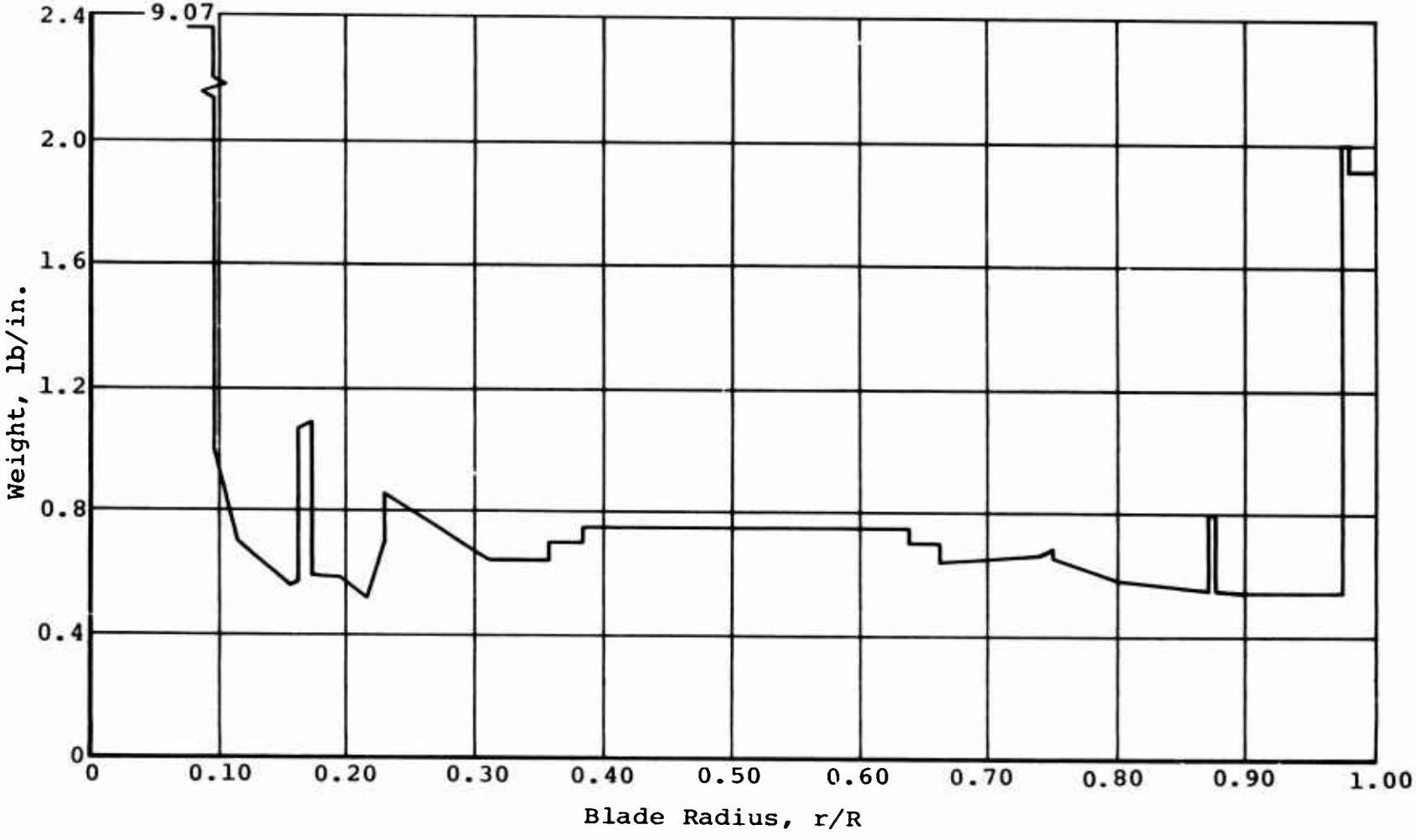

Figure 16. Ballistically Tolerant Blade Weight Distribution - Design 2.

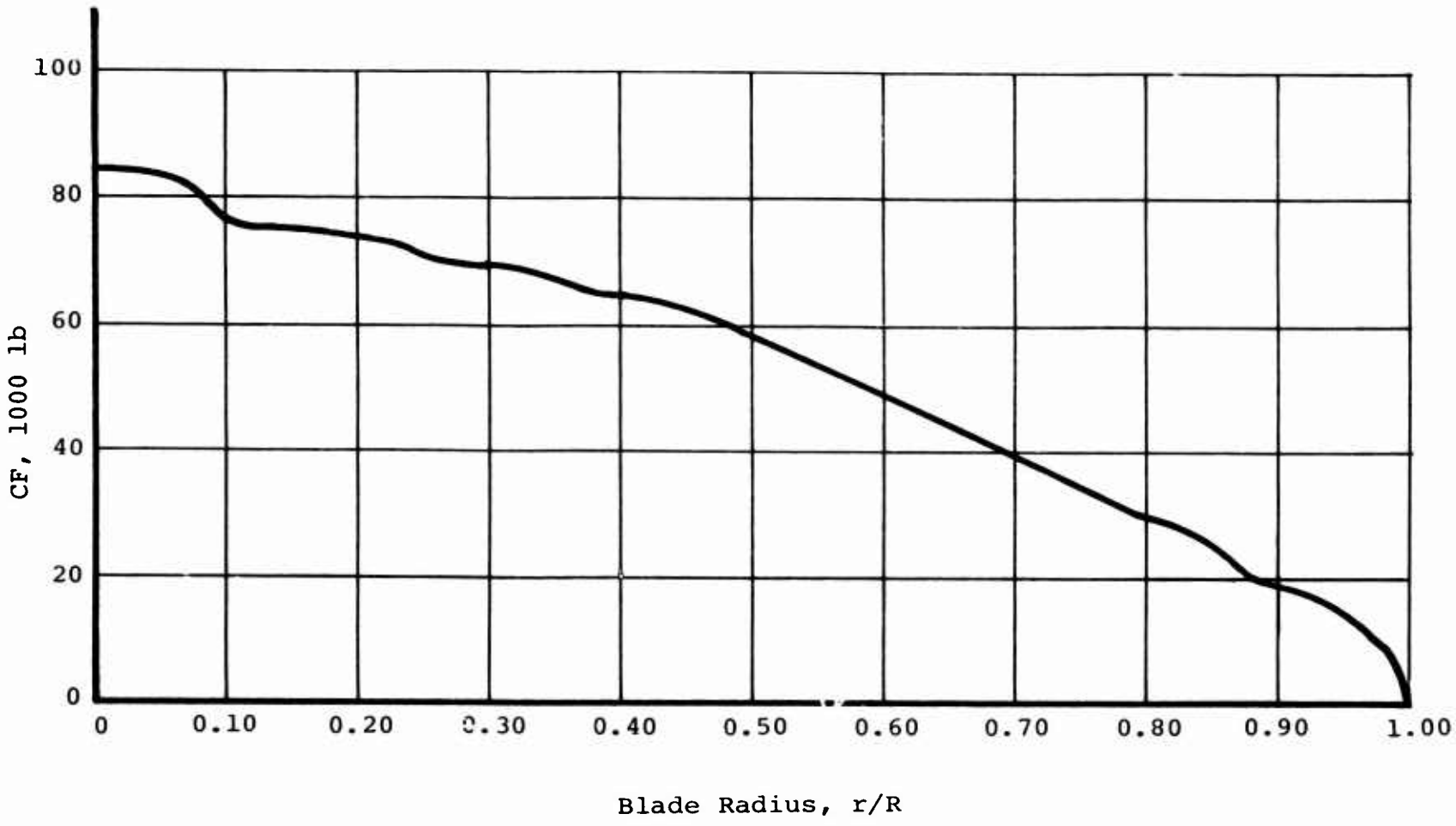

Figure 17. Ballistically Tolerant Blade CF Distribution - Design 2.

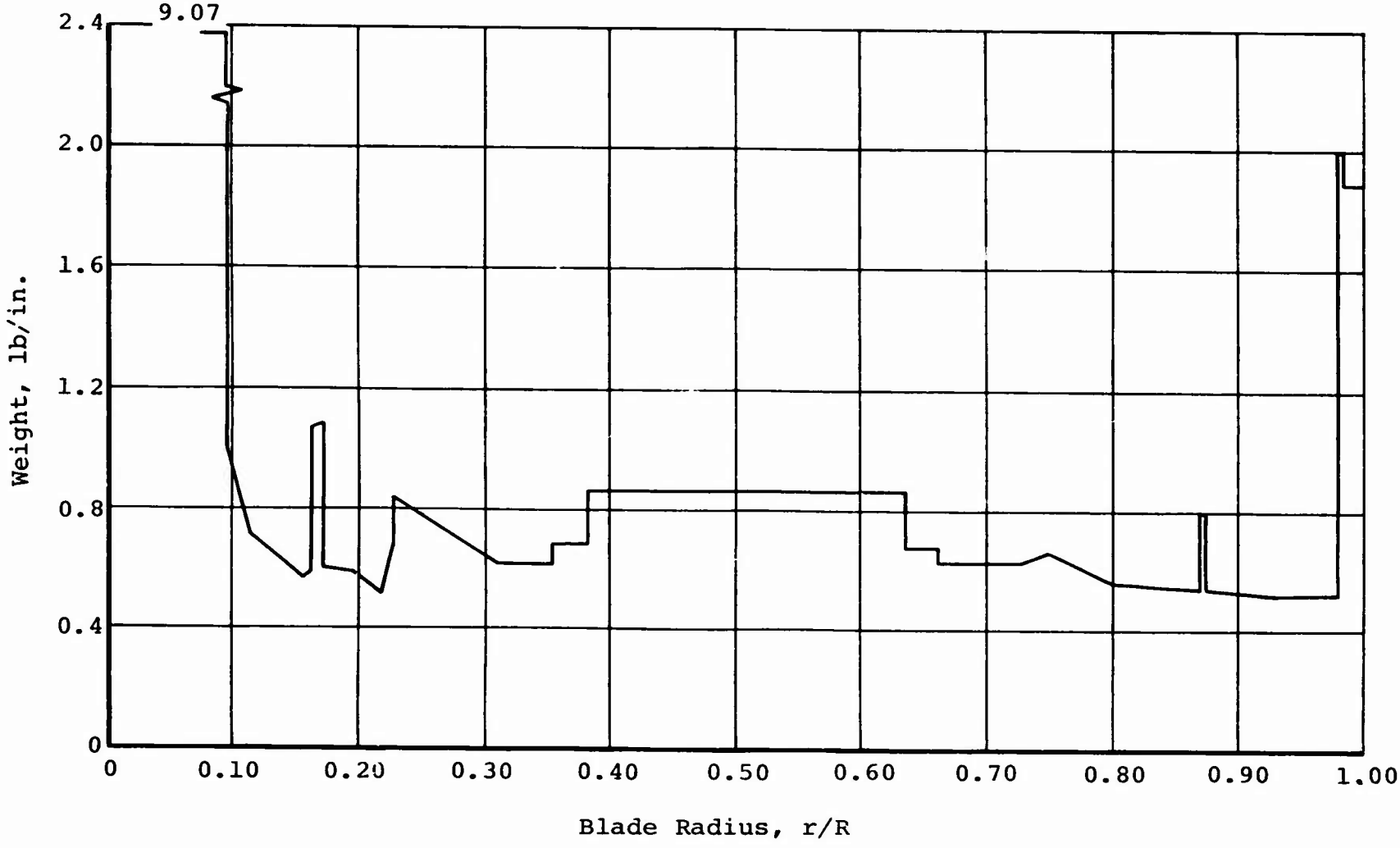

Figure 18. Ballistically Tolerant Blade Weight Distribution - Design 3.

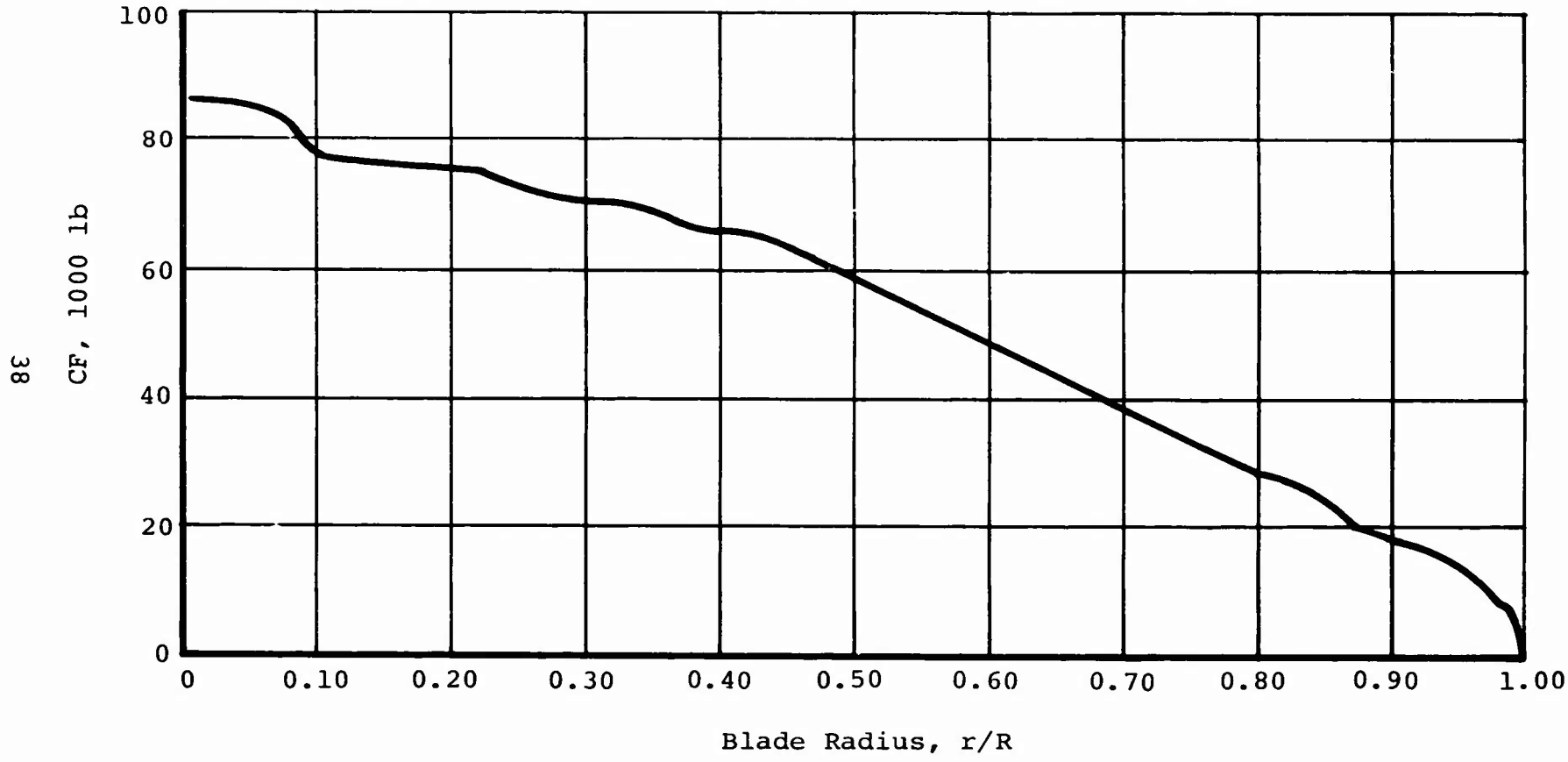

Figure 19. Ballistically Tolerant Blade CF Distribution - Design 3.

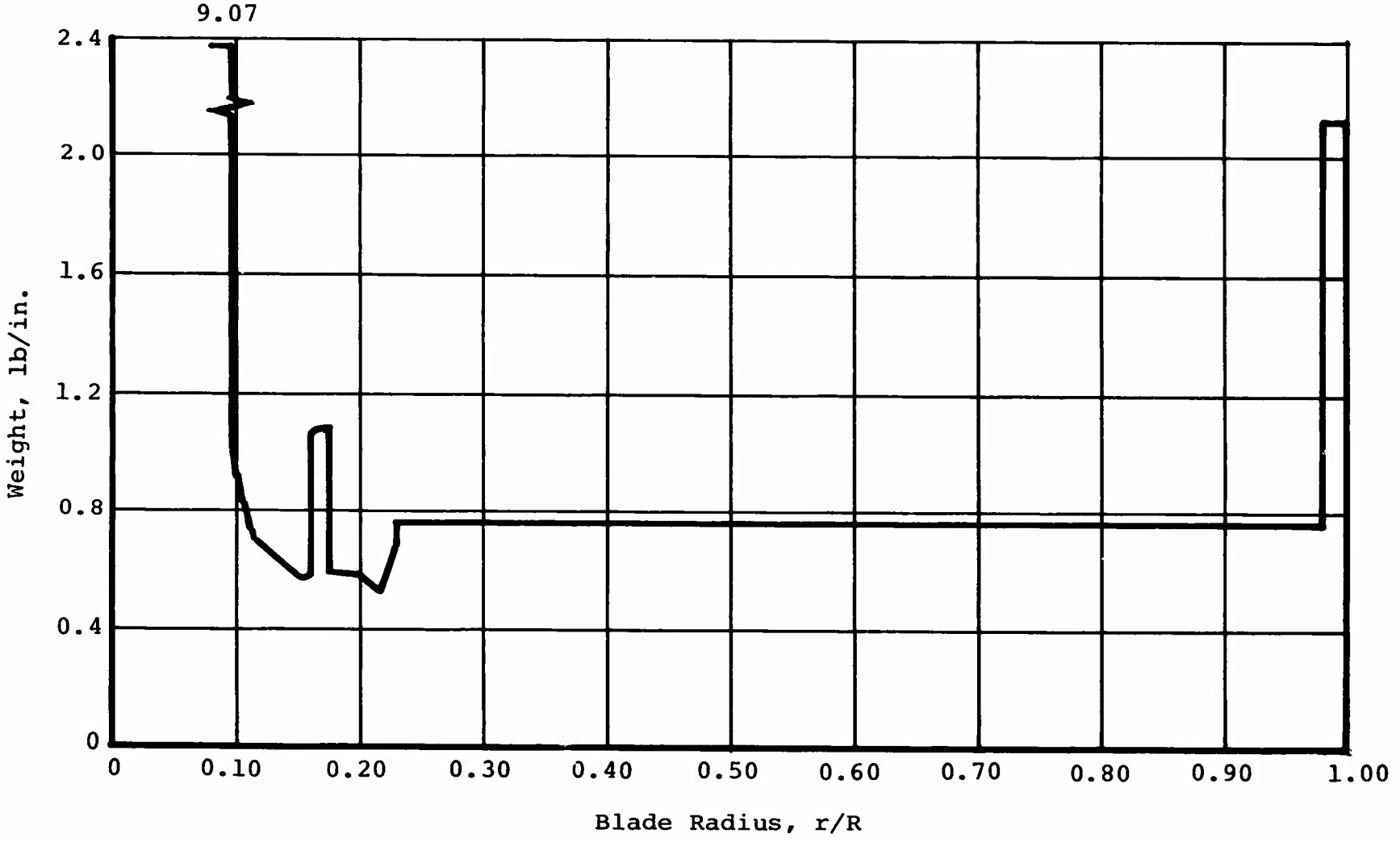

Figure 20. Ballistically Tolerant Blade Weight Distribution - Design 6A.

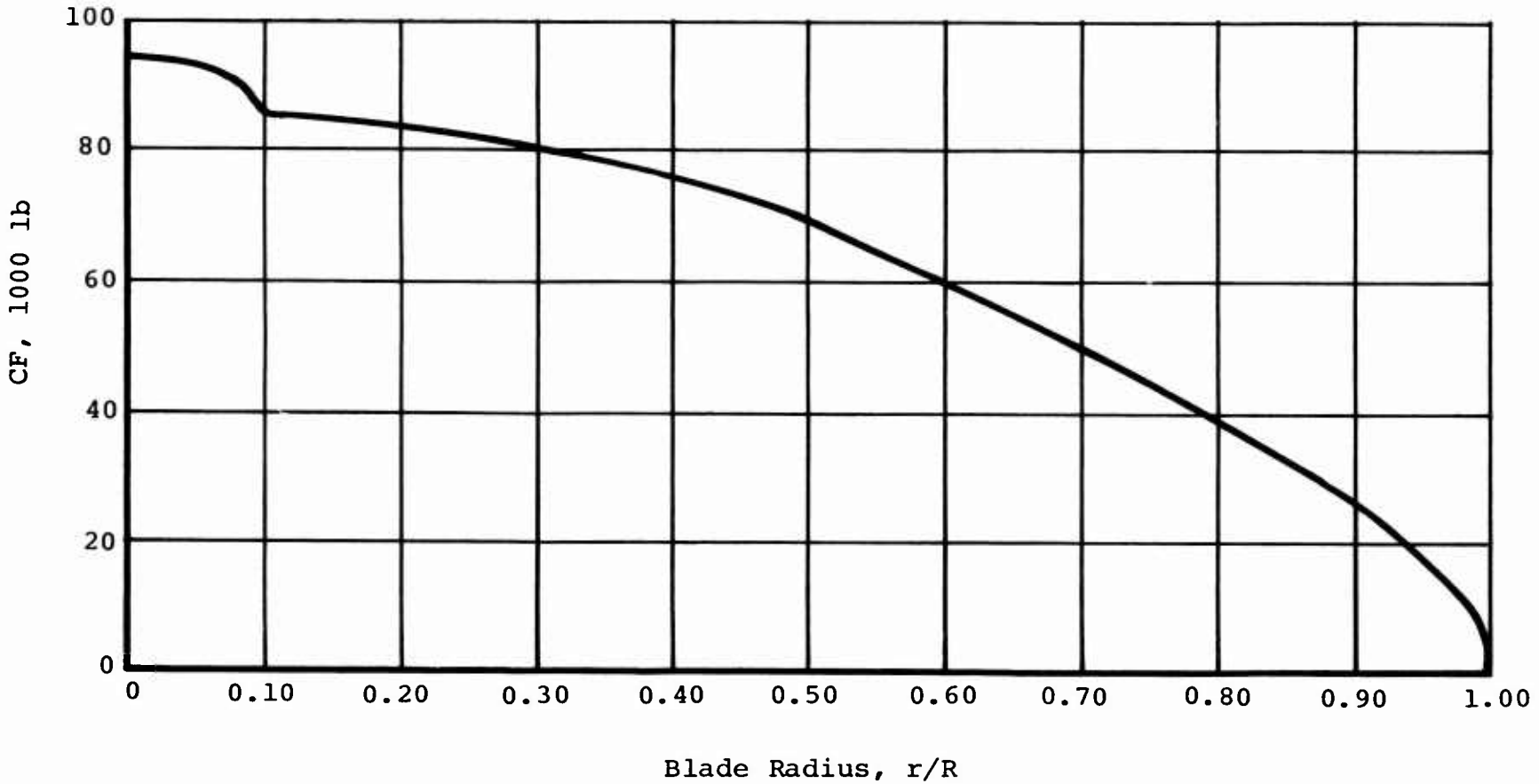

Figure 21. Ballistically Tolerant Blade CF Distribution - Design 6A.

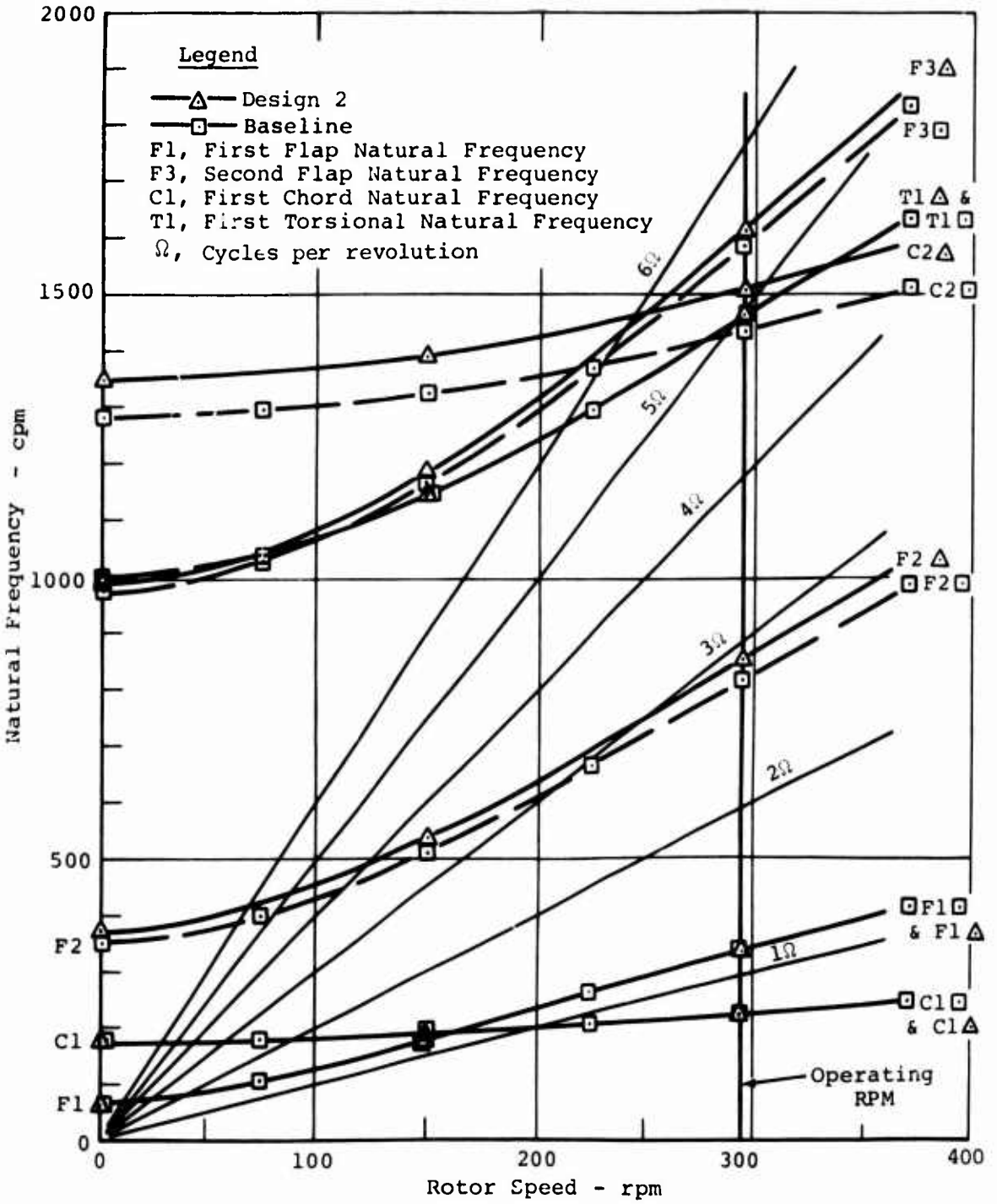

Figure 22. Ballistically Tolerant Blade Frequency Spectrum - Design 2 Blade.

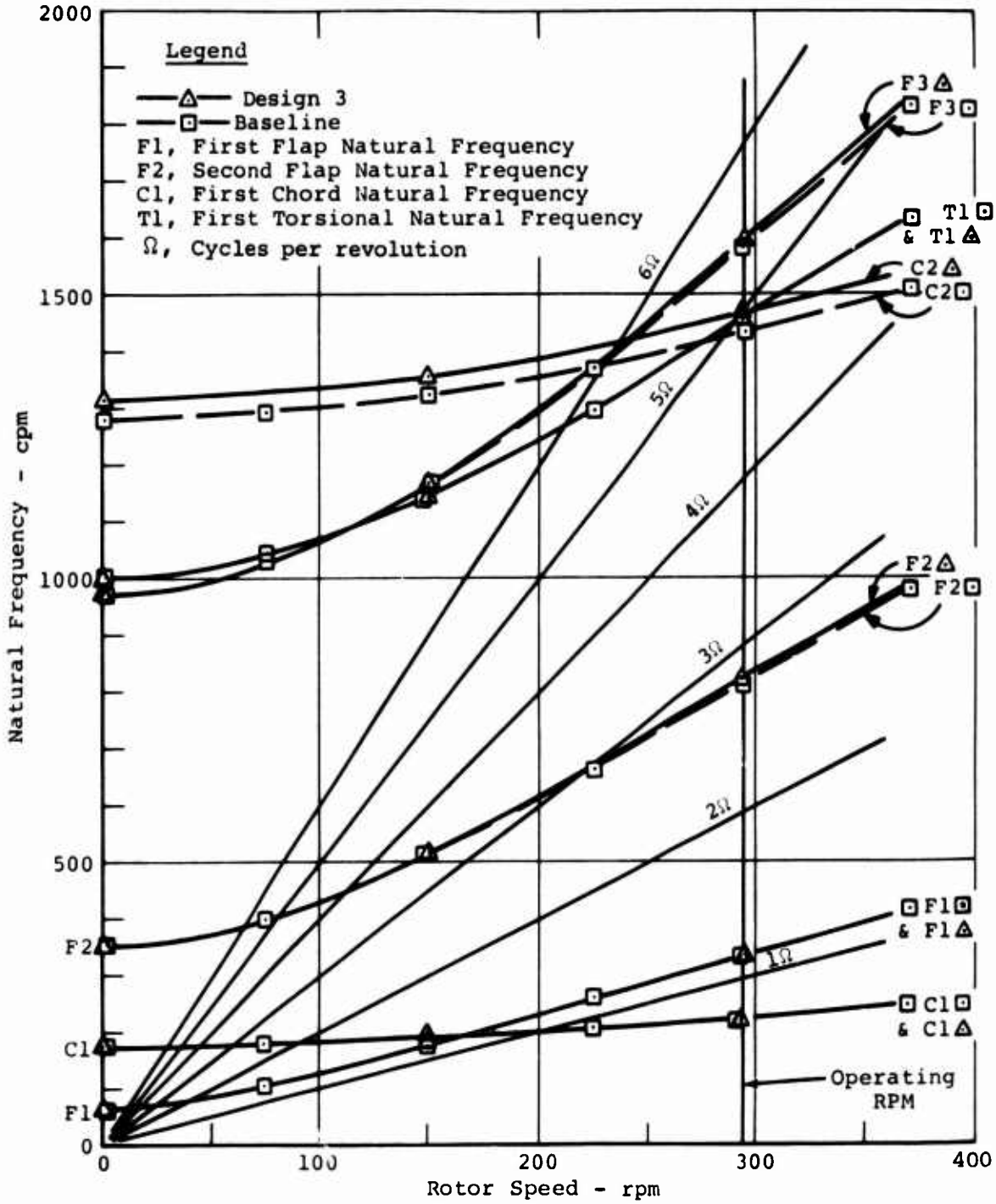

Figure 23. Ballistically Tolerant Blade Frequency Spectrum - Design 3 Blade.

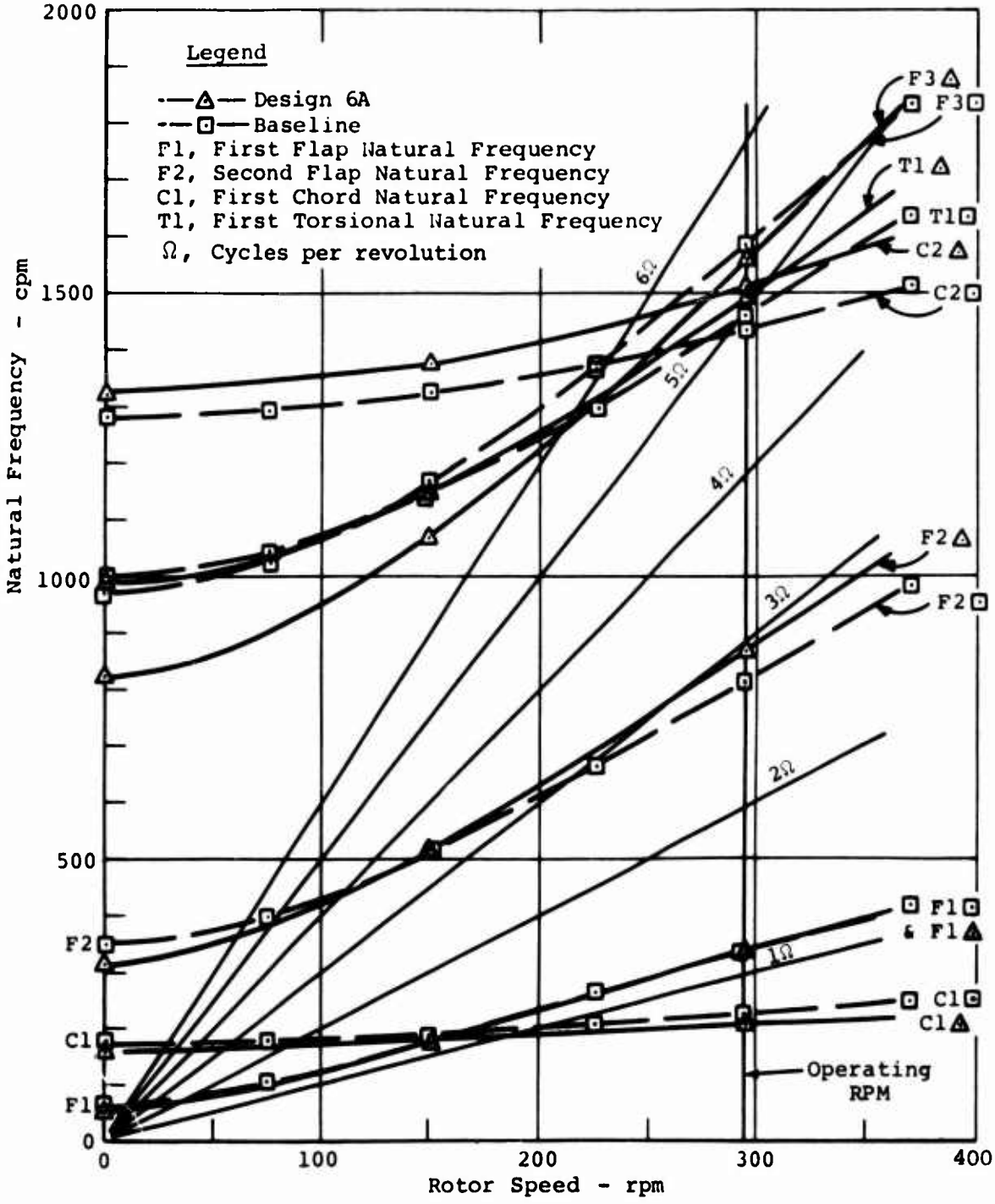

Figure 24. Ballistically Tolerant Blade Frequency Spectrum - Design 6A Blade.

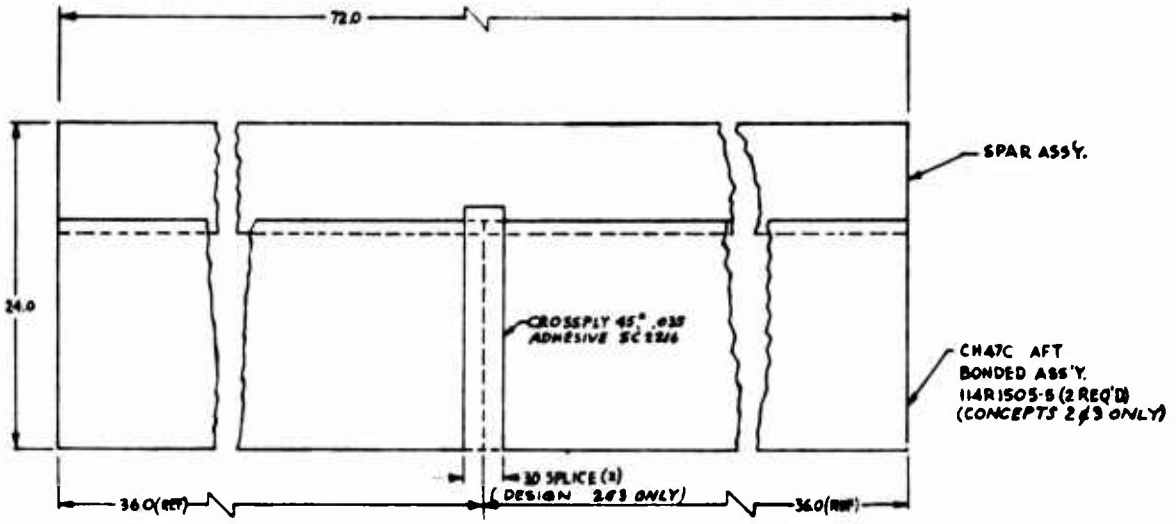

Figure 25. Ballistic Test Specimen Blade - Unloaded.

This dimension was selected to permit two 23mm HEI hits to be made in each section without excessive damage from one hit overlapping the other or extending into the end. The other type of test section (Figure 26) was designed with loading ends to fit into the Ballistic Research Laboratories blade loading rig, and also into a Boeing fatigue test machine. The ends were designed to carry blade tension and blade bending loads encountered at V_{max} through steel plates bonded and bolted to the top and bottom of the spar. Inside the spar and inside the plates, which extended beyond the spar, was a bonded-in hardwood filler. The loaded sections on Designs 2 (Figure 27) and 3 (Figure 28) had aft fairing which was only 3 feet in span. Design 6A had a full span aft section. Either length was satisfactory for the loaded sections, since only one hit was to be made on each of the loaded sections.

Designs 2 and 3 were designed with unidirectional and cross-ply "S" glass spars. They were of a constant section matching that portion of the baseline blade, which has a low-density nose filler instead of a nose balance mass. The aft sections were a production configuration built for use on the CH-47C blades. They had fiberglass skins and aluminum honeycomb filler. Designs 2 and 3 also incorporated the stainless steel nose cover which is used on the CH-47C blade.

Blades of the design represented by Design 6A have been built in a variety of forms under USAAMRDL contract by Fiber Science, Inc., of Gardena, California. This design was fabricated by filament winding major components including the spar, tubes and skin. Prior to this program, ballistic tests had been conducted on a blade similar in construction to Design 6A.

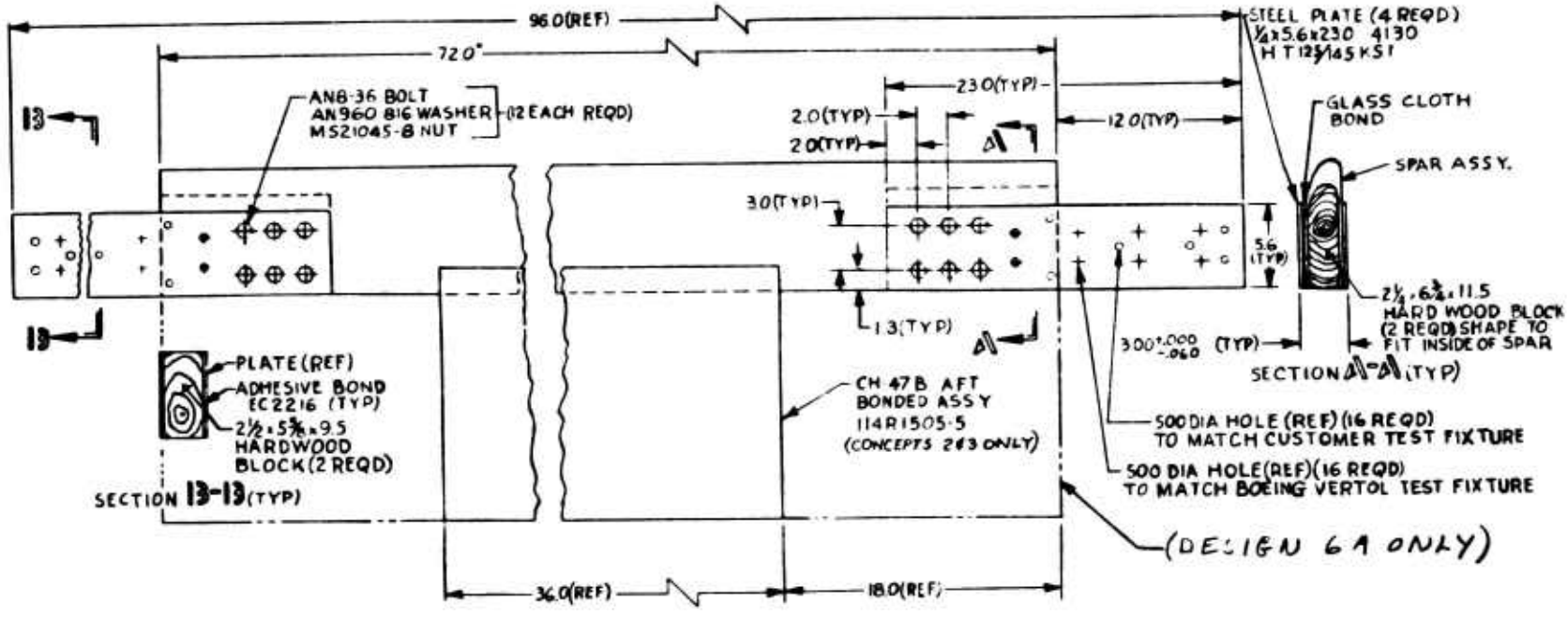

Figure 26. Ballistic Test Specimen Blade - Loaded.

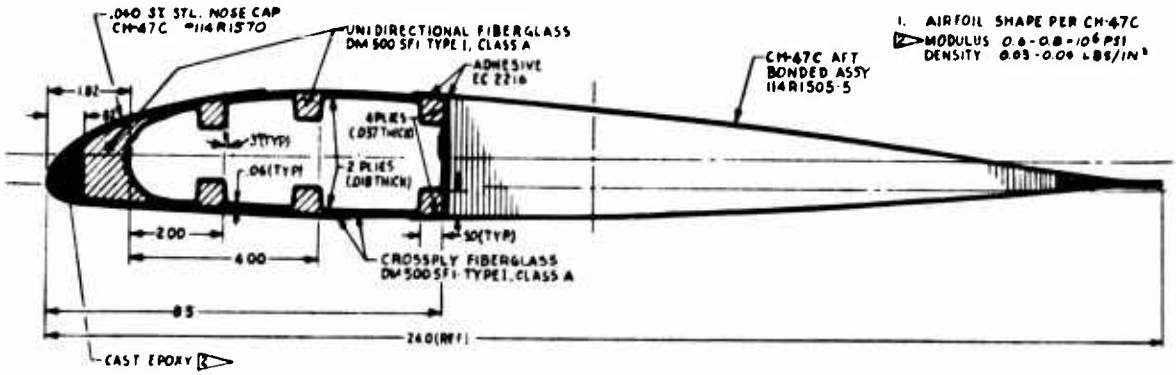

Figure 27. Ballistic Test Specimen Blade - Design 2.

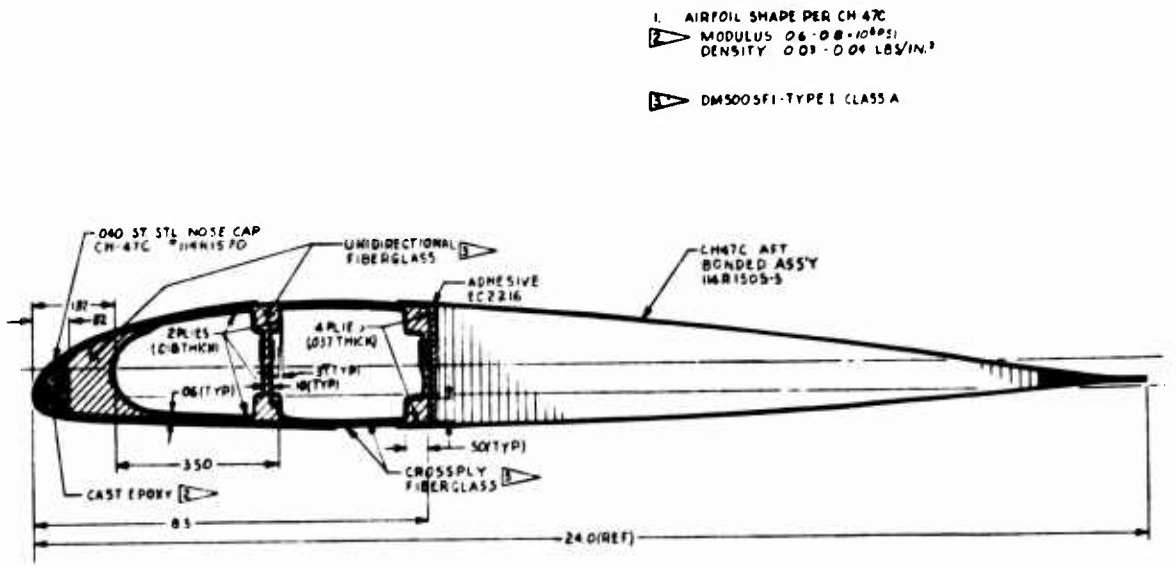

Figure 28. Ballistic Test Specimen Blade - Design 3.

The results were not considered satisfactory, and the Army decided that a redesign was desirable for this program. The resulting design (Figure 29) is designated as 6A. It consists of one large concentrated mass of unidirectional fiberglass at the nose sufficient to balance it chordwise, a filament-wound "D" spar around it, and a large filament-wound "D" spar extending back from the smaller "D" spar. The aft section is of crossply fiberglass skins and a foam filler.

FABRICATION OF BLADE SECTIONS

The ballistic test blades were made to match the size, shape, and construction of the baseline blade as nearly as possible, but with consideration for quick and economical blade fabrication. Designs 2 and 3 were fabricated by conventional hand lay-up. Design 6A was fabricated using the filament winding process, where possible, in addition to hand lay-up.

Designs 2 and 3

Spars for Designs 2 and 3 (Figure 30) were cured in specially made female compression molds. These molds were formed by using a CH-47C blade spar and nose contour pieces with a 1-inch-thick wood strip on the back as a mandrel (Figure 31). This was done to closely match the dimensions of the baseline spar. The mold was made from this mandrel using fiberglass reinforced high-temperature tooling resin. It was made in two halves, upper and lower, with separation near the chord line and formed the outer contour of the spar. Electrical heating elements were fastened to the outer surfaces of the mold and thermocouples strategically located inside. Metal slugs were cast in the resin to improve thermal conductivity. Hardwood mandrels were made in the shape of the spanwise holes through the spar to form the inside. The material used in the spars was Dexter Materials Corporation "S" glass made to Boeing Specification DM500-SF1, Class A. The amount of spar material was calculated to fill the space between the mandrel and the mold in order that proper pressure would be applied. Then the two halves were bolted together and was applied to cure the spar. CH-47C aft sections were then bonded to the spar with EC 2216 adhesive. On the unloaded blades, the two aft sections were connected together by a crossply skin bonded with EC 2216 adhesive.

The above manufacturing approach was the same as that which had been followed in making the test sections of the baseline blades. The only major exception to this was the use of SP250-SF1 fiberglass in the baseline instead of the DM500-SFI used in Designs 2 and 3.

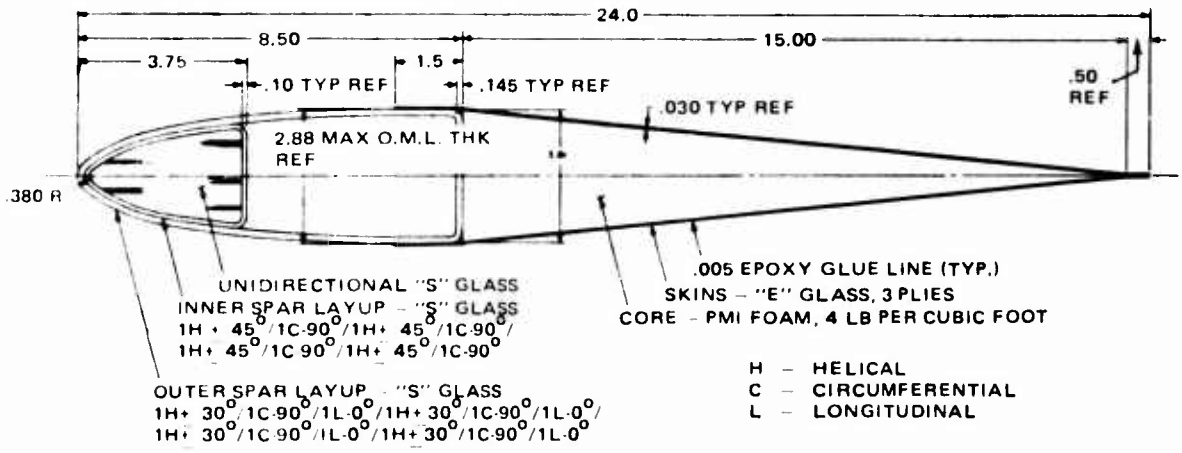

Figure 29. Ballistic Test Specimen Blade - Design 6A.

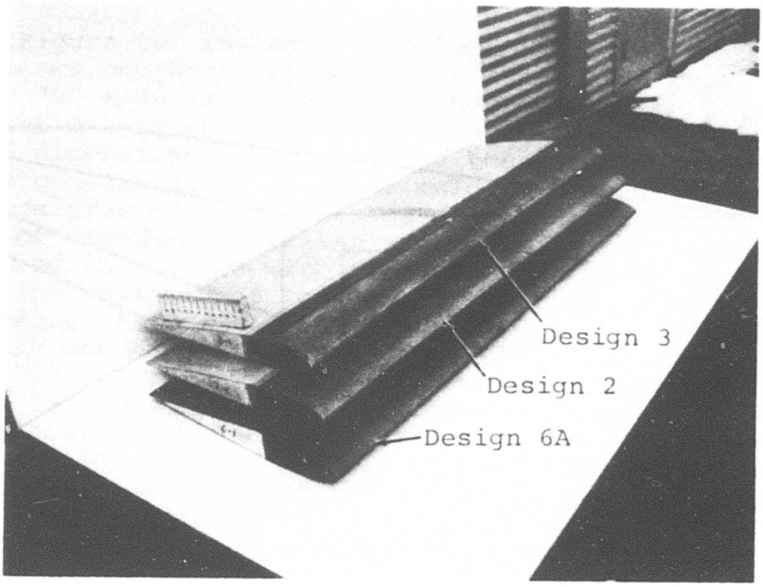

Typical Unloaded Blade Sections
Designs 3, 2, and 6A

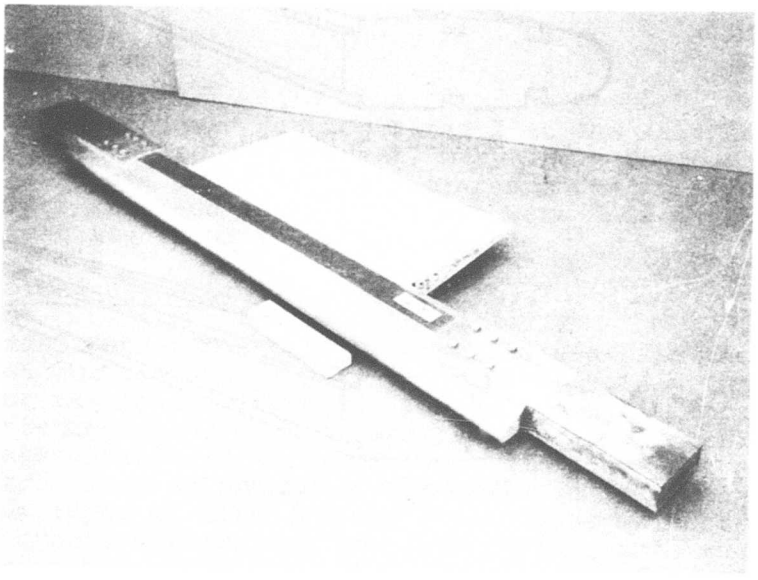

Typical Loaded Blade Sections
Figure 30. Photographs of Blade Sections.

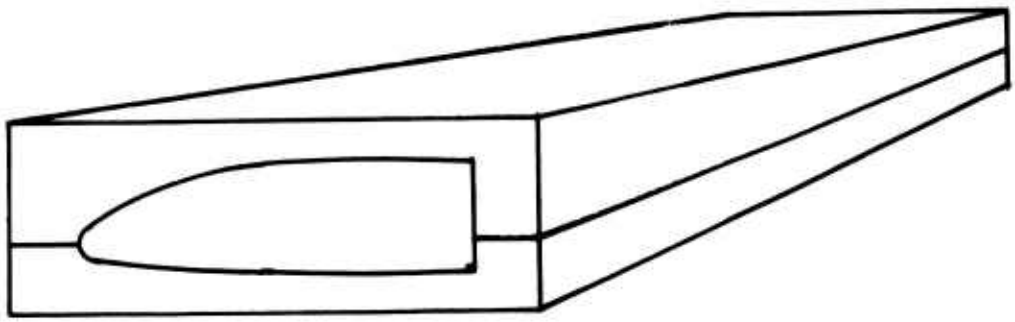

Female Mold - Designs 2 and 3

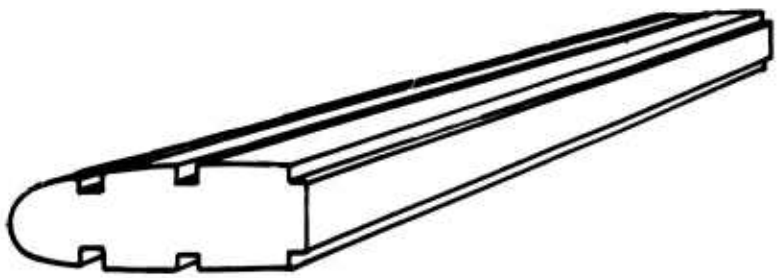

Mandrel - Design 2

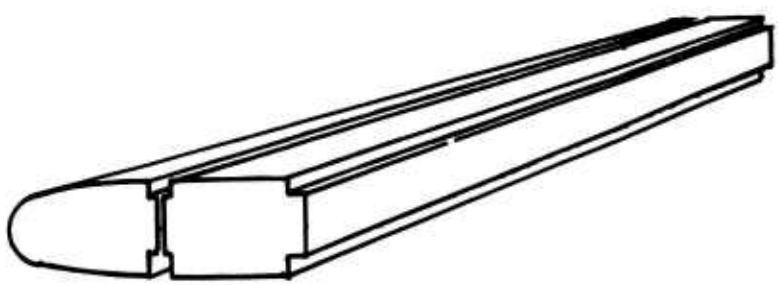

Mandrels - Design 3

Figure 31. Tooling for Designs 2 and 3.

Design 6A

Design 6A (Figure 30) was made by filament winding the inner and outer spars and hand lay-up of the assembly. First the large outer "D" spar was filament wound to a proper diameter. This diameter was selected to provide a finished "D" spar of the desired dimensions. The spar was then placed inside a female mold consisting of an inner mold, 3/8-inch thick of fiberglass reinforced epoxy, backed up with a 3-inch-thick outer mold of low-density filler material (Figure 32). The spar was cured in an oven with pressure applied by an inflatable bag. The small inner spar was also filament wound to a proper diameter, then stuffed with unidirectional fiberglass. This assembly was then flattened and inserted in the front of the larger "D" spar. A pressure bag was inserted into the back of the larger spar, and this was oven cured. The fiberglass used in all of these parts was "S" glass, Ferro S-1014. The resin was 118, Applied Plastic Company, 2434 resin with 2347 hardener made to Fiber Science, Inc., Spec. 118ET. The aft section was 181 cloth "E" glass bonded to an acrylic PMI foam filler with the same resin. It was also bonded to the spar in the same operation with that resin.

Loaded Sections

Load ends were then bolted and bonded with EC 2216 adhesive to the three blade sections which were to be shot under load.

BALLISTIC TESTS

The ballistic testing was done on Range 7 at the Army Ballistic Research Laboraties at Aberdeen, Maryland. Tests made on unloaded blades were conducted in the area shown in Figure 33. Tests on blades stressed to flight loads were done in the blade load test rig shown in Figure 34.

Hits on Unloaded Blade Sections

Unloaded blades were shot first in order to evaluate the damage sustained due to various hits prior to selecting the hit direction for the loaded impacts. The unloaded hit locations used were selected based on the results of previous tests, because they are considered to be the most damaging that a blade can encounter. Each of the three concepts was impacted with the same four types of hits (Figure 35). These were straight-in from the front, straight-up from the bottom, into the front from 30 degrees below the chord line, and up and forward from the back at a specific hit point and angle which causes the delayed round to function on the aft skin and detonate just inside the spar. The first three of these types of hits all utilized an 0.060-inch-thick aluminum function plate placed

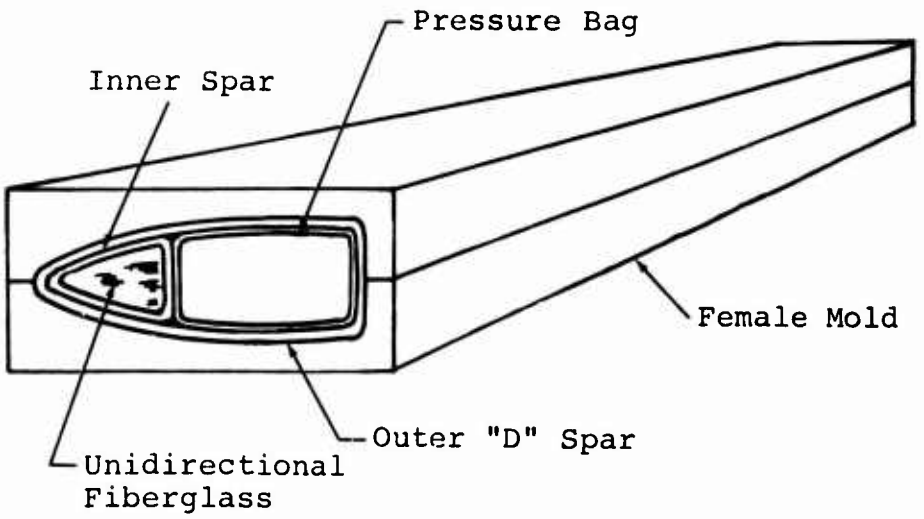

Figure 32. Tooling for Design 6A.

Test Range

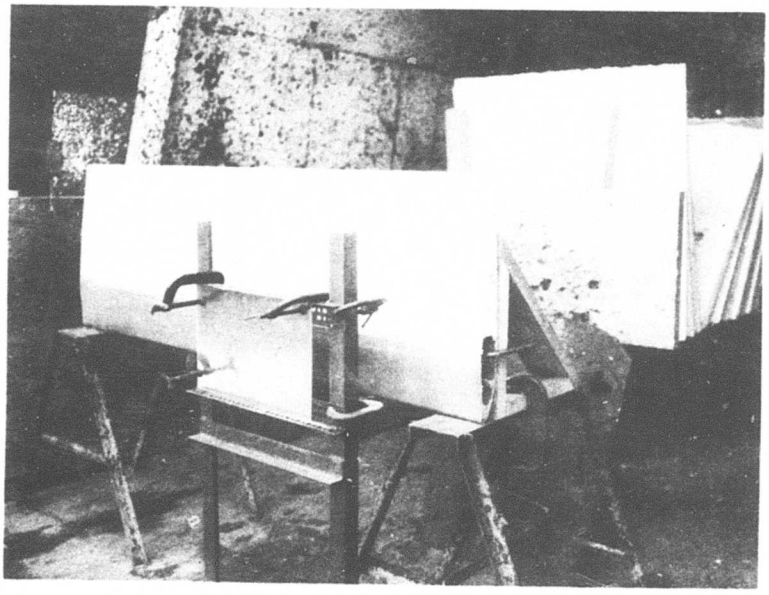

Unloaded Test Setup Showing
Function Plate

Figure 33. Ballistic Test Range - Unloaded Tests.

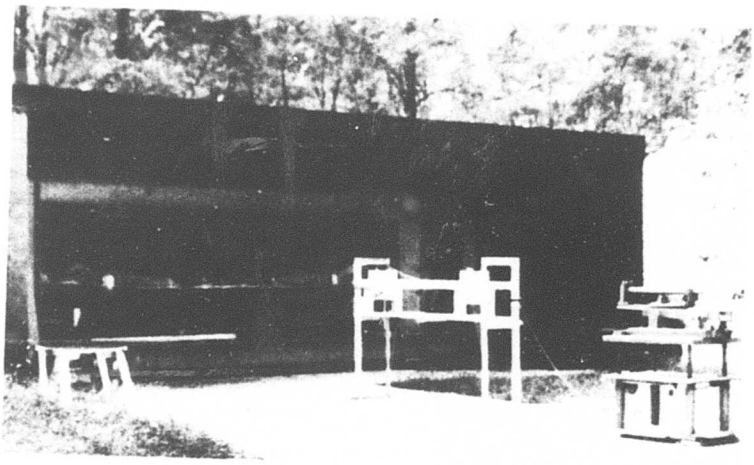

Test Range

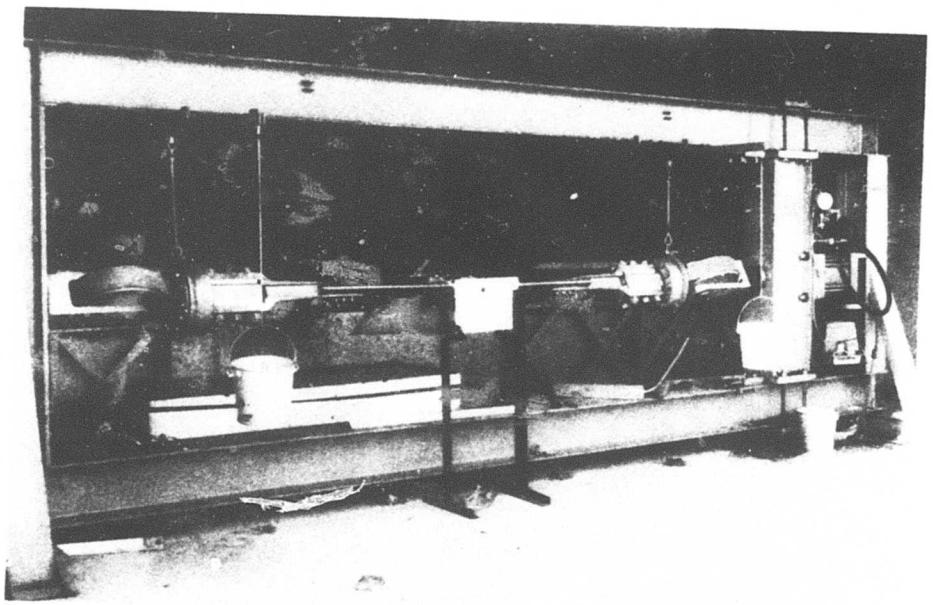

Blade Loading Rig

Figure 34. Ballistic Test Range - Loaded Tests.

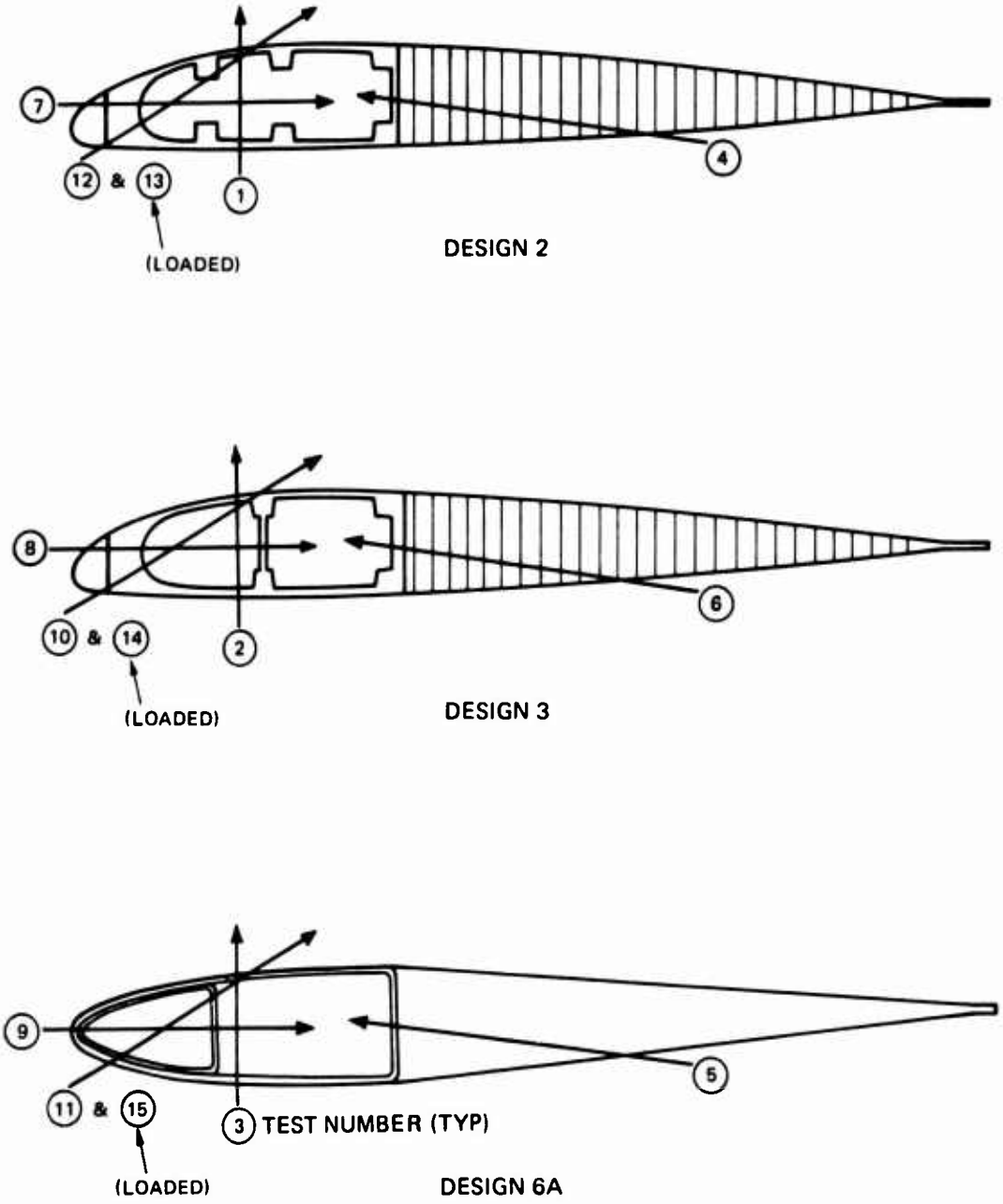

Figure 35. Ballistic Impacts Tested.

approximately 9 inches ahead of the blade surface. A function plate causes an earlier detonation of the round, and thereby permits the use of available delayed 23mm HEI-T rounds to simulate the effect of superquick rounds which detonate immediately on impact with the surface. The rounds used were all 23mm HEI-T OFZT with MG-25 delay fuses.

In all, 12 hits were made on unloaded sections, four for each blade design (Table 3). All hits were made at muzzle velocity, which is believed to be conservative for the types of blade spar sections being tested. Shrapnel density and velocity are both greater at muzzle velocity and, therefore, more damaging than at lower velocity. Blast effect does not vary significantly with impact velocity.

When using delayed 23mm HEI rounds to simulate the effect of superquick, some variation may be experienced in the detonation point from round to round. The detonation point is critical to blades. If the round detonates too early, the blast effect is diminished and the shrapnel is more diffused. If it detonates too late, excessive blast may occur inside the blade and the effect of the shrapnel on the entrance surface is diminished. The detonation points were correct in all cases except two. Hit number 021474P2 detonated slightly early but was considered acceptable. Hit number 021474P8 detonated too late, doing little damage to the blade. The hit was then repeated in the same spot and detonation was proper.

After the hits on the unloaded sections were made, the blades were sawed through chordwise across the damaged area. They were examined before and after cutting to determine the type and extent of damage sustained due to each hit. Several types of damage were noted. On some of the hits of all three concepts, the aft part of the blade separated from the spar. This was aggravated by the fact that the two hits on each section were close together and close to the end of the section. Also, on Design 6A the large section of unidirectional fiberglass and the inner "D" spar tended to separate from the outer "D" spar. This is understandable, since they are held together only by one bond of resin which covers the upper and lower front surfaces of the inner "D" spar, but not the back of it.

Hits on Loaded Blade Sections

The results of the various hits made on unloaded sections were evaluated in order to decide how the loaded specimens should be hit. Only one hit was to be made on each design while loaded, and it was considered desirable to use the most damaging hit in order to provide total invulnerability. However, evaluation of the unloaded hits showed that no distinct pattern could be discerned in which one type of hit was clearly the most

TABLE 3. TABULATION OF BLADE TESTS

Test No.	Hit Designation	Blade Design	Load Sustained			Location	Remarks
			Before Hit	After Hit	Reload		
1	021474P1	2	-	-	-		Aft section separated
2	021474P2	3	-	-	-		Aft section separated
3	021474P3	6A	-	-	-		Aft section separated
4	021474P4	2	-	-	-		Aft section separated
5	021474P5	6A	-	-	-		Aft section separated
6	021474P6	3	-	-	-		Aft section stayed on
7	021474P7	2	-	-	-		Aft section separated
8	021474P8	3	-	-	-		Aft section separated
9	021474P9	6A	-	-	-		Aft section stayed on
10	021574P1	3	-	-	-		Aft section stayed on
11	021574P2	6A	-	-	-		Aft section stayed on
12	021574P3	2	-	-	-		Aft section separated
13	041074B1	2	93,000	53,000	92,900		Aft section separated
14	041774B1	3	57,000	44,000	57,000	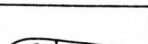	Aft section stayed on Fatigue tested - no failure
15	041774B2	6A	69,300	32,500	32,500	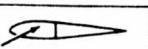	Aft section stayed on

damaging (this is discussed in more detail later in this report). Therefore, it was decided that the hit from the front at 30 degrees below the nose should be used, since it is a most probable type of hit in flight.

Determination of Static Test Loads To Be Applied

A major aim of the loaded ballistic test was to simulate as closely as possible the stresses in the damaged blade which occur in flight at V_{max}. These stresses result primarily from the tension load due to centrifugal force plus the flapwise and chordwise bending. Determination of the best method of setting the load machine to simulate these flight stresses offered some problems. To understand these problems, it is necessary to describe the Ballistic Research Laboratories' blade loading rig (Figure 34). This device can pull tension, representing centrifugal force, on a blade section with a force up to 100,000 pounds by means of a hydraulic cylinder. When this force is aligned with the blade's flapwise and chordwise neutral axes, no bending will be applied to the blade section. However, load offset adjustments are incorporated in the machine. These can be used to move the alignment of the tension load away from the blade flap and chord neutral axes so that in-flight blade bending can be simulated. Pin joints are located in the machine just beyond the ends of the blade section about which rotation occurs when the blade bends. Analysis of the local loads on a damaged blade in flight indicated that the magnitude of the flap and chord bending moment at the damaged spot is reduced due to the local loss of stiffness (Figures 36 and 37). However, the short distance between pins in the loading rig could cause a greater increase in bending of the test blade as the neutral axes shifted upon being damaged than would occur in flight. In order to minimize this effect, it was decided that the blade would be loaded in tension on its neutral axes so that no original bending would occur. To compensate for this lack of bending, the tension load would be increased to account not only for centrifugal force but also for strains due to steady and alternating bending loads. Thus, the effect of an unrealistically excessive shift in blade neutral axes due to damage would be minimized.

Test of Design 2

The first blade to be tested was Design 2 (Figure 27). A tension load of 93,000 pounds was applied. Fifty-eight thousand (58,000) pounds of this represented centrifugal force and the rest simulated bending stress. Centrifugal force was based on an L-01 analysis which used the actual weight of the ballistic test specimen (Figures 16 and 17). No offset was used and virtually no initial blade bending occurred. The blade was shot, after which the load dropped to 53,000 pounds.

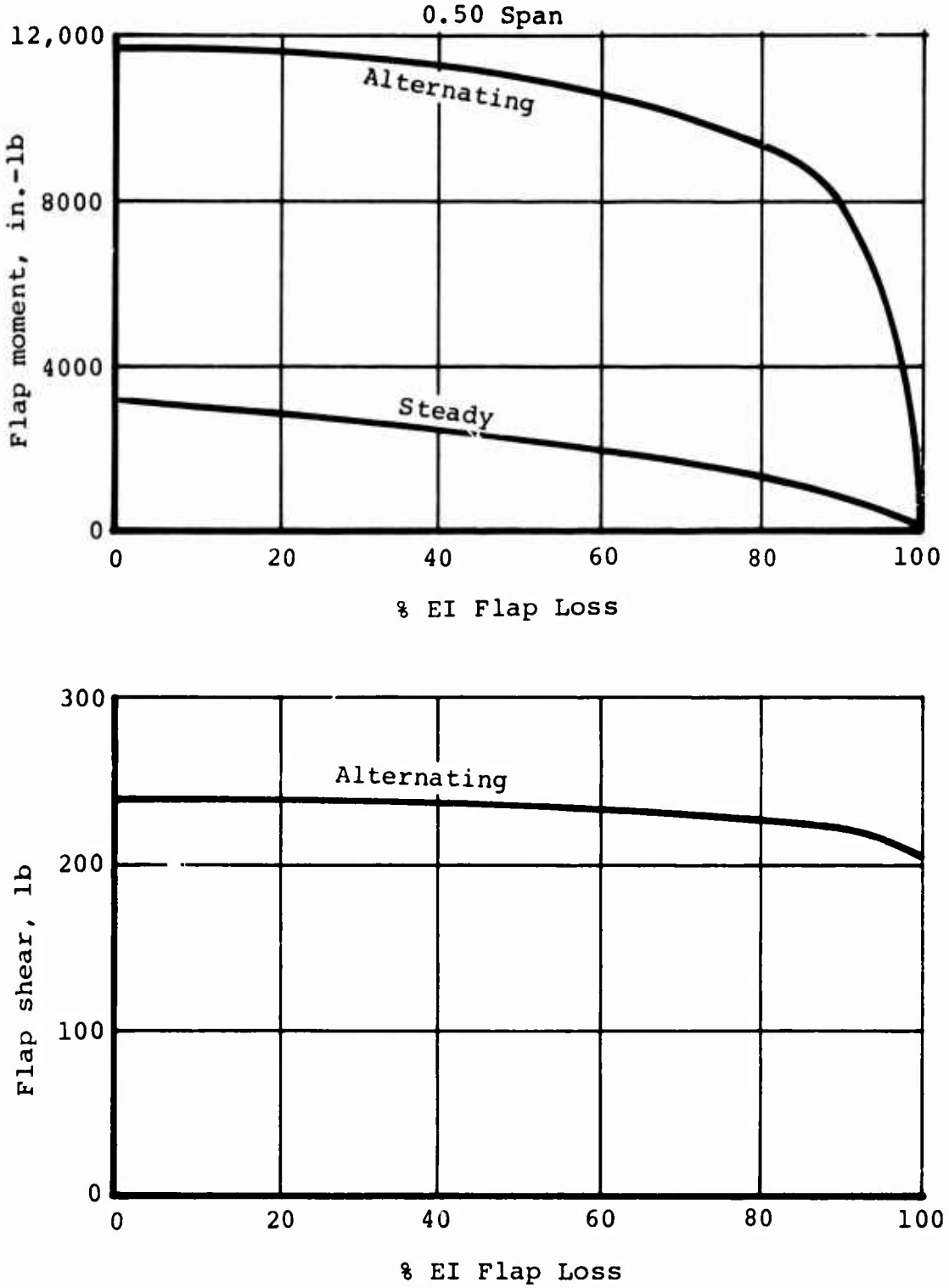

Figure 36. Variation of Moments and Shears With Loss of Flapwise Stiffness.

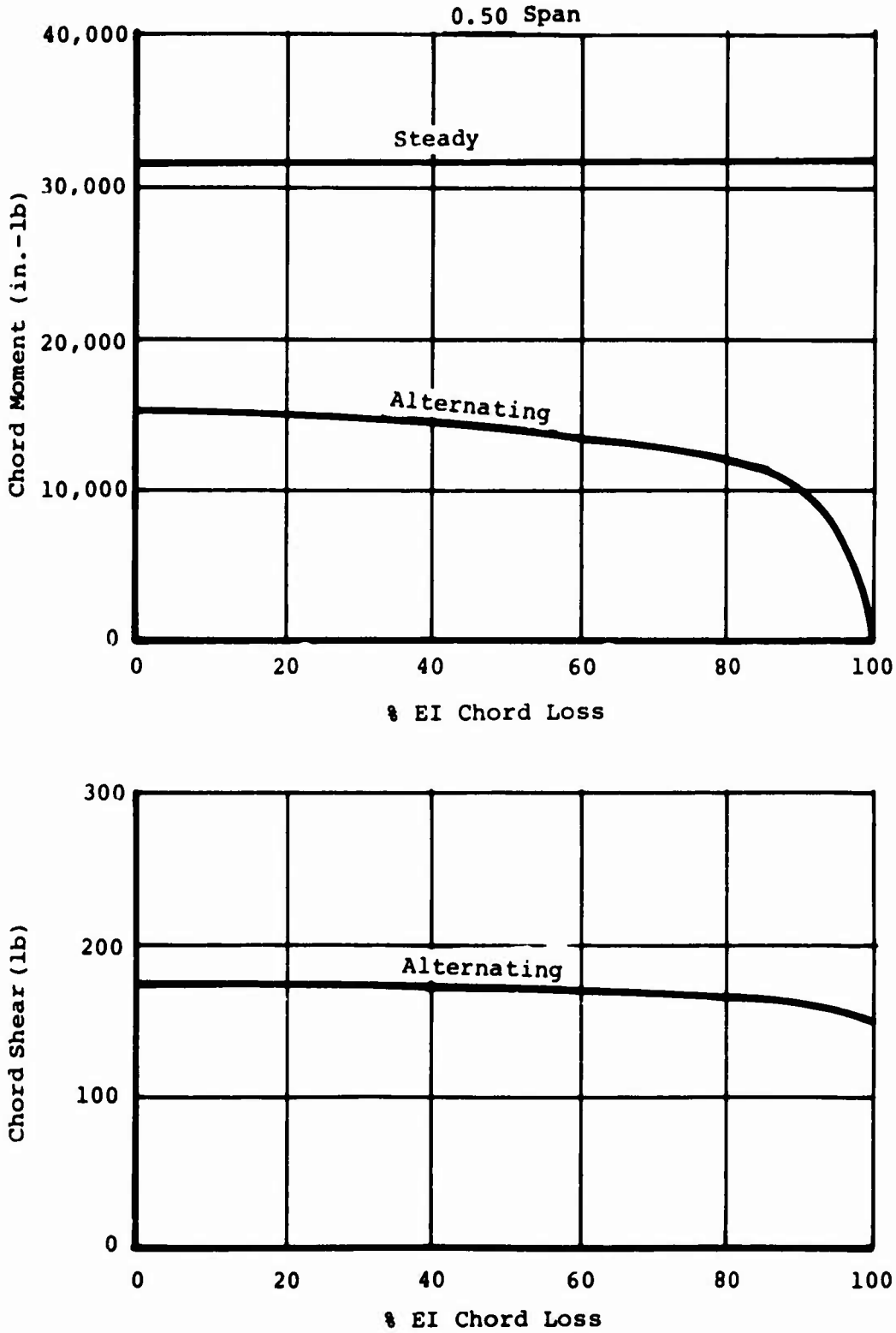

Figure 37. Variation of Moments and Shears With Loss of Chordwise Stiffness.

This load dropoff was due to a reduction of axial stiffness at the damaged area. The BRL blade loading rig incorporates a hydraulic accumulator, intended to compensate for such stiffness changes. However, this feature was not functioning at the time of the test. Therefore, the post-impact load was then gradually increased to within 100 pounds of the original 93,000 pounds tension, when a failure occurred. This was evidenced by sounds of breaking from the blade and by a dropoff in the load reading. Further actuation of the loading cylinder failed to increase the load and continued to separate the blade. The mode of failure was not the tension/bending failure at the damage point which had been anticipated. Instead, the failure mode was interlaminar shear in which the remaining unidirectional fiberglass at the damage point held and pulled out these extended fibers from one side of the test section (Figure 38).

In reviewing the results of that test, it was decided that in spite of precautions, the loading could have been unnecessarily severe. The reason is that, in a flying blade, that portion of the damage area strain caused by bending would be alleviated due to the reduction in bending stiffness of the blade (Figures 36 and 37). In the test configuration, the bending stresses were simulated by higher tension loads which were not alleviated by reduced bending stiffness. Additionally, the neutral axes were displaced due to the short coupling between pins of the test rig which caused additional bending stresses.

To help prevent the separation of the other blade sections due to improper overload, it was decided to shoot the Design 3 section while loaded only with a tension equal to centrifugal force and not to simulate bending other than that which naturally would occur due to the resulting shift in neutral axes.

Test of Design 3

In testing Design 3 (Figure 28), a tension load of 57,000 pounds to simulate centrifugal force only was applied with no offset from the neutral axes. This load was also based on an L-01 program which used actual blade test section weight (Figures 18 and 19). The section was shot after which the load dropped to 44,000 pounds. The load was restroed to 57,000 pounds and the blade held.

Test of Design 6A

Lastly, Design 6A (Figure 29) was tested. The centrifugal force for this design was 69,300 pounds. This load was also based on an L-01 program which used actual blade test section weight (Figures 20 and 21). After ballistic impact, the load dropped from 69,300 pounds to 32,500 pounds. Continued

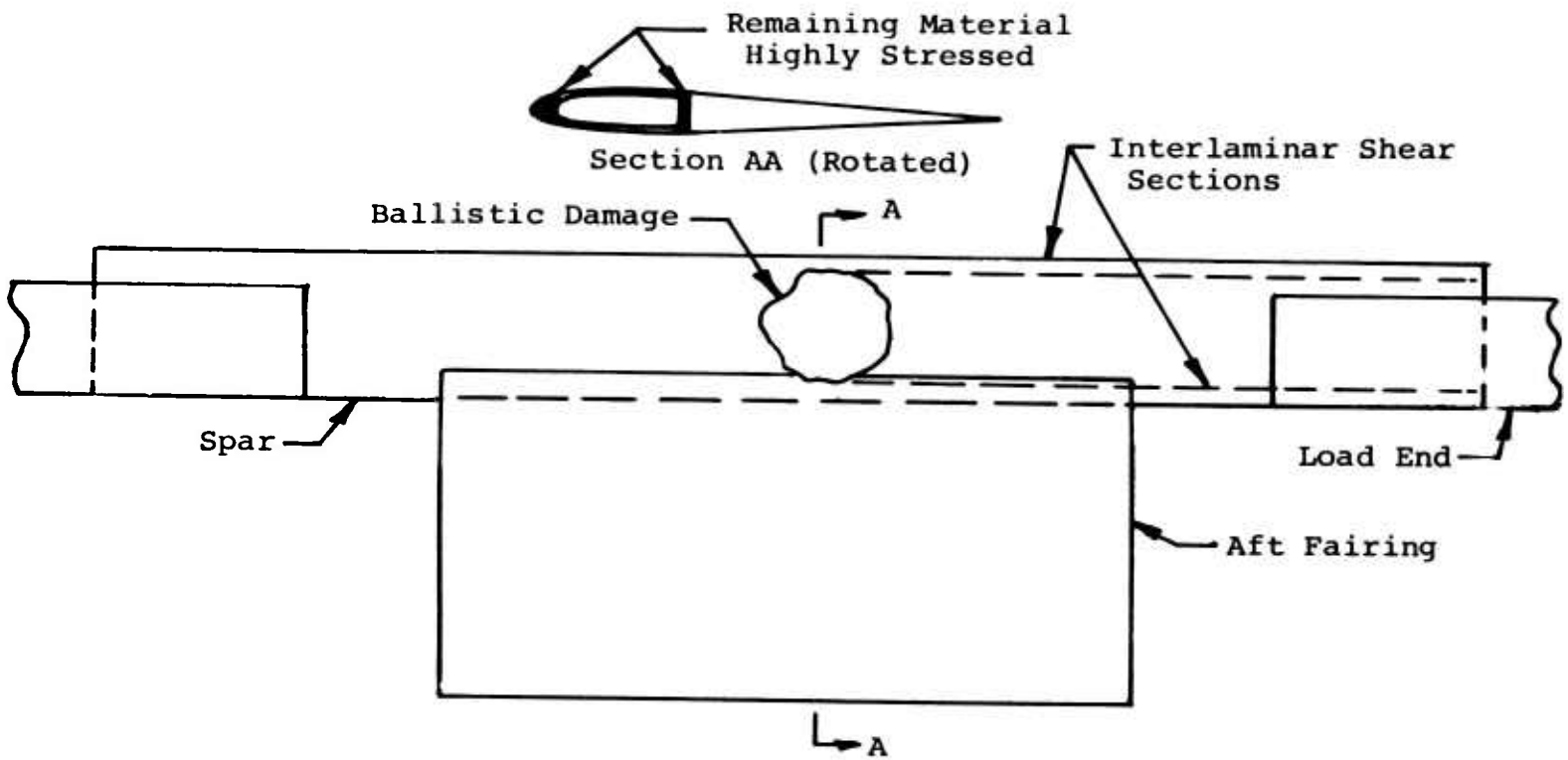

Figure 38. Interlaminar Shear Failure.

actuation of the hydraulic cylinder failed to increase this load, and a further dropoff was experienced along with the sounds of blade failure. The failure mode in this test was also interlaminar shear. The heavy section of unidirectional fiberglass in the nose pulled out of the blade section on one side of the damage area. As previously noted, this heavy structural section is connected to the outer "D" spar only by one cure-bonded surface. Also, as was noted in the unloaded tests, this section separated from the "D" spar due to ballistic impact alone.

Net results of blade ballistic testing under load were: Designs 2 and 6A failed under static load; only Design 3 survived to permit fatigue test.

Reading of Test Loads

It may be questioned why strain gages were not used in these tests. Previous tests had shown that any strain gages located near the damage area were likely to be destroyed by the impact. If not destroyed, they would still be of no value unless their strain readings could be accurately related to the amount and location of residual load-carrying material. This could not be done with any degree of accuracy until after the section was cut through and examined. Thus, the only value of strain gaging would be to determine preimpact stresses. It was decided that the calibrated hydraulic pressure gage on the test rig would be sufficiently accurate for reading tension loads. Preimpact blade bending was eliminated by adjusting the retention pins to the blade neutral axes and checking the blade for straightness.

FATIGUE TESTS

The purpose of fatigue testing a damaged blade is to determine whether progressive failure will occur when it is subjected to the steady and alternating loads associated with the anticipated flight conditions. The ability of a blade to hold up under such loads for a number of cycles equal to or exceeding those experienced in making a forced landing or returning to base is convincing evidence that it would have done so in actual flight.

The fatigue testing of damaged blades in this program was limited to Design 3, Test 14, since the other two designs failed on impact as previously described. The Boeing blade fatigue test machine (Figure 39) imposes both tension and bending loads to the specimen. Torsional loads are not applied; however, basic analysis indicates that they are not important to fatigue life. The tensile load simulated blade centrifugal force at 50-percent span based on that of the

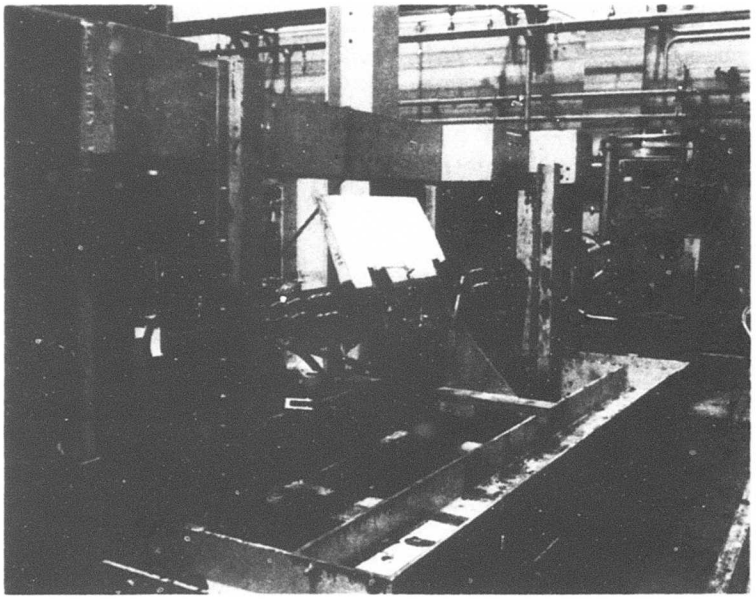

Fatigue Test Machine
With Damaged Blade

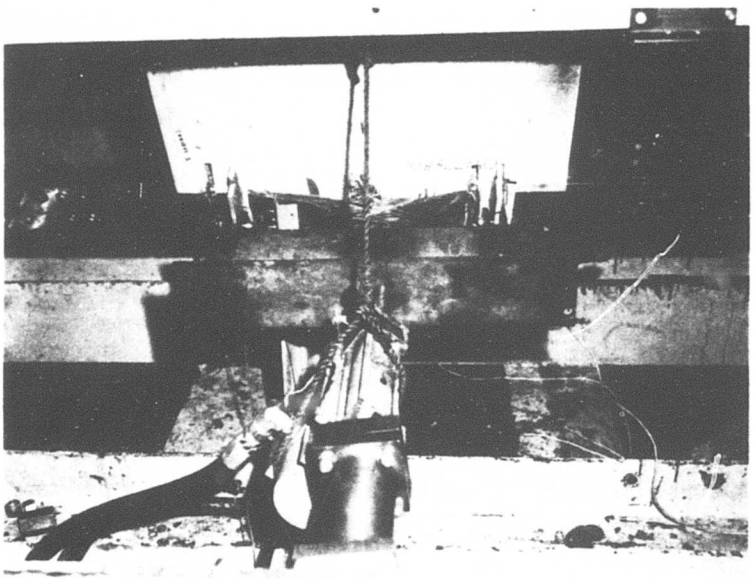

Actuator Drives Blades
Through Whiffletree (I Beam)

Figure 39. Blade Fatigue Test.

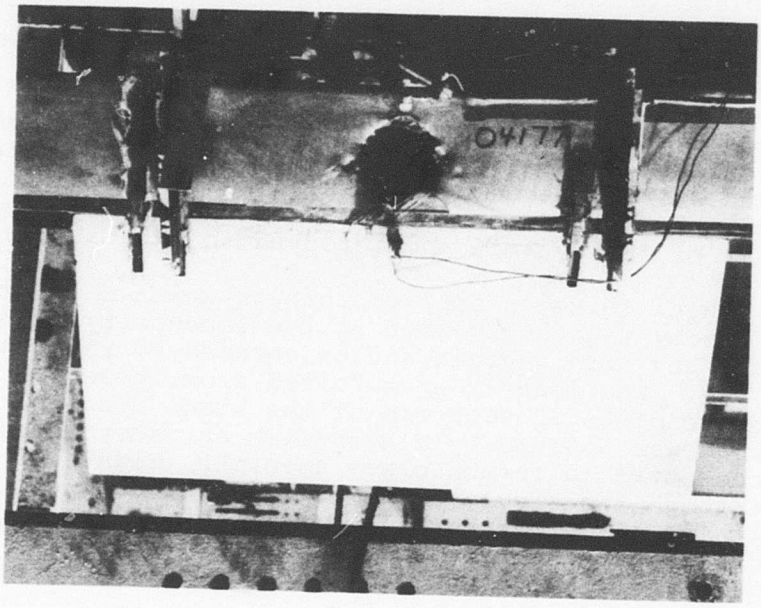

Damaged Blade in Fatigue Test
Machine (Side Away From Actuator)

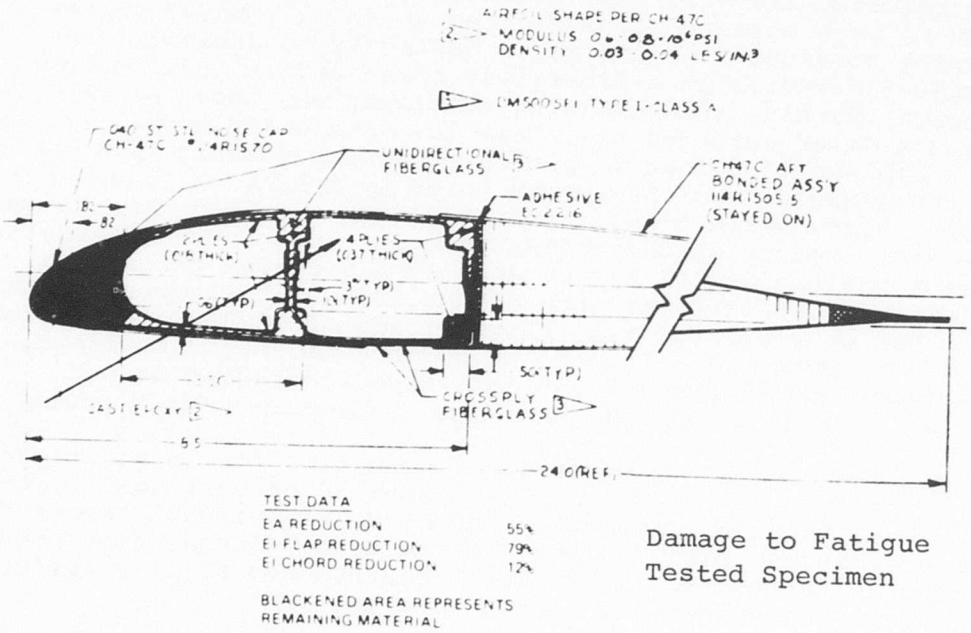

Damage to Fatigue
Tested Specimen

Figure 39(cont.)

baseline blade factored by the increased weight of Design 3. The bending loads simulated the steady and alternating flapwise and chordwise blade moments that would be experienced by the blade during flight.

The imposed test loads were based on the blade in-flight loads calculated by Boeing Computer Program L-02, including the effects due to the damaged area. This program yields the theoretical blade loads during the prescribed flight condition as a result of the dynamic and aerodynamic excitation.

The centrifugal force is applied through preloading compression springs by tightening nuts on the load-carrying bolts. These bolts are strain gaged and calibrated to read specimen tensile load. The load is transferred from these bolts into a steel flexure plate at each end of the blade section. The bending load was applied by a hydraulic actuator through a whiffletree attached to the blade specimen (Figure 39) and was reacted through the single plane flexures at each end of the specimen. The blade can be tilted relative to these flexures in order to adjust the ratio of flapwise-to-chordwise bending moment. The whiffletree applied loads unequally to each side of the damage point to provide the in-flight simulation of shear and moments across the damaged section. The NASTRAN computer program was used to establish the whiffletree kinematics.

The required flapwise and chordwise moments at the damaged section were obtained from Figures 36 and 37, based on remaining stiffness. Since it is difficult to estimate the residual material in a fiberglass blade before it is sawcut through the hit, the remaining stiffness was based on the previous similar unloaded hit, Test 10. The whiffletree arrangement applied side load to generate bending moment. Test moment at the damaged section was monitored by measuring blade deflection. Blade deflections associated with required moments were predetermined using the NASTRAN computer program. Alternating moment was applied at a frequency of 4.9 cycles per second, which is the 1/rev frequency of the assumed helicopter. The test ran at simulated V_{max} flight loads of 10,000 ±10,000 inch-pounds flapwise moment (0.53 ±0.53 inch midspan flapwise deflection) and 15,000 ±15,000 inch-pound chordwise moment (0.04 ±0.04 inch midspan chordwise deflection) for 8 hours.

It was then run at 1.50g maneuver condition for an additional 6 minutes (V_{max} moments were increased 50 percent to simulate the 1.50g maneuver moments). The blade was visually monitored for progressive damage either in the tension/bending or interlaminar shear modes. No failure occurred and no propagation of damage was discernible during the test.

ANALYSIS OF DAMAGE

The analysis was done on each hit by measuring the amount, type, and location of residual material and analyzing for the following survivability parameters:

- Residual strength to prevent separation
- Remaining fatigue life
- Possibility of flutter
- Predicted blade out-of-track

Figures 40 to 69 illustrate the damage incurred by each of the 15 hits. They show:

- Photographs of entrance and exit holes
- Cross-sectional drawings illustrating residual material after each hit
- Percentage of strength and stiffness reduction
- Whether aft section remained on spar

Residual Strength To Prevent Separation

Prior Tests of the Baseline Blade - Prior to the start of this investigation, the baseline blade, Figures 6 and 7, had been ballistically tested against nonexplosive rounds up to 23mm API and explosive rounds of 20mm HEI and 23mm HEI. The hits by nonexplosive rounds were all survivable by a wide margin. The reductions in strength after hits by 20mm HEI and 23mm HEI are shown in Figure 70. These reduced strengths are calculated based on tension/bending stresses at the impact point. The upper shaded area represents probable spar separation, while its lower limit indicates sufficient strength remaining to permit approximately 30 minutes of flight at V_{max}.

Hits numbers B1 to B5 are in the oval swan neck section and show a high degree of survivability to the 20mm HEI rounds used. Hits on the 50-percent span section ranged between 15- and 45-percent reduction in strength for the 20mm HEI. Of the three 23mm HEI hits, two were survivable while the highly improbable hit through the back of the blade which detonated in the spar (Number B19) was unsurvivable. At the 87 1/2-percent span position, with this 9-percent airfoil, hit numbers B15 (20mm HEI) and B22 (23mm HEI) were both survivable. Hit number B23, again the improbable aft hit into the spar, was with 23mm HEI and was unsurvivable.

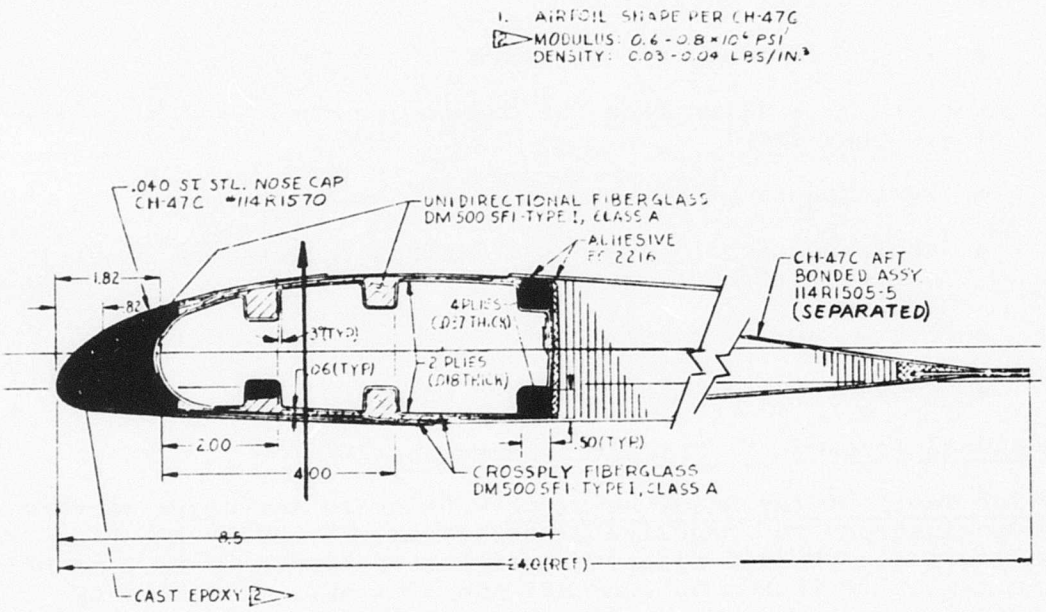

Figure 40. Damage Due to Hit Number 021474P1 - Test 1, Design 2.

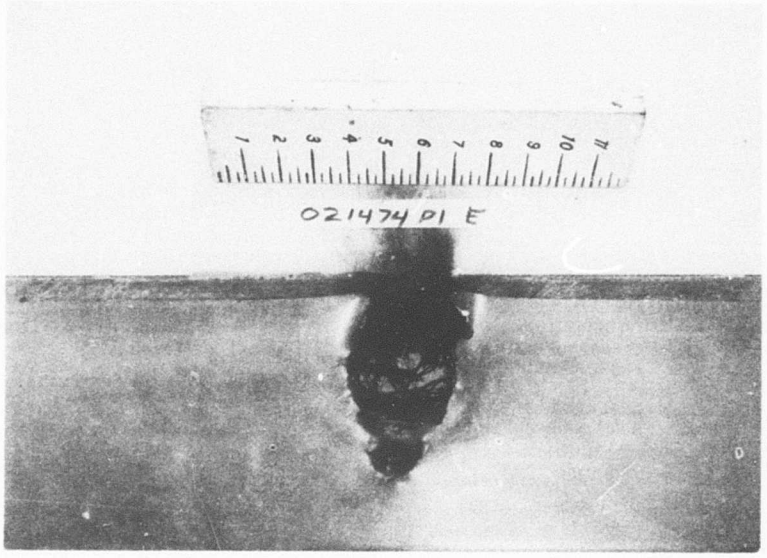

Entrance

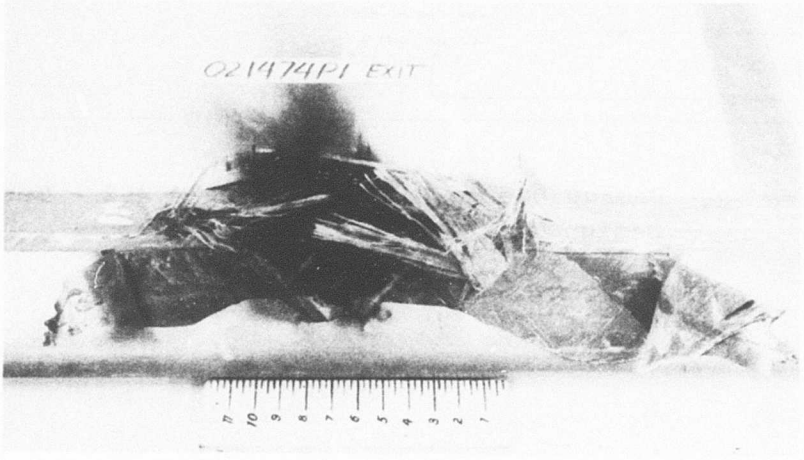

Exit

Figure 41. Photographs of Hit Number 021474P1 - Test 1.

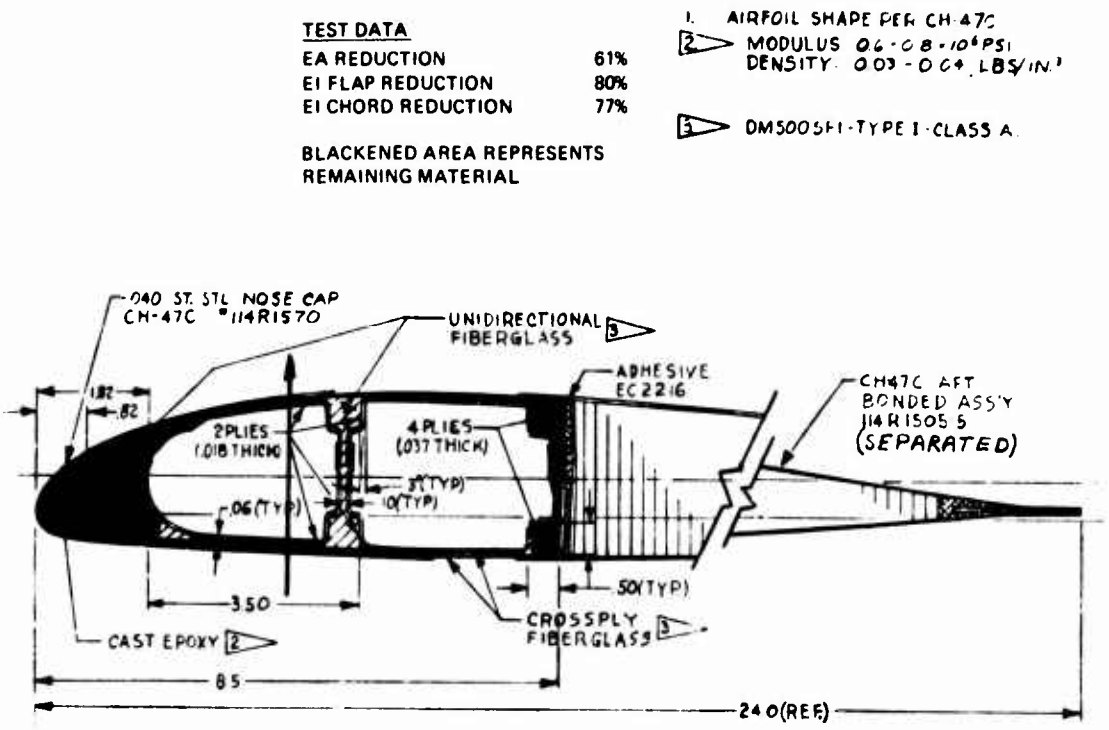

Figure 42. Damage Due to Hit Number 021474P2 - Test 2, Design 3.

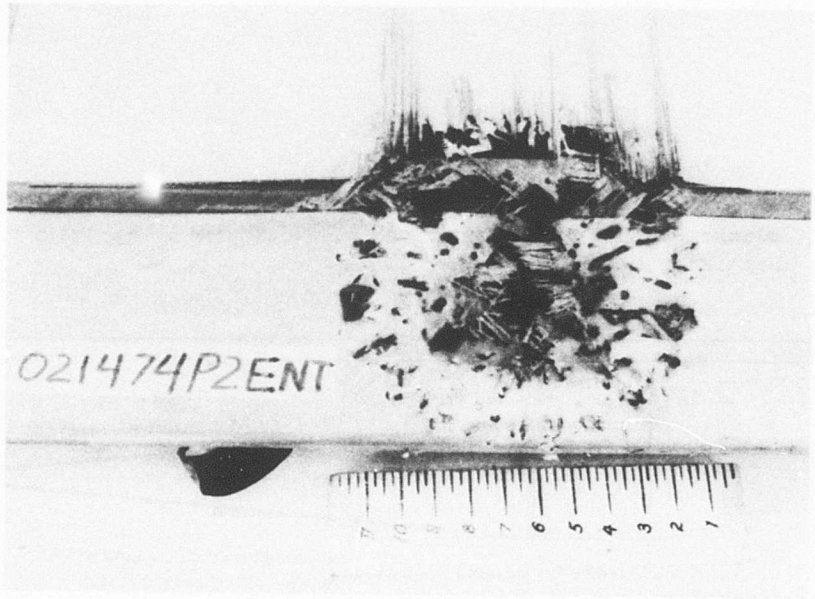

Entrance

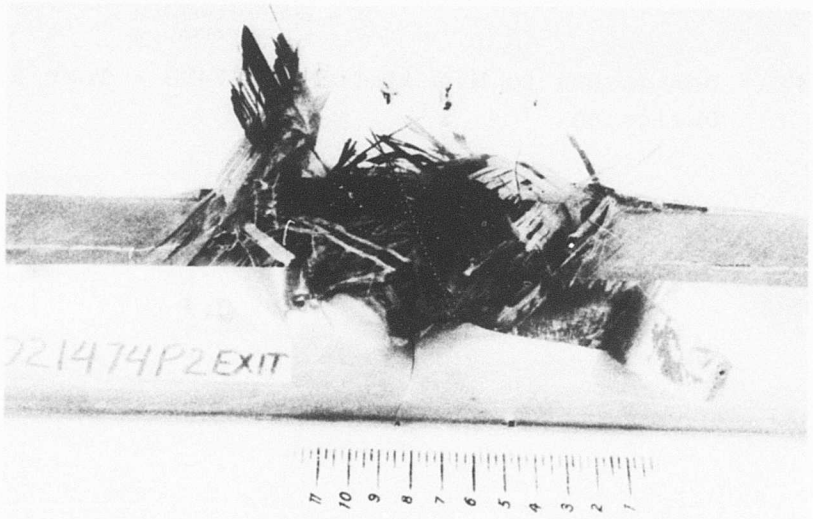

Exit

Figure 43. Photographs of Hit Number 021474P2 - Test 2.

Blackened Area Represents
Remaining Material

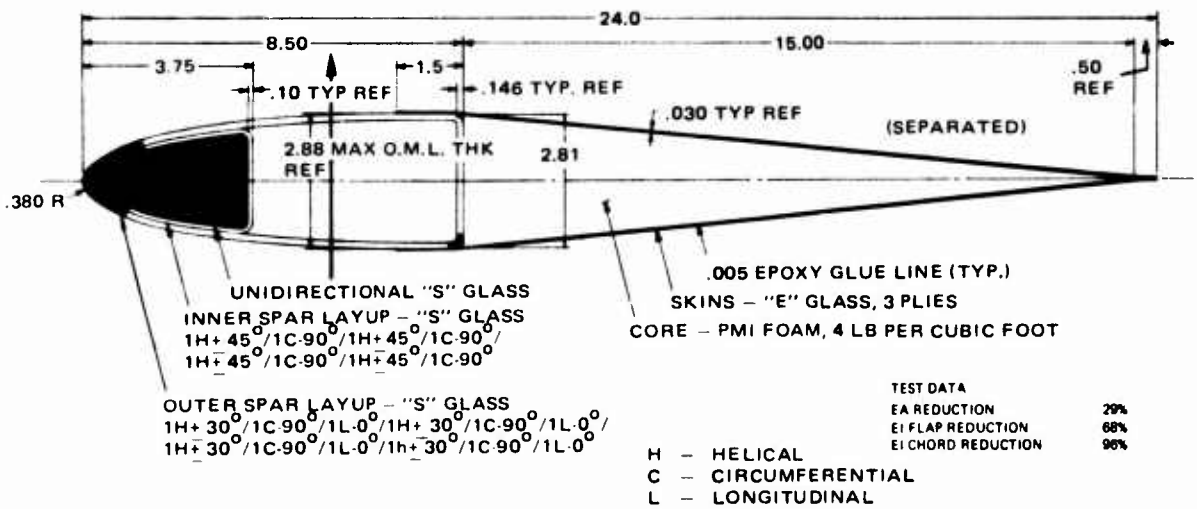

Figure 44. Damage Due to Hit Number 021474P3 - Test 3, Design 6A.

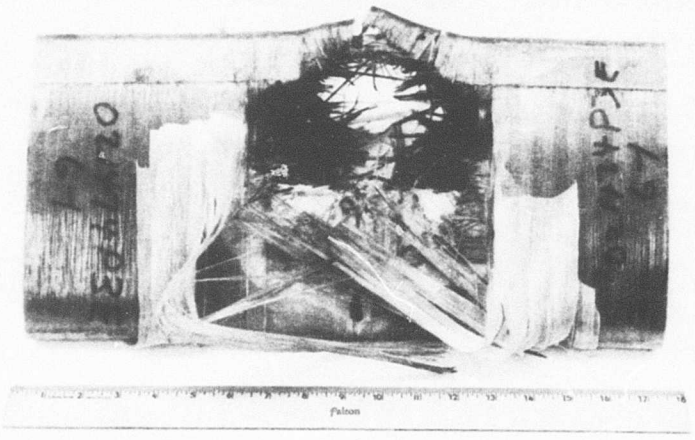

Entrance

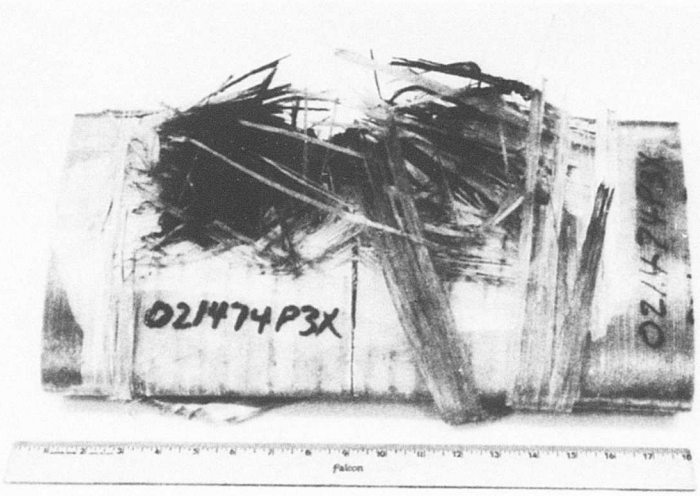

Exit

Figure 45. Photographs of Hit Number 021474P3 - Test 3 (Photographed After Cutting Section).

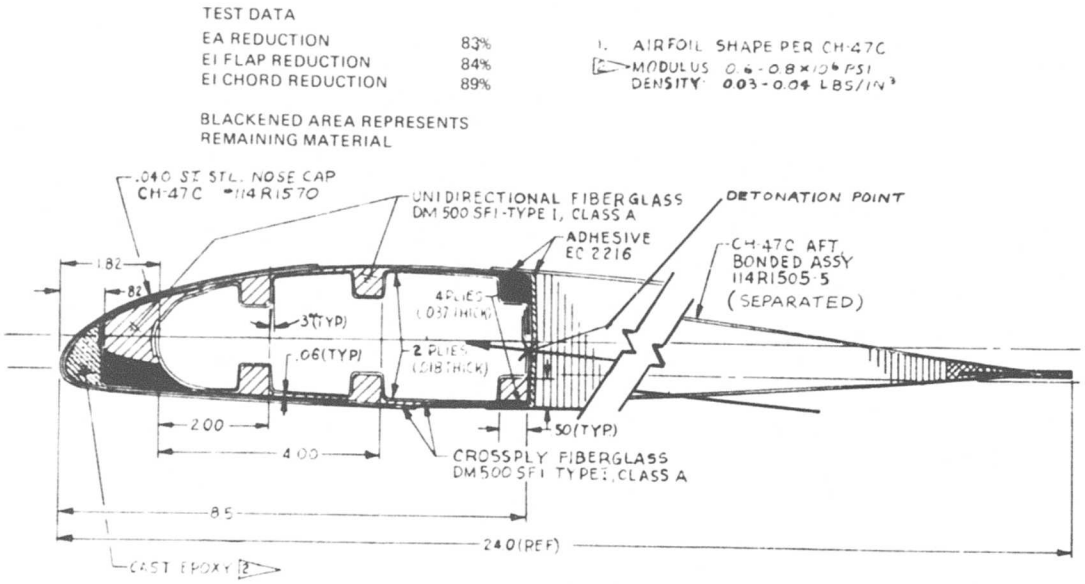

Figure 46. Damage Due to Hit Number 021474P4 - Test 4, Design 2 .

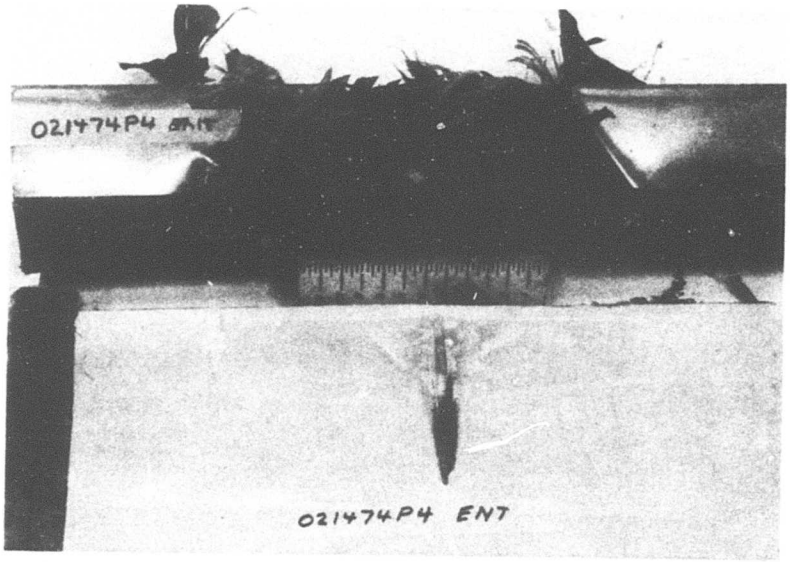

Bottom View

Figure 47. Photograph of Hit Number 021474P4 - Test 4.

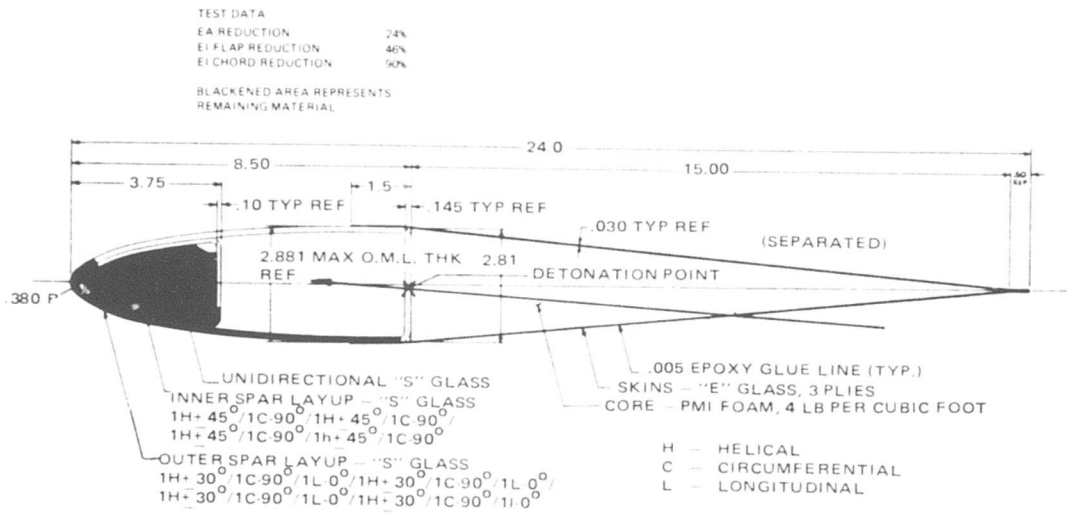

Figure 48. Damage Due to Hit Number 021474P5 - Test 5, Design 6A.

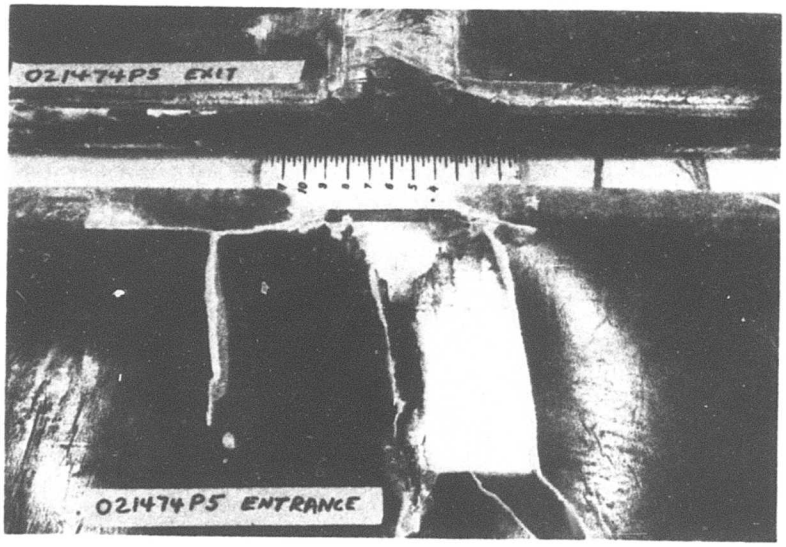

Bottom View

Figure 49. Photograph of Hit Number 021474P5 - Test 5.

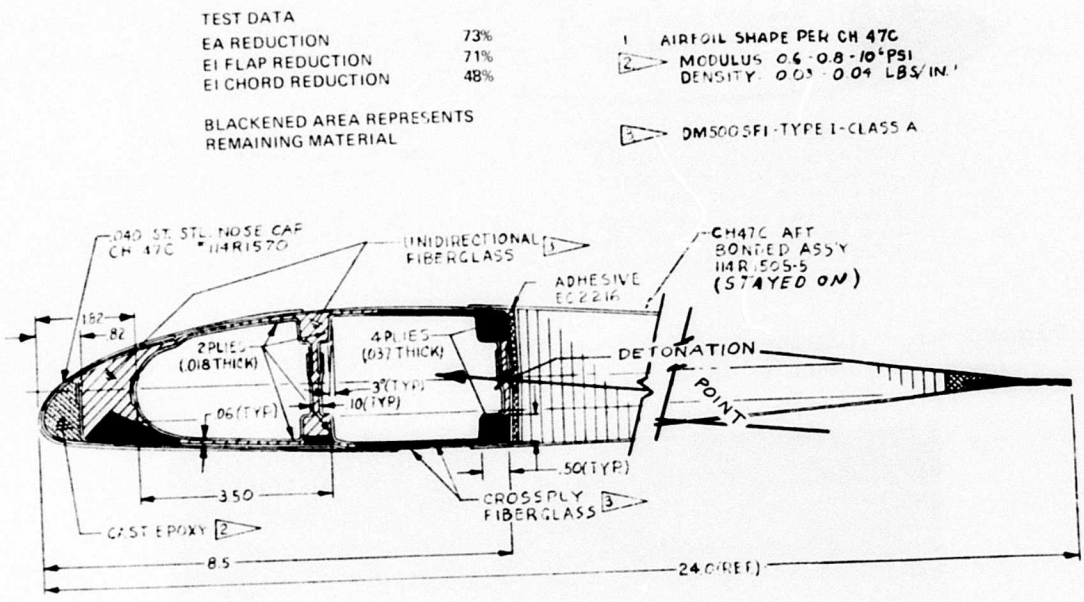

Figure 50. Damage Due to Hit Number 021474P6 - Test 6, Design 3.

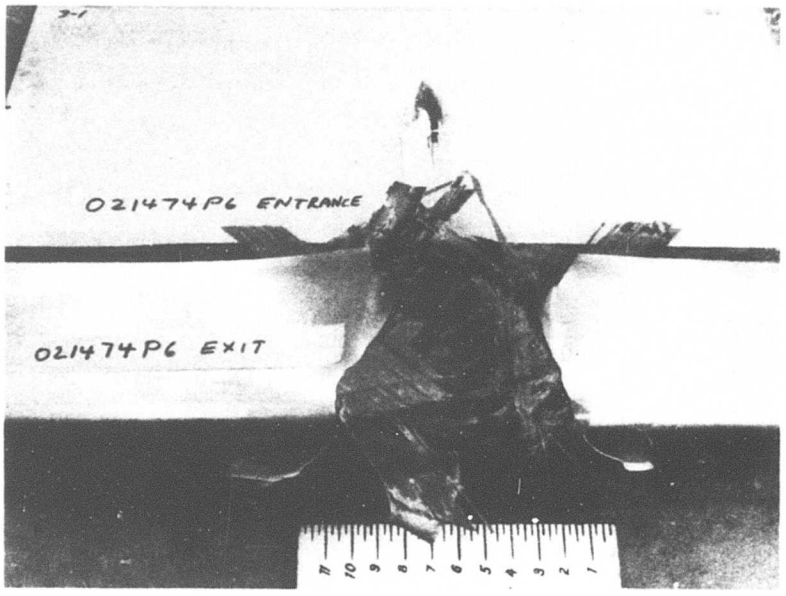

Bottom View

Figure 51. Photograph of Hit Number 021474P6 - Test 6.

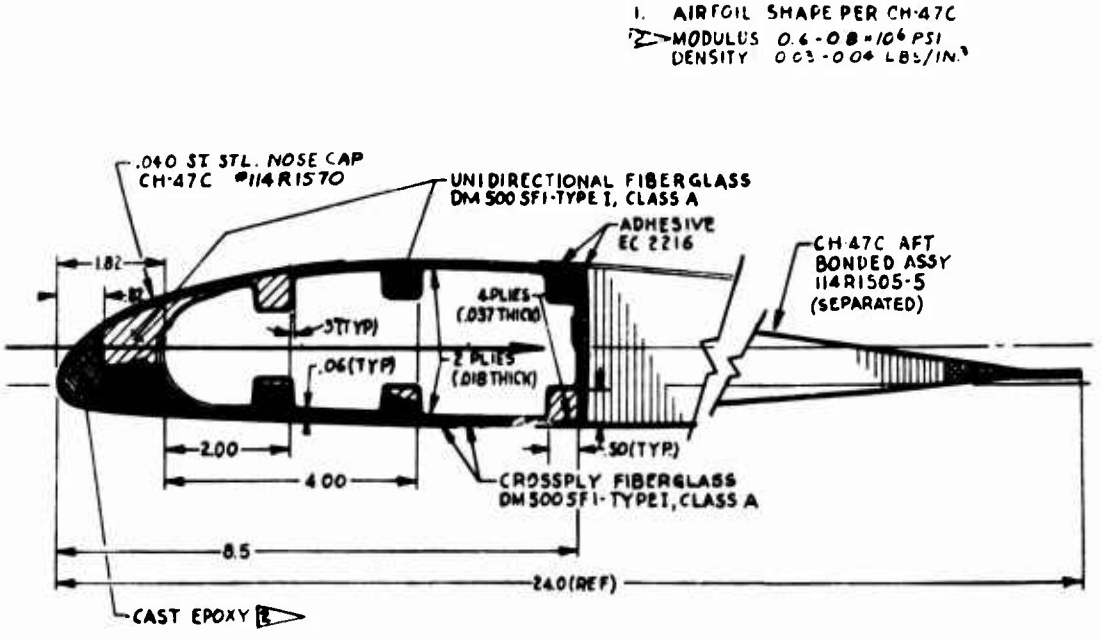

TEST DATA

EA REDUCTION	69%
EI FLAP REDUCTION	76%
EI CHORD REDUCTION	88%

BLACKENED AREA REPRESENTS
REMAINING MATERIAL

Figure 52. Damage Due to Hit Number 021474P7 - Test 7 Design 2.

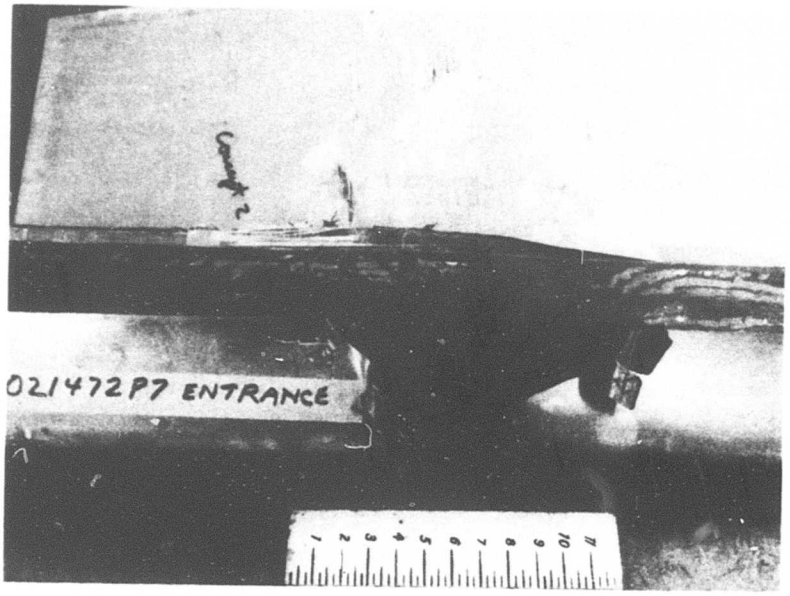

Top View

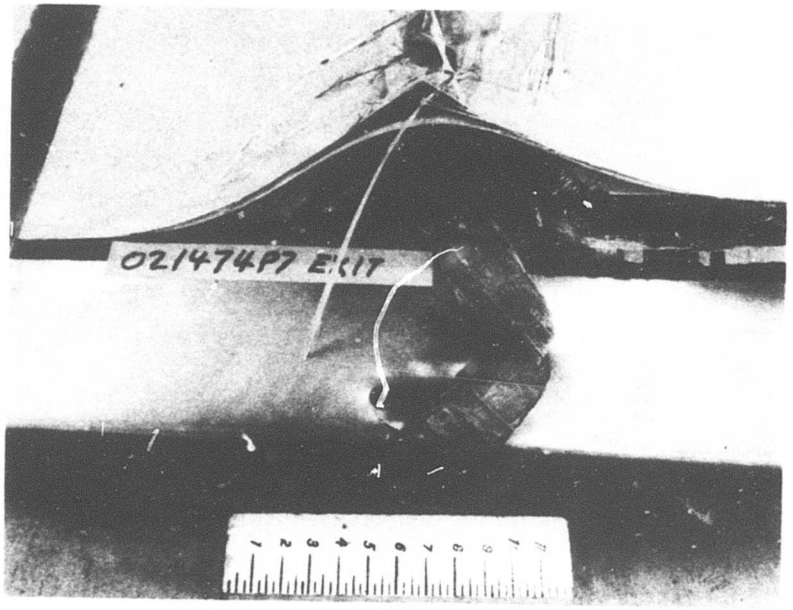

Bottom View

Figure 53. Photographs of Hit Number 021474P7 - Test 7.

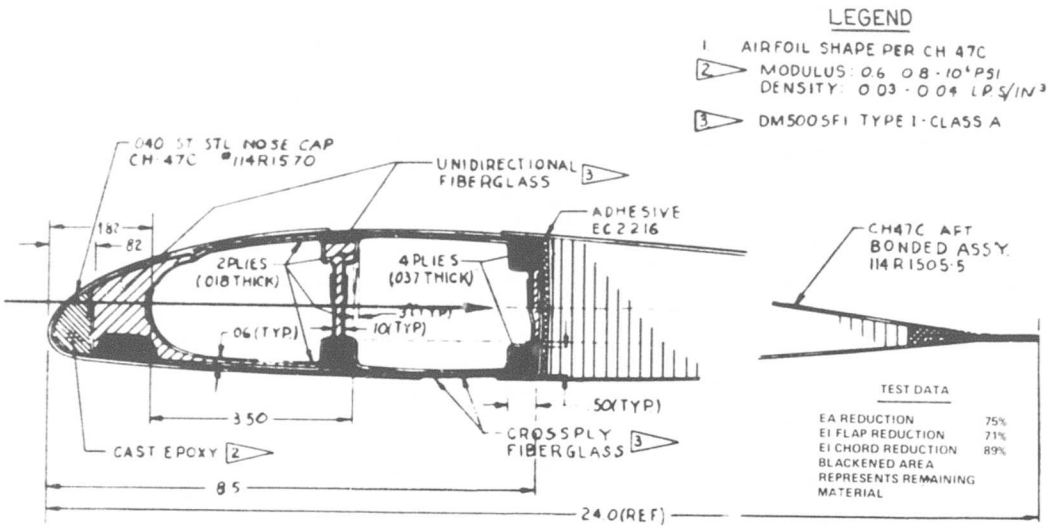

Figure 54. Damage Due to Hit Number 021474P8 - Test 8, Design 3.

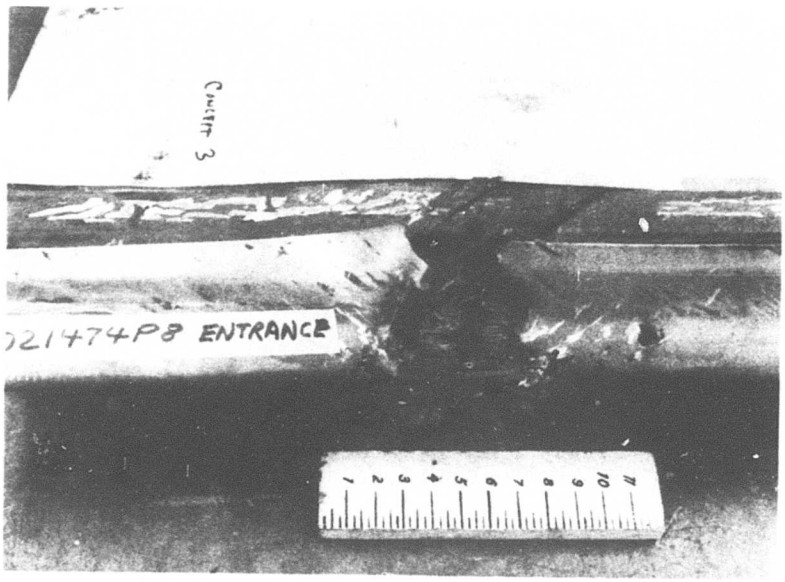

Top View

Figure 55. Photograph of Hit Number 021474P8 - Test 8.

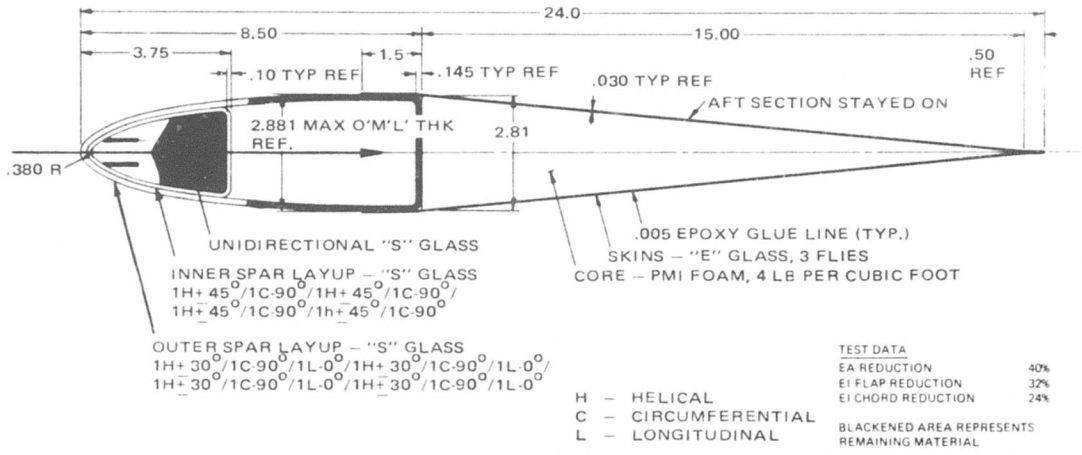

Figure 56. Damage Due to Hit Number 021474P9 - Test 9, Design 6A.

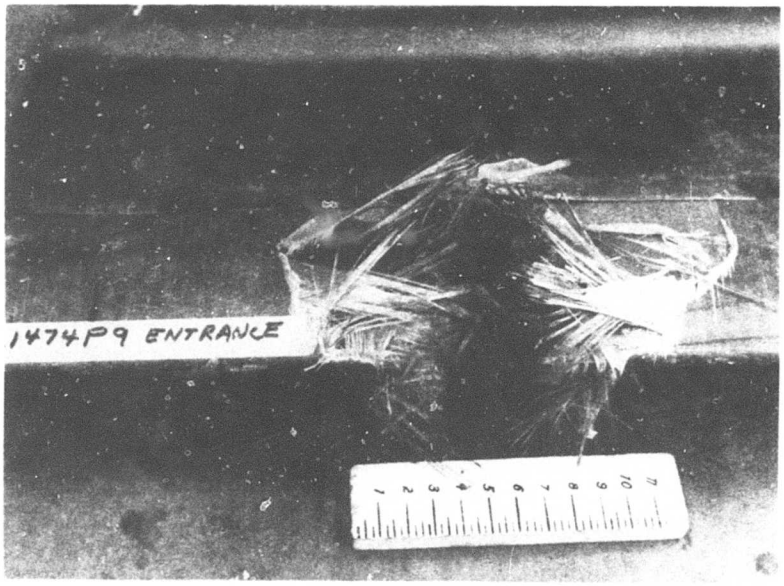

Top View

Figure 57. Photograph of Hit Number 021474P9 - Test 9.

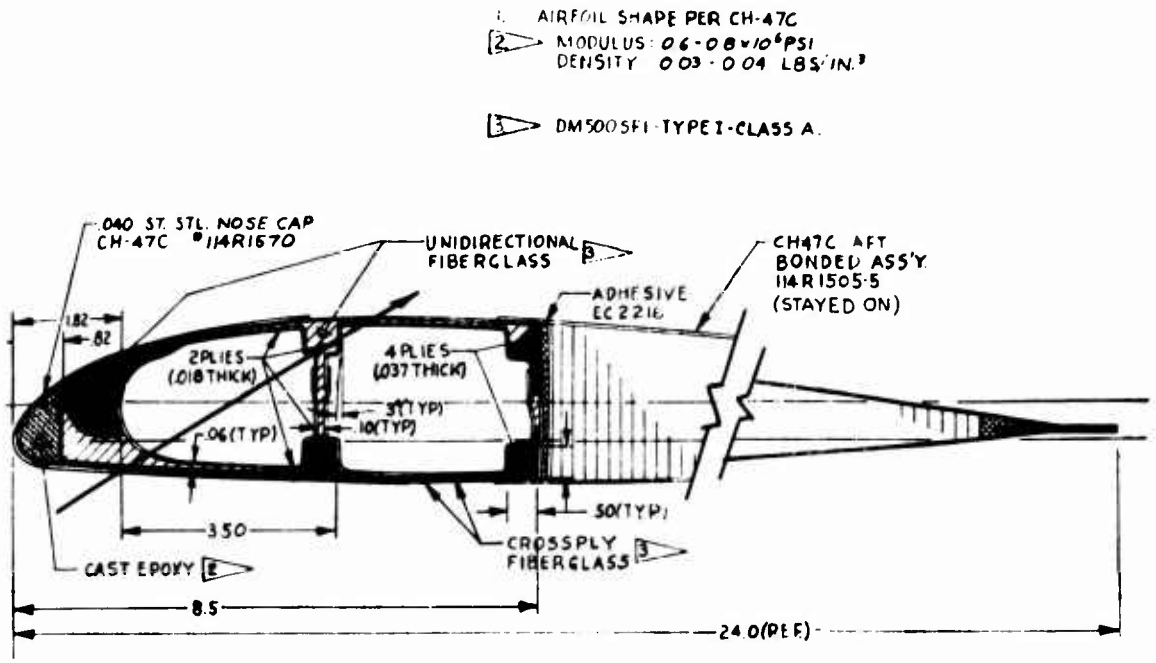

TEST DATA	
EA REDUCTION	68%
EI FLAP REDUCTION	77%
EI CHORD REDUCTION	35%

BLACKENED AREA REPRESENTS REMAINING MATERIAL

Figure 58. Damage Due to Hit Number 021574P1 - Test 10, Design 3.

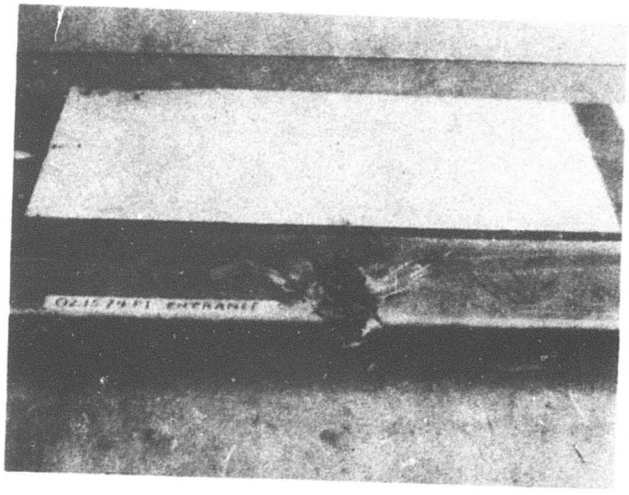

Entrance

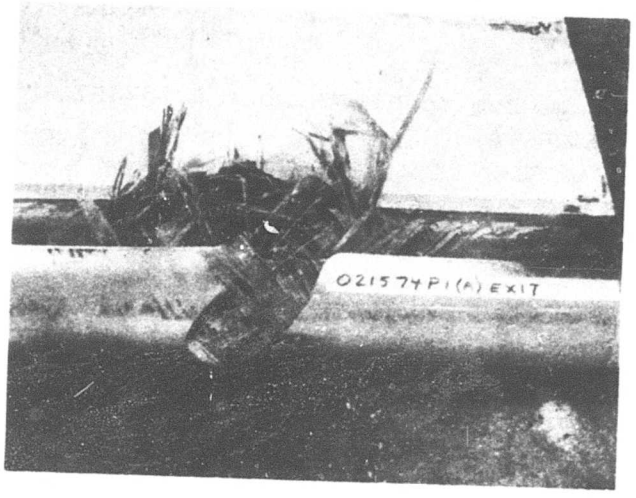

Exit

Figure 59. Photographs of Hit Number 021574P1 - Test 10.

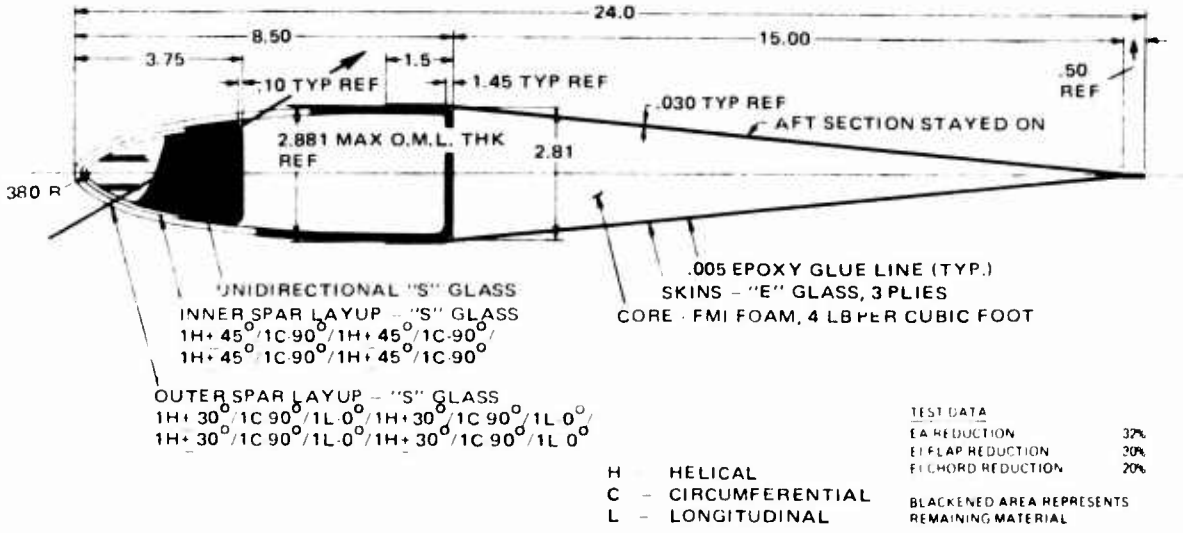

Figure 60. Damage Due to Hit Number 021574P2 - Test 11, Design 6A.

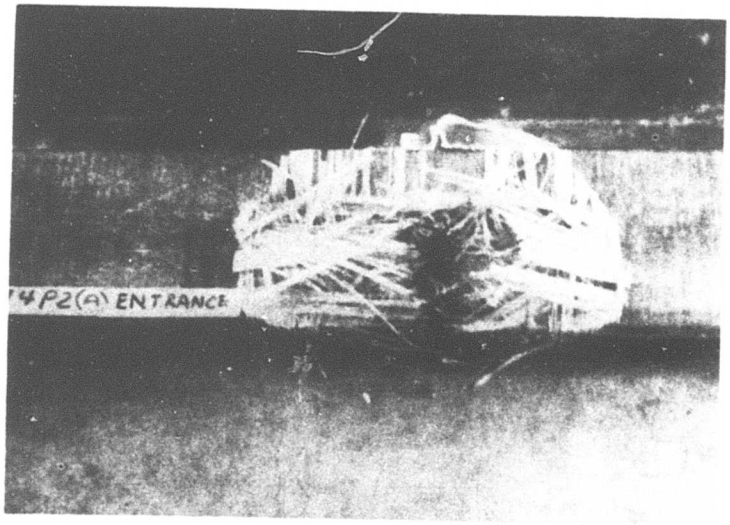

Entrance

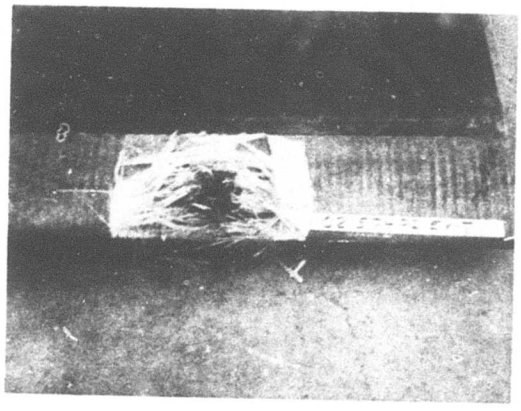

Exit

Figure 61. Photographs of Hit Number 021574P2 - Test 11.

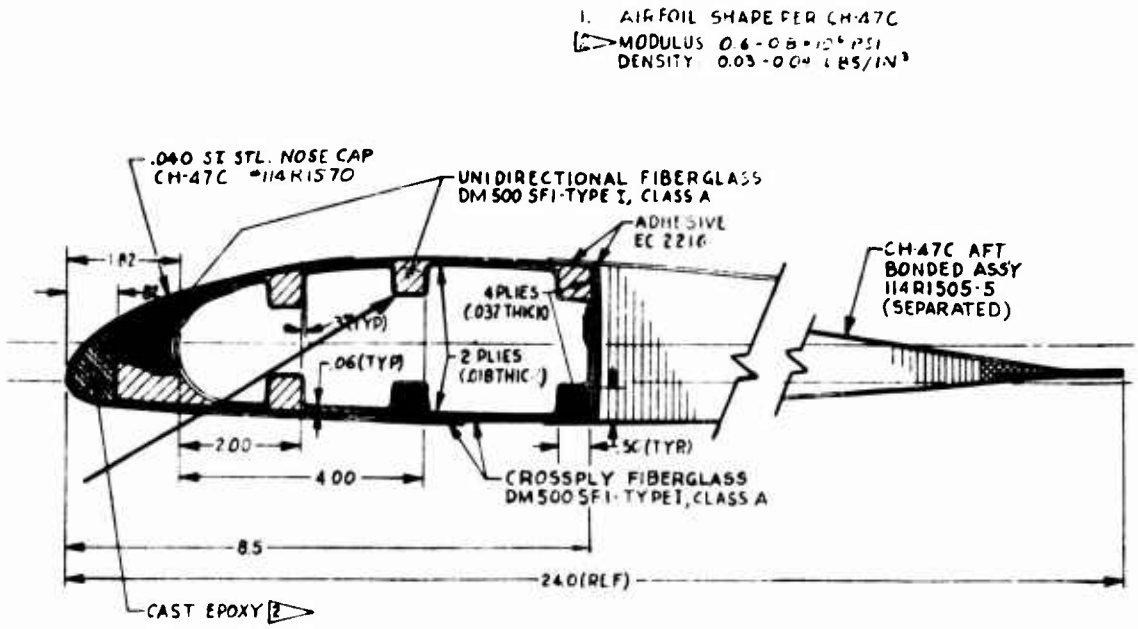

TEST DATA

EA REDUCTION	76%
EI FLAP REDUCTION	90%
EI CHORD REDUCTION	88%

BLACKENED AREA REPRESENTS
REMAINING MATERIAL

Figure 62. Damage Due to Hit Number 021574P3 - Test 12, Design 2.

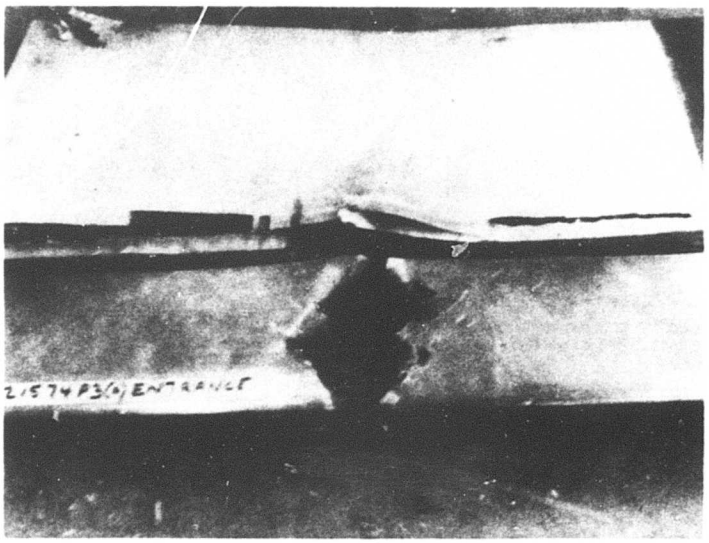

Entrance

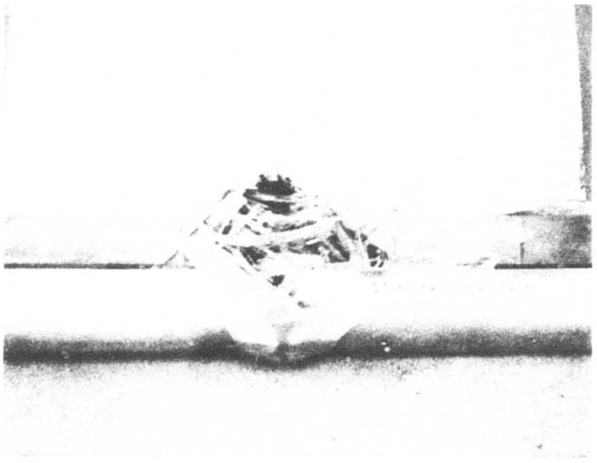

Exit

Figure 63. Photographs of Hit Number 021574P3 - Test 12.

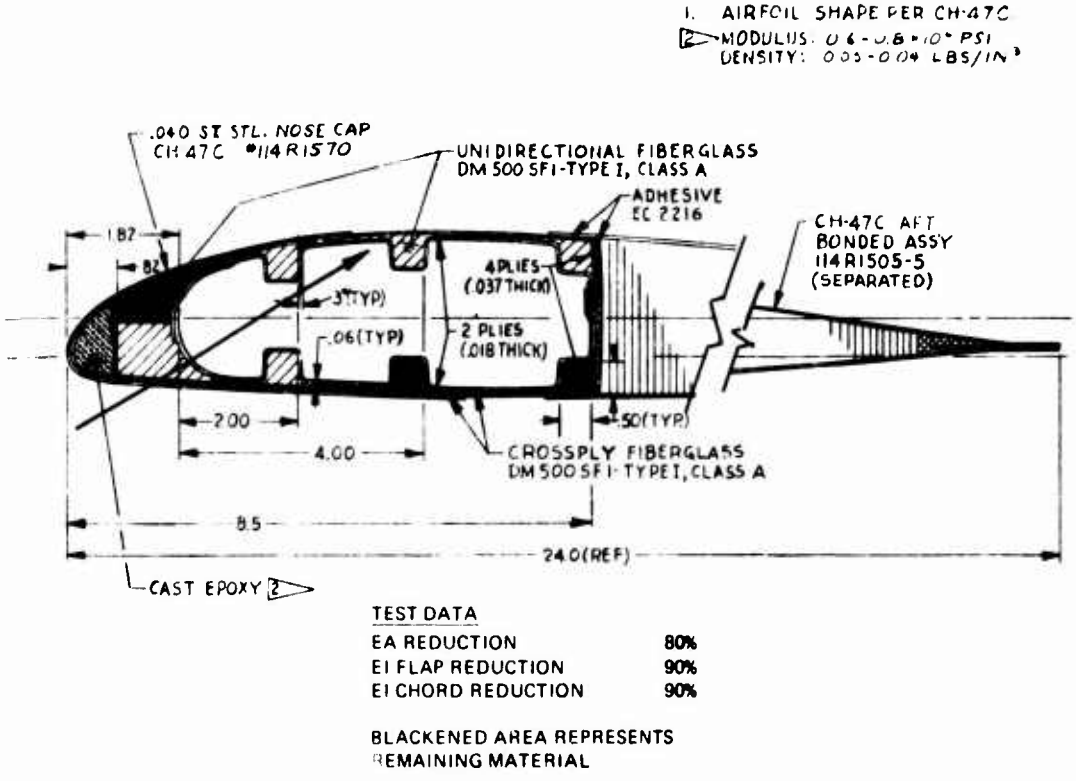

Figure 64. Damage Due to Hit Number 041074B1 - Test 13, Design 2.

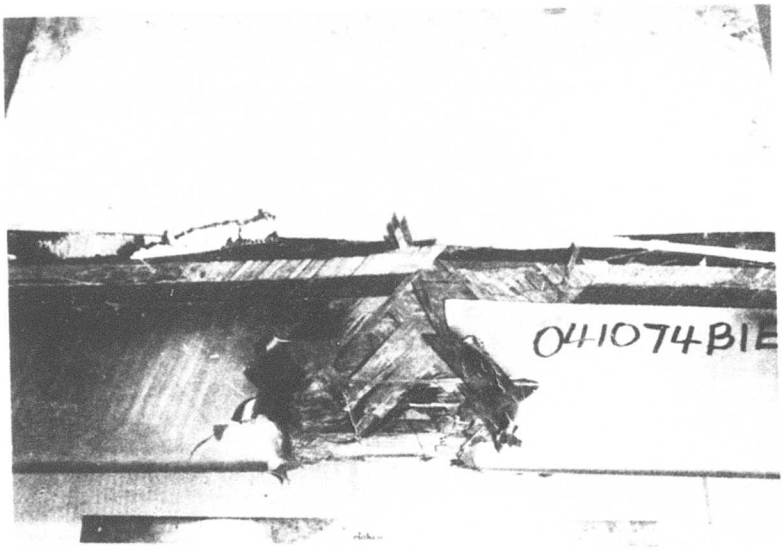

Entrance

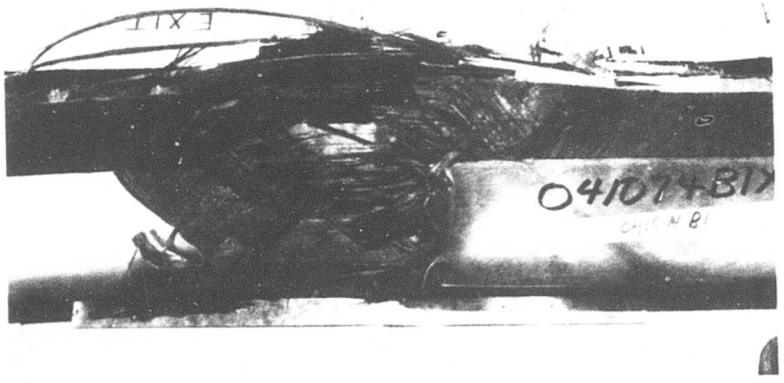

Exit

Figure 65. Photographs of Hit Number 041074B1 - Test 13.

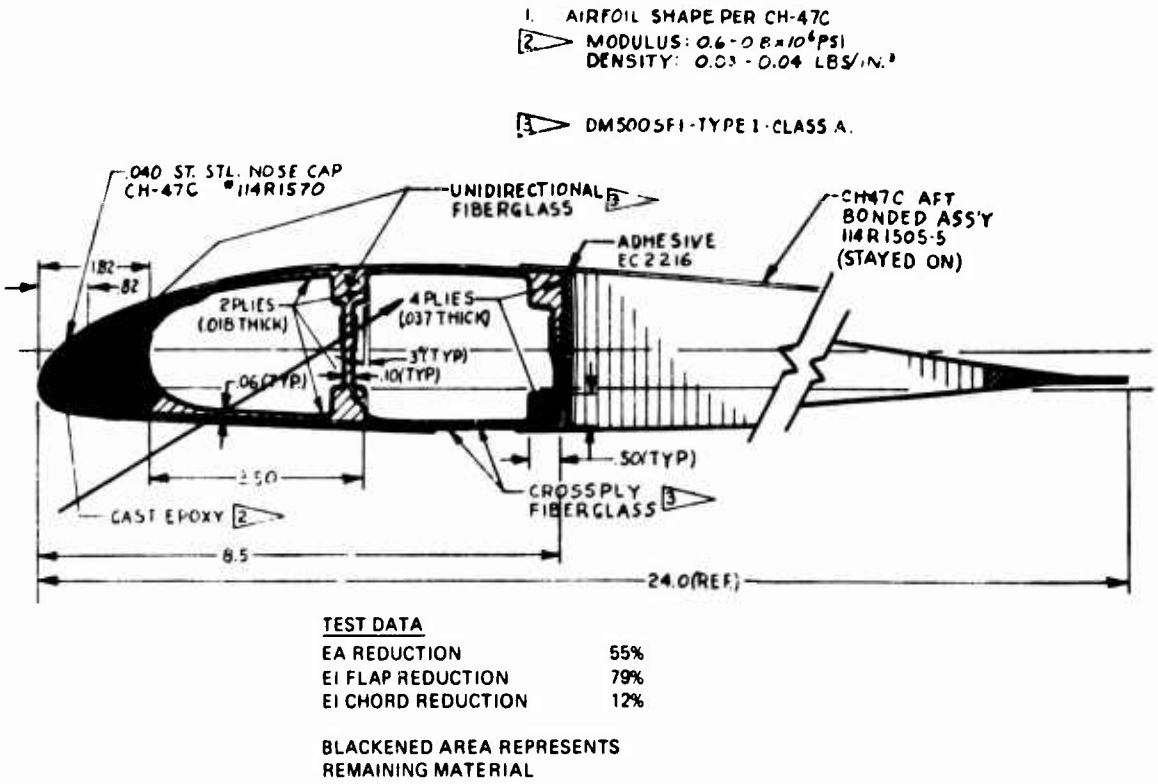

Figure 66. Damage Due to Hit Number 041774B1 - Test 14, Design 3.

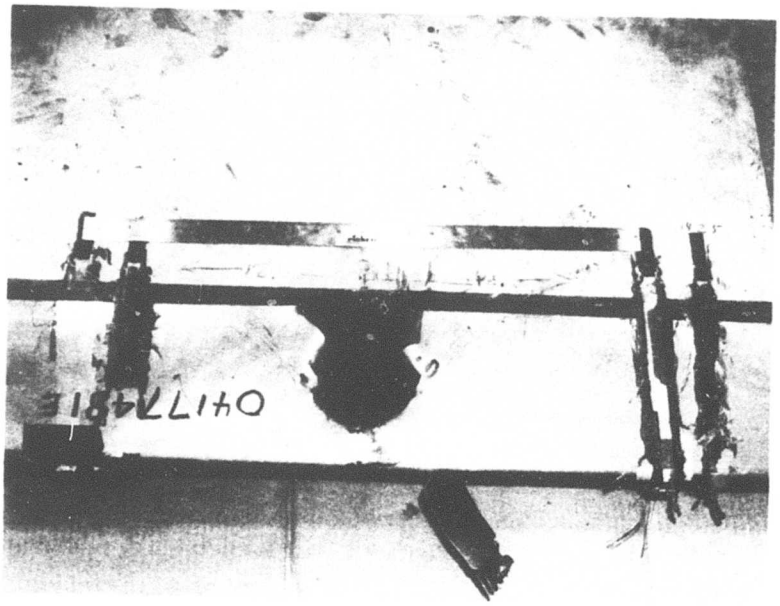

Entrance

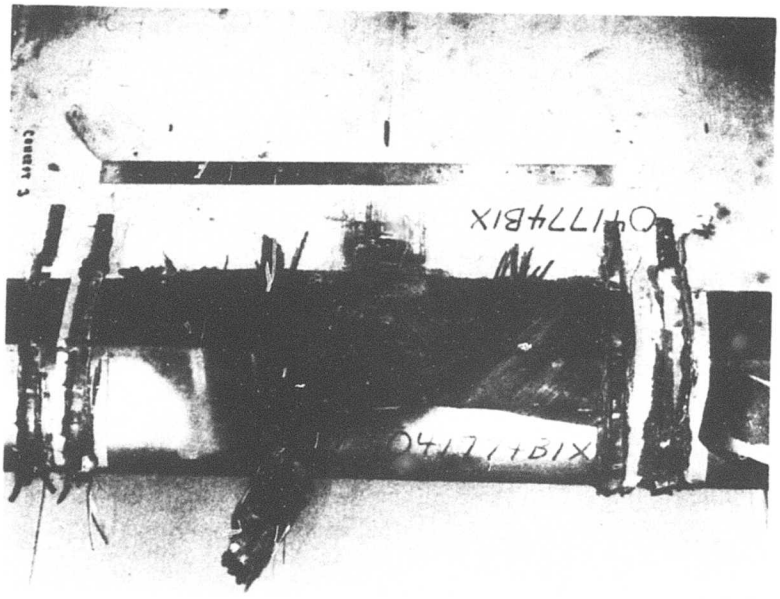

Exit

Figure 67. Photographs of Hit Number 041774B1 - Test 14.

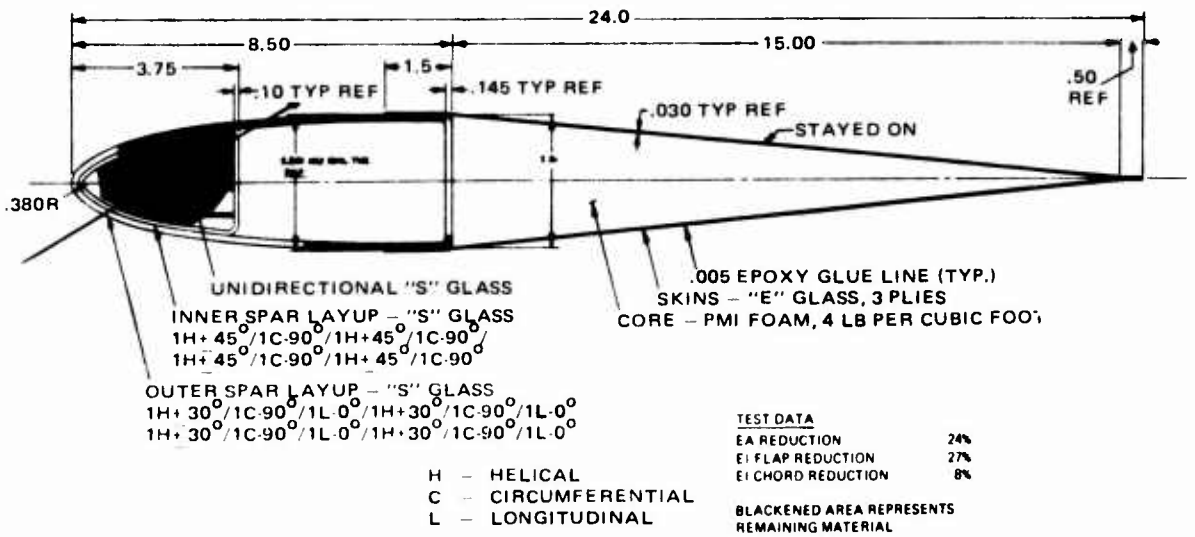

Figure 68. Damage Due to Hit Number 041774B2 - Test 15, Design 6A.

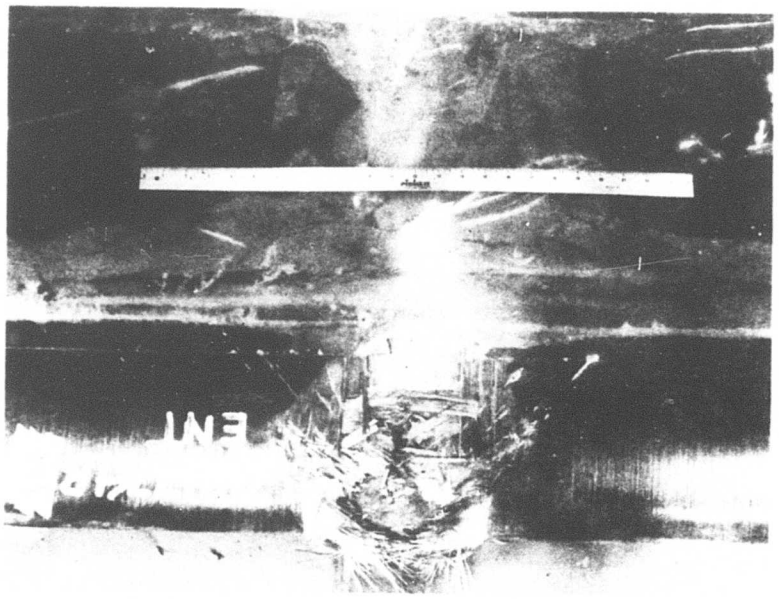

Entrance

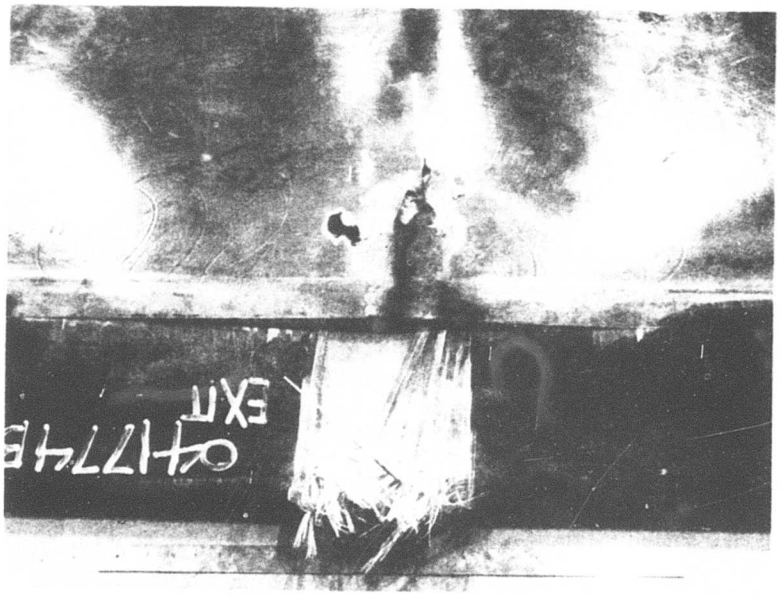

Exit

Figure 69. Photographs of Hit Number 041774B2 - Test 15.

Hits numbers B4, B6 and B15 were made with the blade under simulated static flight loads at V_{max} including centrifugal force, steady bending, and alternating bending. None of these blades failed on impact. The blade, which was used for hit number B15 and which had lost a calculated 48% of its strength, was also fatigue tested under simulated V_{max} flight conditions for the equivalent of 6 hours of flight plus 8 minutes of 1.56g maneuvering loads. No signs of progressive failure were observed during this test.

Comparison of Survivable Designs With Baseline - The tests made on the baseline blade at 50 percent of span were the most marginal of the three spanwise positions tested. They can now be compared with those made on the survivable designs. The difficulty in making such a comparison lies in the fact that most of the previous tests were of 20mm HEI while all the tests in this program were of 23mm HEI. It is helpful to recognize that where the blade section is thin enough for a 20mm HEI round to completely remove all material in the shrapnel cone, as in hit B15, the 23mm HEI, as in hit B22, does not generally do more damage. However, in stronger sections which partially defeat the 20mm HEI, as in hits at 12-1/2-percent span and 50-percent span, the 23mm HEI will be more damaging. The degree to which the 23mm HEI is more damaging varies with the blade construction and the hit angle; but, for hits at the 50-percent span, it may be roughly estimated at about 25 percent more reduction in residual strength.

Analysis of Survivable Design Tests - All of the 15 hits were analyzed for residual axial and bending strength, i.e., axial stiffness (EA), flapwise stiffness (EI_{flap}) and chordwise stiffness (EI_{chord}). Residual EA is the sum of the intact fiber areas multiplied by the respective moduli of elasticity and is one of the more important measures of blade strength to prevent separation. Residual flapwise and chordwise stiffness are calculated assuming that a full shear tie exists between all remaining material at the damaged section. A summary of these calculations is presented in Table 4. The results in terms of EA reduction are also plotted in Figures 71, 72, and 73.

The percentage reduction in EA varied considerably among blade designs. Design 6A had the least loss, Design 3 was next and Design 2 lost the most. None of the hits indicated the probability of immediate blade separation; however, several were marginal.

The degree of damage due to the different hit directions does not show any distinct pattern; nor is there any indication that blades shot under load incur more damage than those shot unloaded. Designs 3 and 6A actually had less damage in the loaded hits than in the same hit direction while unloaded.

TABLE 4. PERCENTAGE OF STIFFNESS LOSS DUE TO BALLISTIC DAMAGE

	Test No.	Axial Stiffness (EA) Loss (%)	Flapwise Stiffness (EI_{flap}) Loss (%)	Chordwise Stiffness (EI_{chord}) Loss (%)
Blade Design 2	1	66	83	83
	12	76	90	88
	4	83	84	89
	7	69	76	88
	13	80	90	90
Blade Design 3	10	68	77	35
	2	61	80	77
	6	73	71	48
	8	75	71	89
	14	55	79	12
Blade Design 6A	11	32	30	20
	3	29	68	96
	5	24	46	90
	9	40	32	24
	15	24	27	8

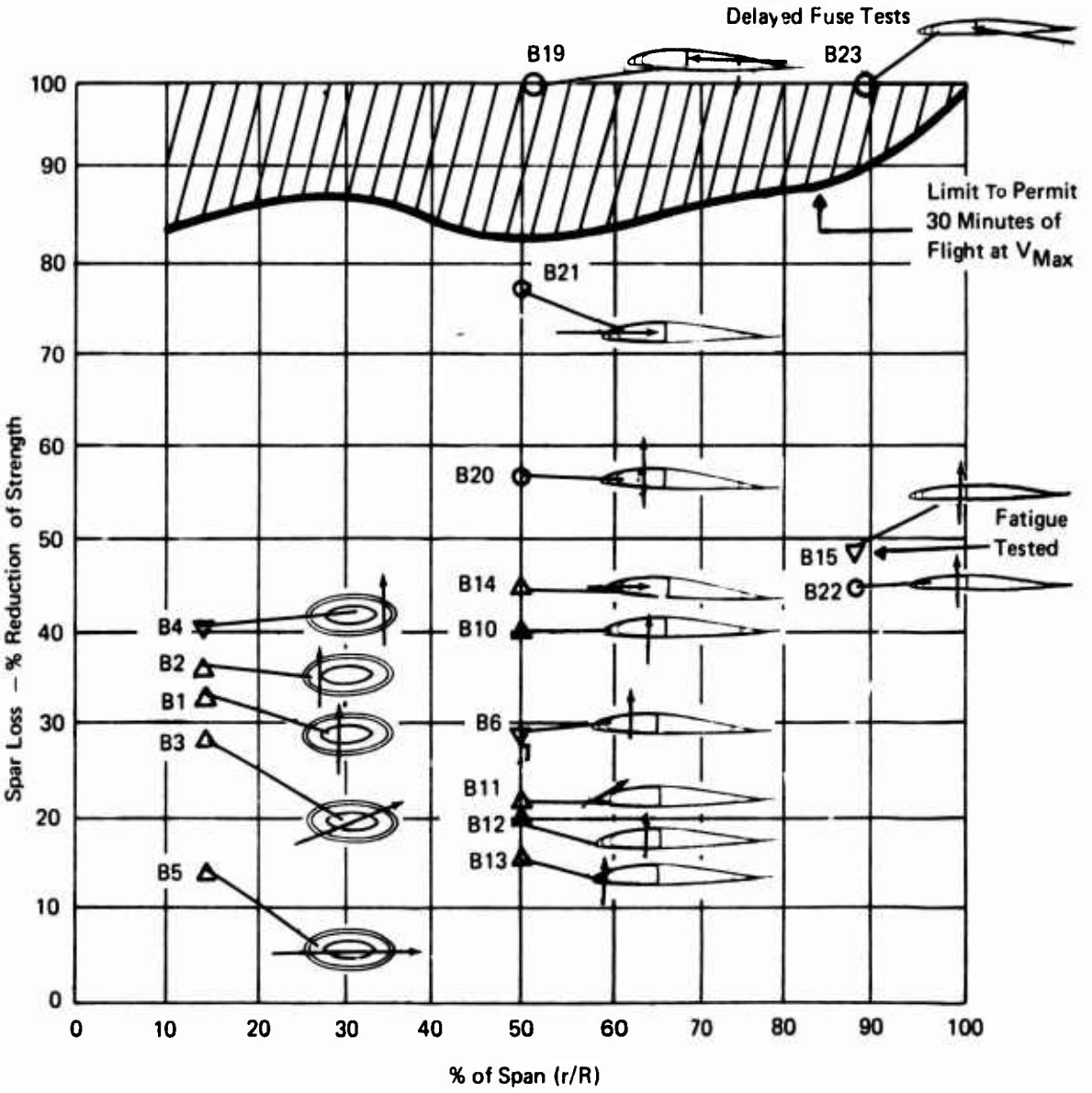

Legend:

△ – Unloaded (20mm HEI)
▽ – Loaded (20mm HEI)
○ – Unloaded (23mm HEI)

All Tests were with "Superquick" Fuses, the Major Threat for Composite Blades, Except Tests 19 and 23

Figure 70. Reduction of Strength Due to HEI Hits - Baseline Blade.

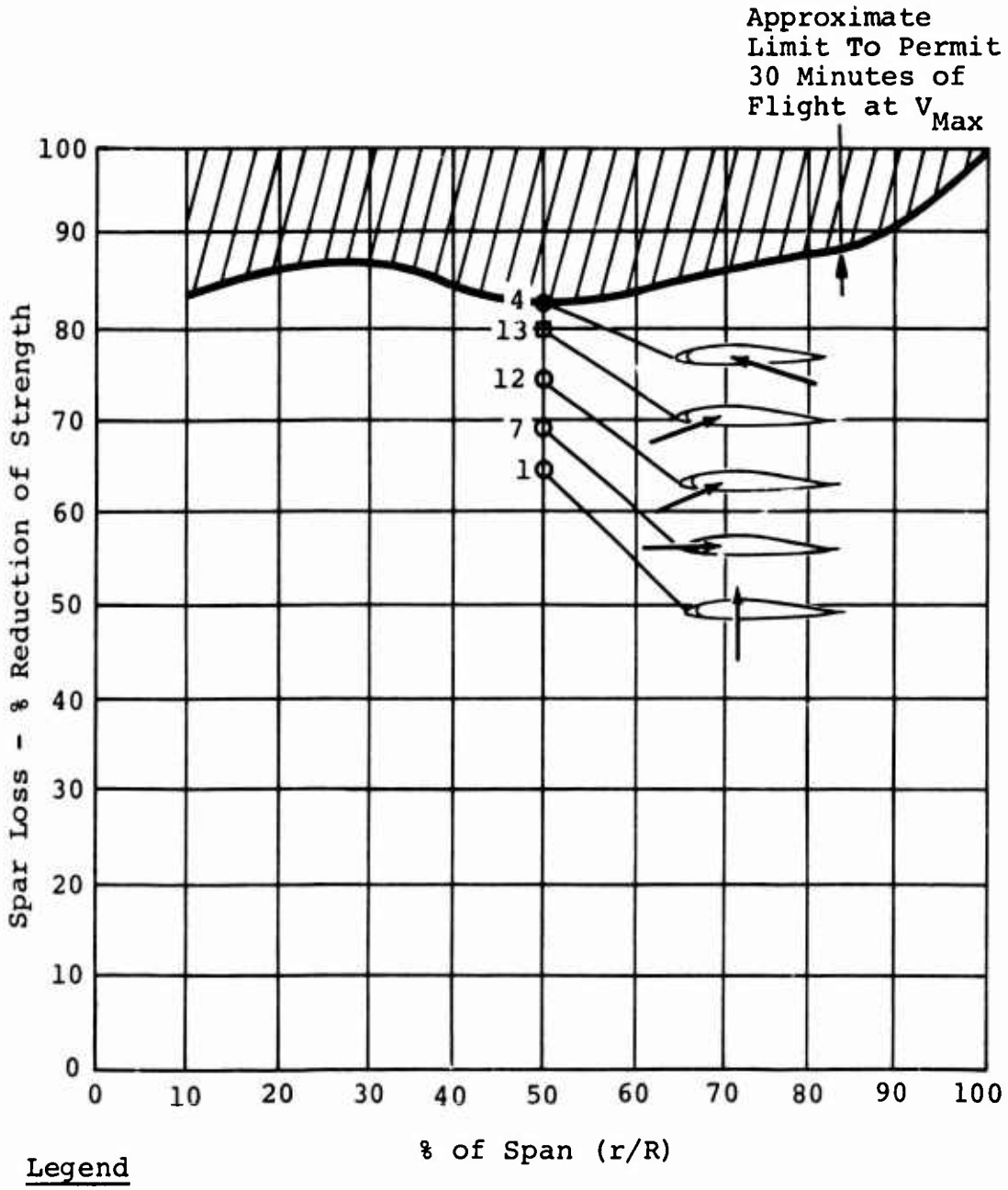

Legend

O Unloaded (23mm HEI)
□ Loaded (23mm HEI)

Figure 71. Reduction of Strength Due to 23mm HEI Hits - Design 2.

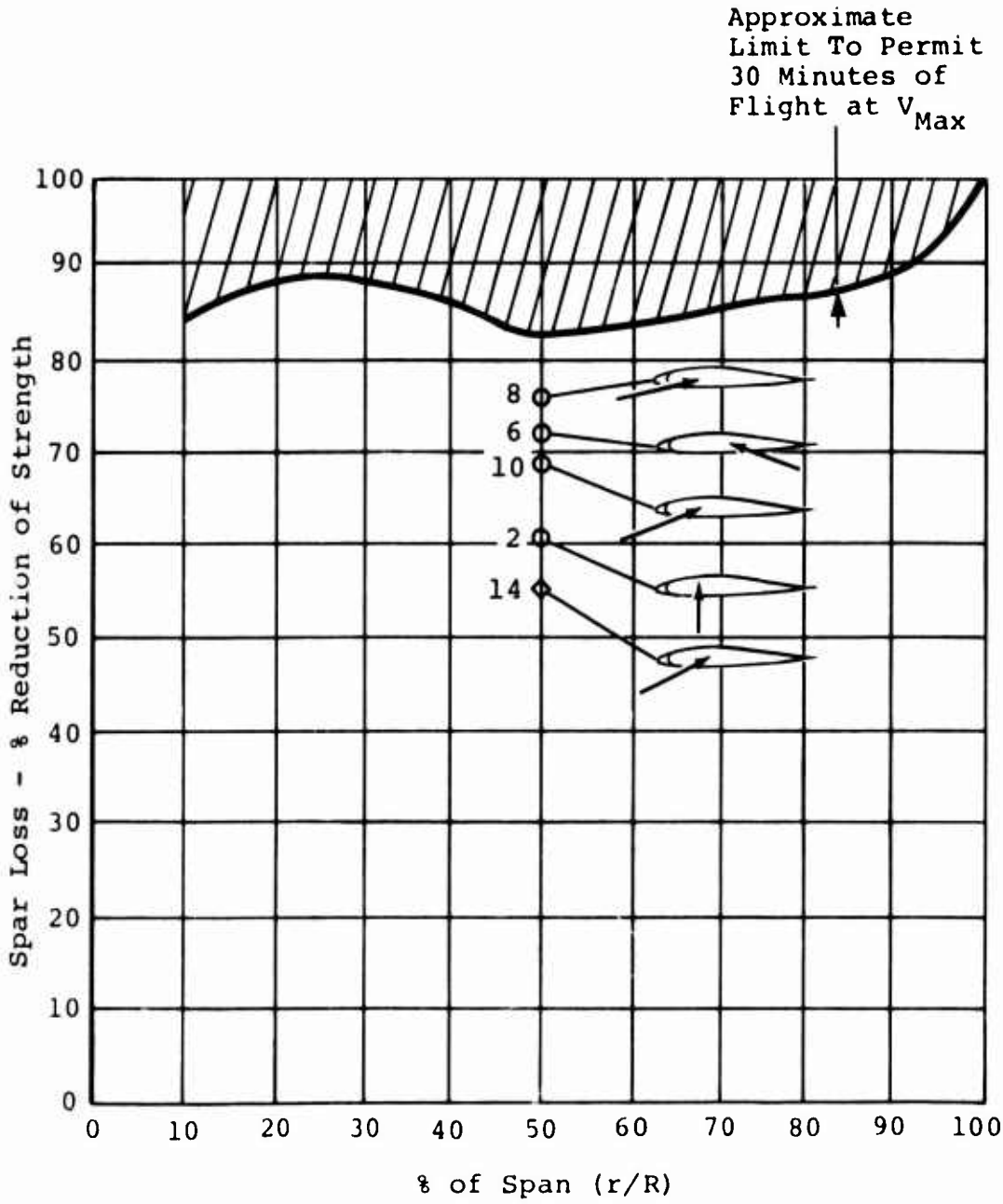

Legend

○ Unloaded (23mm HEI)
◇ Loaded and Fatigue Tested (23mm HEI)

Figure 72. Reduction of Strength Due to 23mm HEI Hits - Design 3.

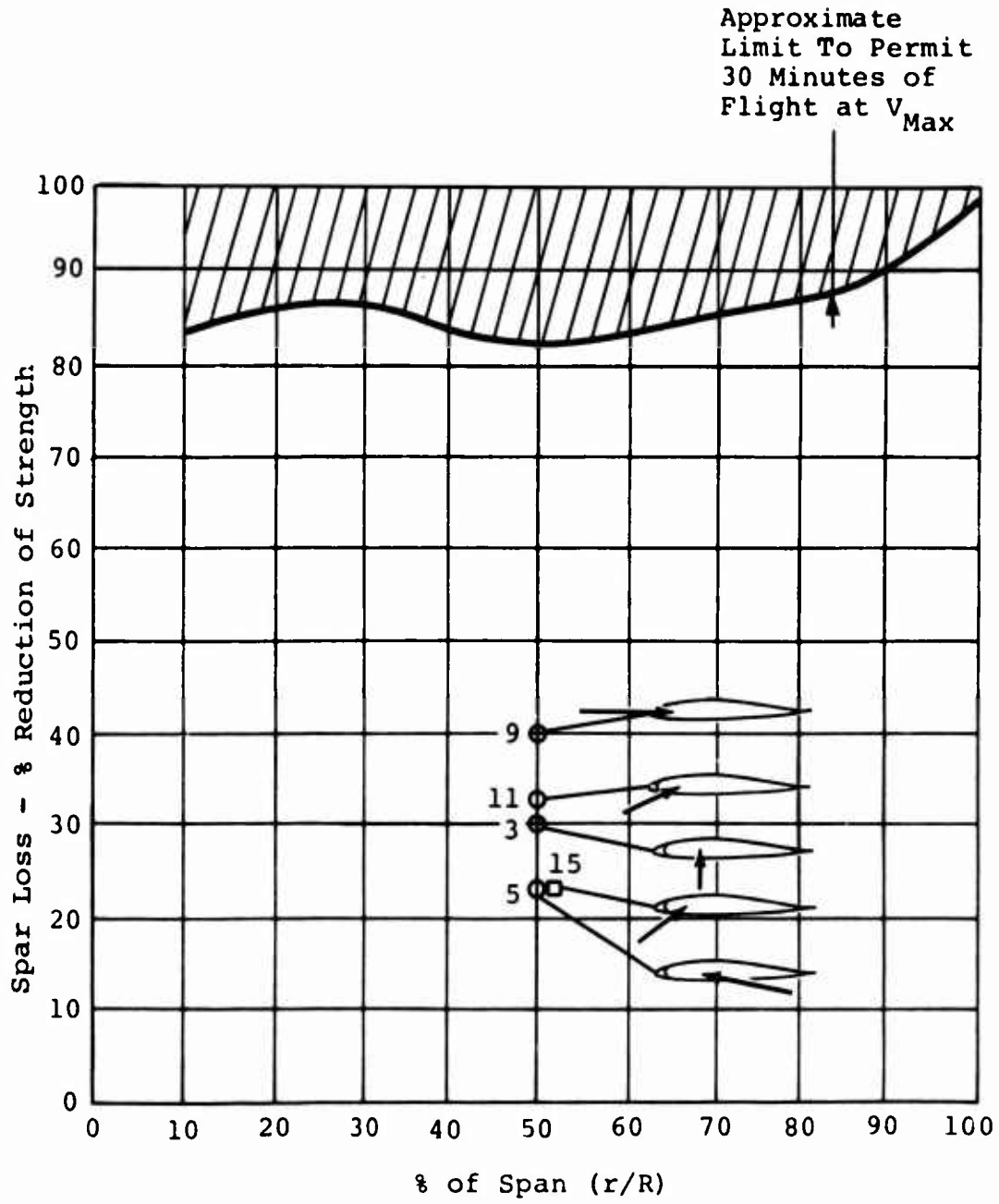

Legend

O Unloaded (23mm HEI)
□ Loaded (23mm HEI)

Figure 73. Reduction of Strength Due to 23mm HEI Hits - Design 6A.

Note that one of the most damaging of all the hits was the loaded hit of Design 2, Test 13, which had lost 76 percent of EA and which separated in interlaminar shear at a load that may have been slightly excessive. Test 15, of Design 6A, which separated under load and which also failed in interlaminar shear, had lost only 24 percent of EA. This indicates a large difference in interlaminar shear strength among designs and/or fabrication methods.

Strain Levels at V_{max} - Steady and alternating strain levels were calculated at the most critical point of the damaged section for each of the 15 hits. Flapwise and chordwise moments for each hit (Figures 36 and 37 were obtained using the blade property reductions of Table 4 to obtain the strain levels summarized in Table 5.

The equation to obtain strain is

$$\frac{MC}{EI}$$

where

M = Applied moment, in.-lb
C = Distance from neutral axis to outer fiber, in.
EI = Stiffness at remaining blade section

Remaining Fatigue Life

The fatigue life remaining in a ballistically damaged blade is dependent on the physical characteristics and the stress levels in the residual material. The damaged blade spars in these tests contained a mixture of unidirectional fiberglass, crossply fiberglass and, in all designs except 6A, a steel nose cap. Each of these materials has different fatigue strengths, cross-sectional areas, moments of inertia, and moduli of elasticity.

The life expectancy was calculated for each hit by comparing the calculated alternating strains at V_{max} in Table 5 to the S-N curve shape for zero degree unidirectional fiber in Figure 74. The endurance limit was obtained by entering the Goodman diagram of Figure 75 with the calculated steady strains. In all six specimens, where part of the steel nose cap remained (Design 2, Tests 1, 12, and 13; and Design 3, Tests 2, 10, and 14), the flight strains are of sufficient magnitude to cause immediate failure of the remaining nose cap material. The fatigue lives in Table 6 for these specimens, therefore, have been based only on the remaining composite material.

Possibility of Flutter

Possibility of blade flutter due to a local loss of stiffness was calculated on Boeing Vertol Program L-01. This program yields the natural frequencies and mode shapes for the

TABLE 5. STRAIN LEVELS AT V_{MAX}

	Test No.	Hit No.	Applied Moment (in.-lb^2) Flap Steady	Flap ±	Chord Steady	Chord ±	CF	Applied Strains (μ in./in.) Flap Steady	Flap ±	Chord Steady	Chord ±	Total Steady	Total ±
Design 2	1	021474P-1	1200	8900	31580	11500	4403	343	2542	1541	541	6287	3103
	12	021474P-3	1500	800	31580	10400	6066	401	2141	2041	672	8508	2814
	3	021274P-4	1200	8900	31580	9900	8780	363	2692	2124	666	11267	3358
	7	021474P-7	1900	10000	31580	10500	4747	259	1574	1810	602	6856	2176
	13	041074B-1	900	8000	31580	9800	7251	203	1800	2035	631	9489	2431
	-	Intact Blade	3200	11800	31580	15400	1480	71	268	960	468	2511	736
Design 3	10	021574P-1	1700	9500	31580	14400	4588	372	2083	185	84	5146	2168
	2	021474P-2	1700	9200	31580	12000	3775	373	2020	1130	429	5278	2449
	6	021474P-6	1600	10000	31580	13900	5514	301	1881	51	22	5866	1903
	8	021474P-8	1600	10000	31580	10000	6039	269	1682	1081	342	7389	2024
	14	041774B-1	1800	9300	31580	15100	3288	285	1474	238	114	3811	1588
	-	Intact Blade	3200	11800	31580	15400	1490	75	276	933	455	2488	731
Design 6A	11	021574P-2	2600	11400	31580	14900	2375	243	1066	206	97	2824	1163
	3	021474P-3	1750	10100	31580	6800	2145	240	1387	1650	355	4035	1742
	5	021474P-5	2000	10600	31580	6800	2063	198	1052	1603	517	3864	1569
	9	021474P-9	2600	11400	31580	14800	2670	248	1089	195	91	3113	1180
	15	041774B-2	2700	11500	31580	15200	1969	247	1053	234	112	2450	1165
	-	Intact Blade	3200	11800	31580	15400	1415	0	0	932	455	2347	455

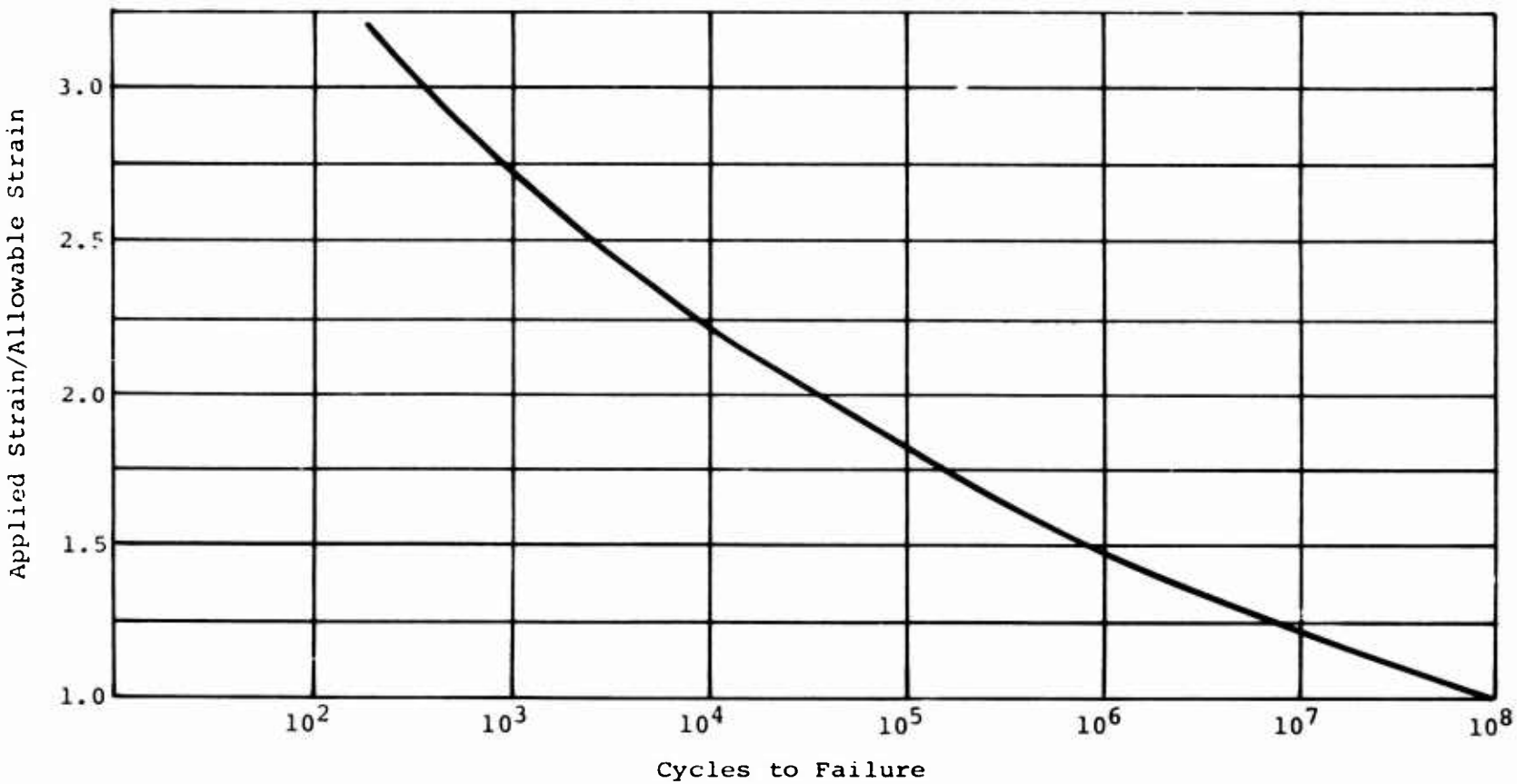

Figure 74. S-N Curve for Unidirectional XP250-1014S Glass Laminate Loaded in Tension-Tension Fatigue.

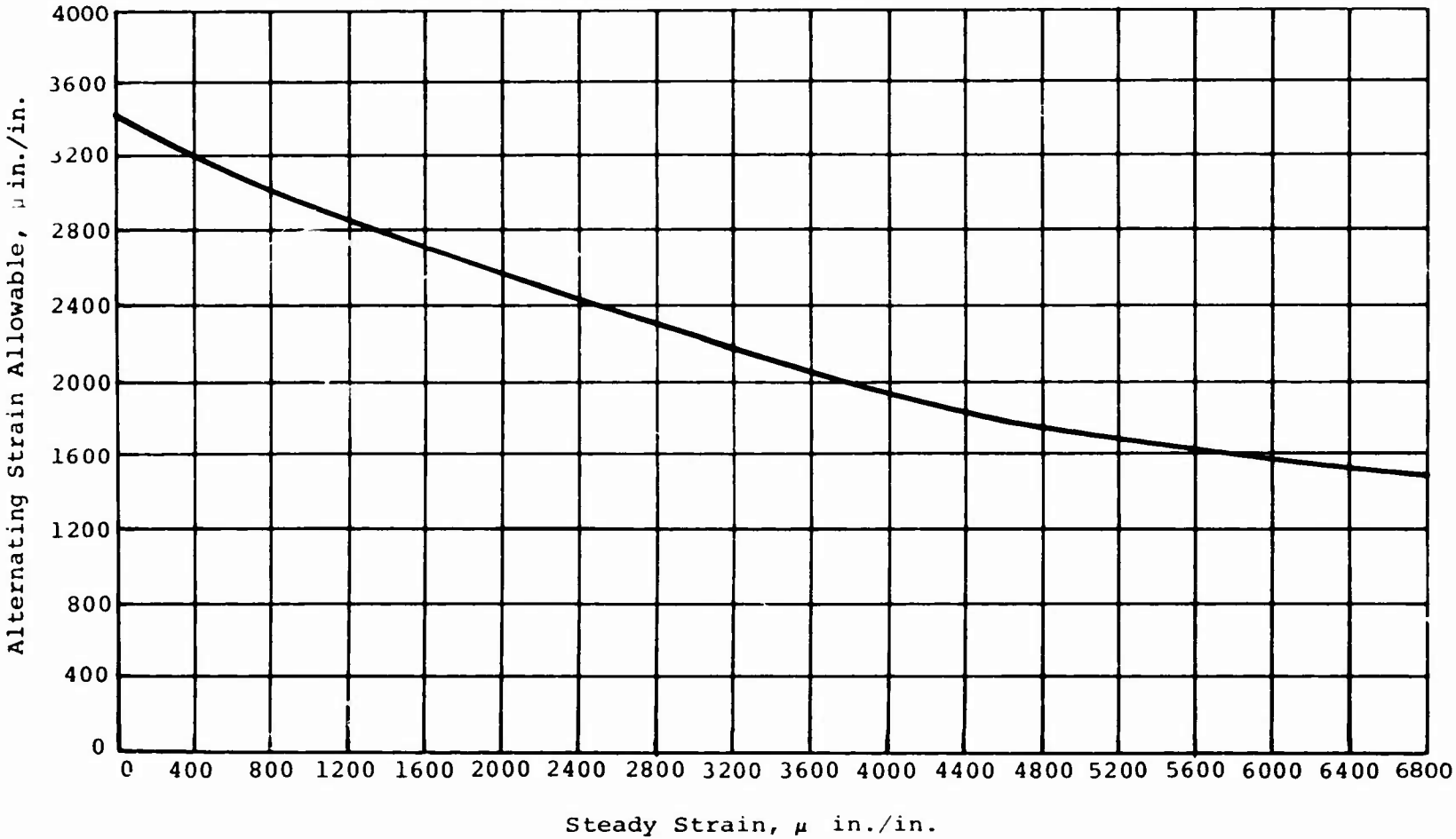

Figure 75. Goodman Diagram for XP 250-SFI Glass Laminate at 10^8 Cycles.

TABLE 6. FATIGUE LIFE EXPECTANCY

		From Table 5				
		V_{max} Strain		Allowable Strain*		Expected Life, Hours @ 295 rpm
Design	Test No.	Steady, μ in./in.	±, μ in./in.	μ in./in.	Cycles To Fail	
2	1	6287	3103	±1560	4.3×10^4	2.4
	12	8508	2814	±1350	2.5×10^4	1.4
	4	11267	3358	±1030	1.01×10^3	.06
	7	6856	2176	±1520	1.6×10^6	90
	13	9489	2432	±1120	1.06×10^4	0.6
3	10	5146	2168	±1720	7.2×10^6	400
	12	5278	2449	±1710	1.7×10^6	96
	6	5866	1903	±1600	1.6×10^7	900
	8	7389	2024	±1480	2.8×10^6	158
	14	3811	1588	±2000	∞	Unlimited
6A	11	2824	1163	±2350	∞	Unlimited
	3	4035	1742	±1930	∞	Unlimited
	5	3864	1569	±1980	∞	Unlimited
	9	3113	1180	±2280	∞	Unlimited
	15	2450	1165	±2460	∞	Unlimited

*Adjusted for Steady Strain

uncoupled flap bending, chord bending, and torsional free vibrations of stationary and rotating wings. The theoretical basis of this program is the lumped parameter method of analysis employing finite-difference equations to relate the dynamic aeroelastic quantities of adjacent wing stations, whose maximum number is 50. Trial and error tabular calculations are employed in search of the wing natural frequencies, these being attained by satisfaction of the root boundary conditions, including the pinned and cantilever conditions. Having found the natural frequencies, the program proceeds to calculate the deflection, slope, moment, shear, and loading distributions for each natural mode. In addition, the program calculates the critical aerodynamic damping ratios, the damped natural frequencies, damped amplification factors, and phase angles, the latter two for 12 harmonics of exciting frequencies, for each natural mode. Following the solutions for the natural modes, a classical flutter analysis is made for the coupled flap bending and torsion flutter vibrations of the stationary or rotating wing, for all combinations of the natural modes found earlier. The analysis employs generalized coordinate theory with the Theodorsen unsteady aerodynamic theory, wherein the complex circulation function is made unity.

This program showed that classical flutter or divergent oscillation would not occur for any of the hits on any of the concepts.

Blade Out-of-Track

Blade out-of-track is an important consideration since, if excessive, it could cause sufficient cockpit vibration to prevent pilot control or cause blade contact with the fuselage. An analysis was conducted of a baseline blade subjected to 23mm HEI damage to the spar using Boeing Vertol Computer Program L-02 to determine the effect of the damage on blade tracking.

L-02 Program Description - The L-02 Program yields the uncoupled flap bending, chord bending, and torsional steady-state forced vibrations of stationary and rotating blades in response to dynamic and aerodynamic periodic excitations. The theoretical basis for this program is the lumped parameter method of analysis employing finite difference equations to relate the dynamic aeroelastic quantities of adjacent wing stations, whose maximum number is 50. Singular tabular calculations are employed to determine the blades' forced response to each harmonic exciting frequency, the solution being effected by satisfaction of the root boundary conditions. The program then proceeds to calculate the deflection, slope, moment, shear, and loading distributions for each harmonic component; and then it performs a Fourier harmonic summation for each distribution, yielding its maximum and minimum vibratory magnitudes.

The Effect of Flap and Chord Stiffness (EI) Loss on Torsional Stiffness (GJ) - A typical type of spar damage caused by 23mm HEI is a hole amounting to 1 percent of the blade span where the flap and chord EI is reduced by 90 percent and with some material remaining in both the spar nose and heel. For this type of damage, a preliminary analysis was undertaken to determine the blade torsional stiffness (GJ) in the damaged section as a function of the flap and chordwise stiffnesses.

If, as in most of the hits, the damaged blade spar has centrifugal force paths remaining at the nose and heel, these load paths yield an effective torsional rigidity even though the flap and chordwise stiffness become small. This condition is sometimes referred to as trapeze effect. Figure 76 shows the GJ stiffness relation as a function of the flap and chordwise stiffness (EI).

For the undamaged condition, the GJ was 31.0×10^6 lb-in.^{2}. When the flap and chordwise stiffnesses are reduced by 90 percent, the spar nose and heel material are two slender beams able to deflect vertically in opposite directions (one up and the other down). Vertical components of the centrifugal force at the nose and heel result in a restoring torque causing an effective GJ torsional stiffness value of 15.9×10^6 lb-in.^{2}. For close to 100-percent reduction in flap and chordwise EI, only a flexible cable is assumed to transmit the centrifugal force across the damaged blade sections. This third condition gives an effective GJ of 0.97×10^6 lb-in.^{2}. Together these points were used to generate the curve in Figure 76.

C_t/σ and λ of Damaged Blade - When all the blade physical properties are known for both the undamaged and damaged sections, the L-02 Rotor Loads Computer Program is used to determine how the blade steady and alternating tip deflections react when the blade is ballistically damage. We know that when a blade is struck, several seconds, possibly 15 rotor cycles, may expire before the pilot can react to the damage situation. In the interim, the controls remain unchanged, and this is reflected in the L-02 analysis by maintaining constant collective pitch and a corresponding loss in C_t/σ. This C_t/σ change also induces an inflow ratio change λ through the rotor.

Iterative runs were made in the L-02 analysis varying C_t/σ and λ to match the root collective pitch angle of the damaged blade with that of the undamaged rotor blade. This matching was made for cases where the flap and chord EIs are reduced by 75 percent, 90 percent, and 95 percent, respectively. For these conditions, the blade flap deflections were compared with those for the undamaged blade. The results are shown in

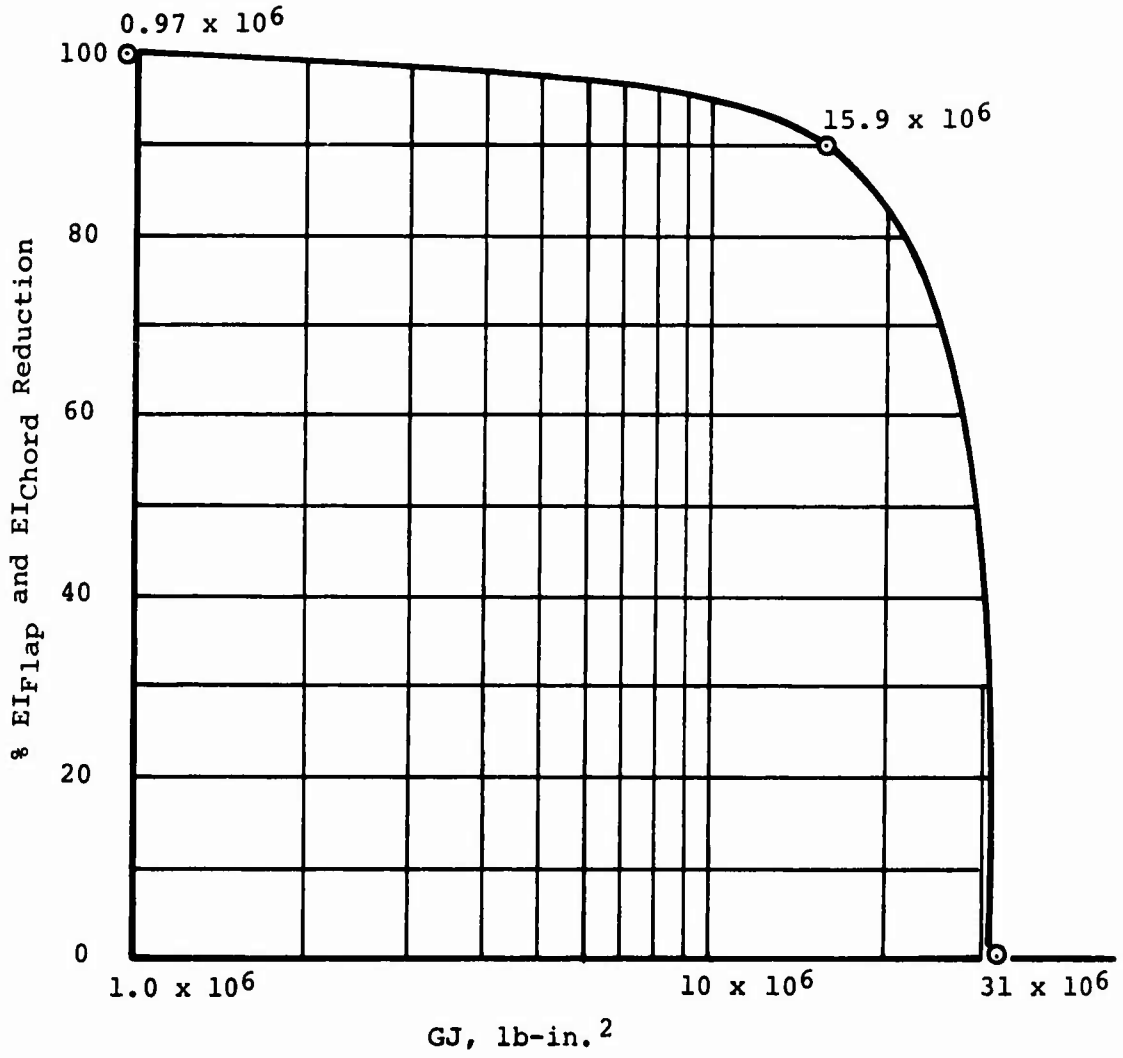

Figure 76. Blade GJ vs % EI_{Flap} and EI_{Chord} Reduction.

Figures 77 through 80 as the damaged blade out-of-track deflection in inches versus percentage reduction in the flap and chord EI stiffness. These plots are conservative in that they do not consider the effect of aft section of blade where they remained. However, none of the hits on the survivable designs caused excessive out-of-track.

Interlaminar Shear Failures

Analysis of a blade's resistance to spar separation after ballistic damage has been based, in this investigation, on tension/bending separation of the remaining material adjacent to the hit. However, the two spars which failed on impact did not separate in that manner. They failed by pulling the continuation of the residual unidirectional fiberglass out of one side of the undamaged part of the blade test section (Figure 38). The probable mechanism of this failure mode is that the unfailed unidirectional fiberglass next to the hit caused a local high shear stress in the resin attaching it to the adjacent unloaded, failed fibers. As the resin failed in shear, this local high shear stress was not relieved and progressed down the blade. This failure mode could be accurately analyzed by a finite element analysis; however, such analysis is time consuming and is beyond the scope of this investigation. A simpler analysis indicates this failure to be reasonable under the applied test loads.

An additional factor to be considered in relation to interlaminar shear strength of composites is the resin used. In Design 2, the material was Dexter Materials Corporation "S" Glass made to Boeing Specification DM500-SF1, Class A. This material incorporates the same glass fiber as the SP250-SF1, Class A material generally used in Boeing blades, but the resin is different. In the case of Design 6A, the resin was 118, Applied Plastic Company, 2434 resin with 2347 hardener made to Fiber Science, Inc., Specification 118ET. Insufficient testing has been done on these materials to understand how they would affect the interlaminar shear experienced in this program.

Another factor which could have affected this situation was the molding and curing processes used. Designs 2 and 3 were made in a bolt-down compression mold in which the volume of fiber and resin must be accurately calculated to achieve the right pressure for curing. This could have permitted areas of the blade to be improperly pressurized during curing. The nor-normal approach would be to have an external mold and an internal pressure bag which would apply even pressure over the entire blade area.

Another consideration is the fact that these blade sections were short and had no mechanical connection of the unidirectional fiberglass at the ends as would be found in an actual blade.

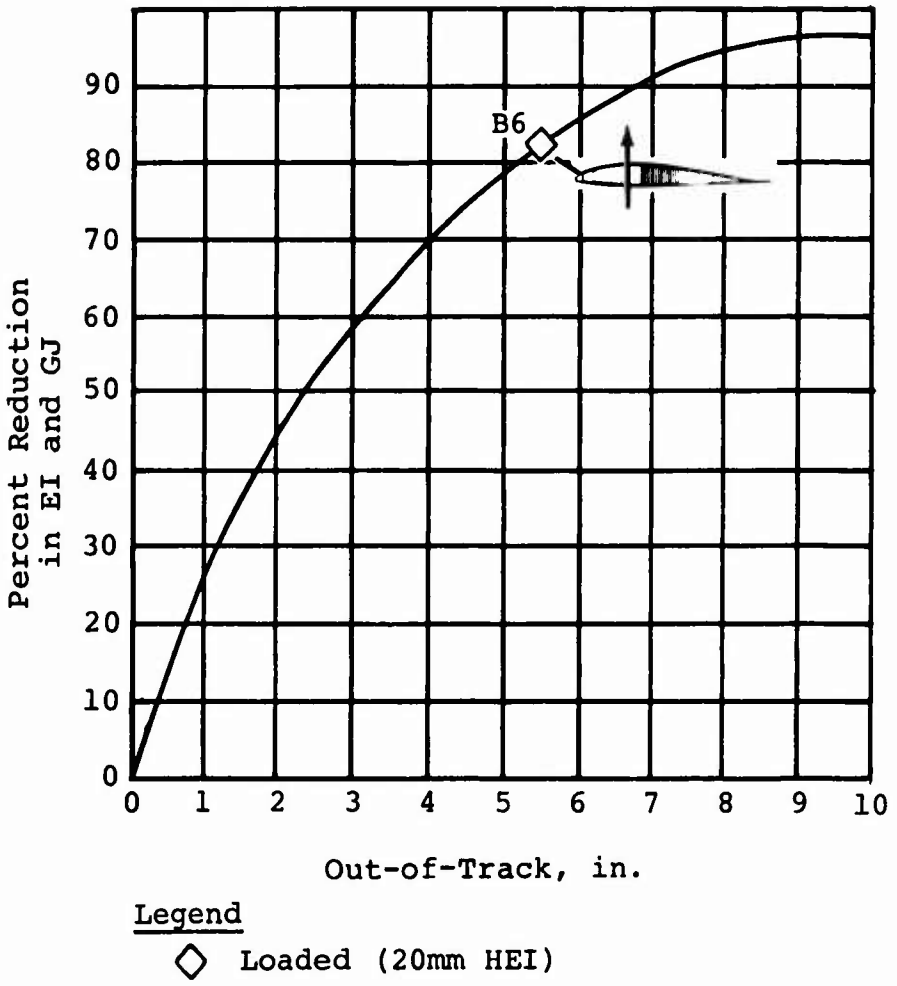

Figure 77. Baseline Blade - Blade Out-of-Track at V_{Max} After 20mm HEI Hits at 50% Radius.

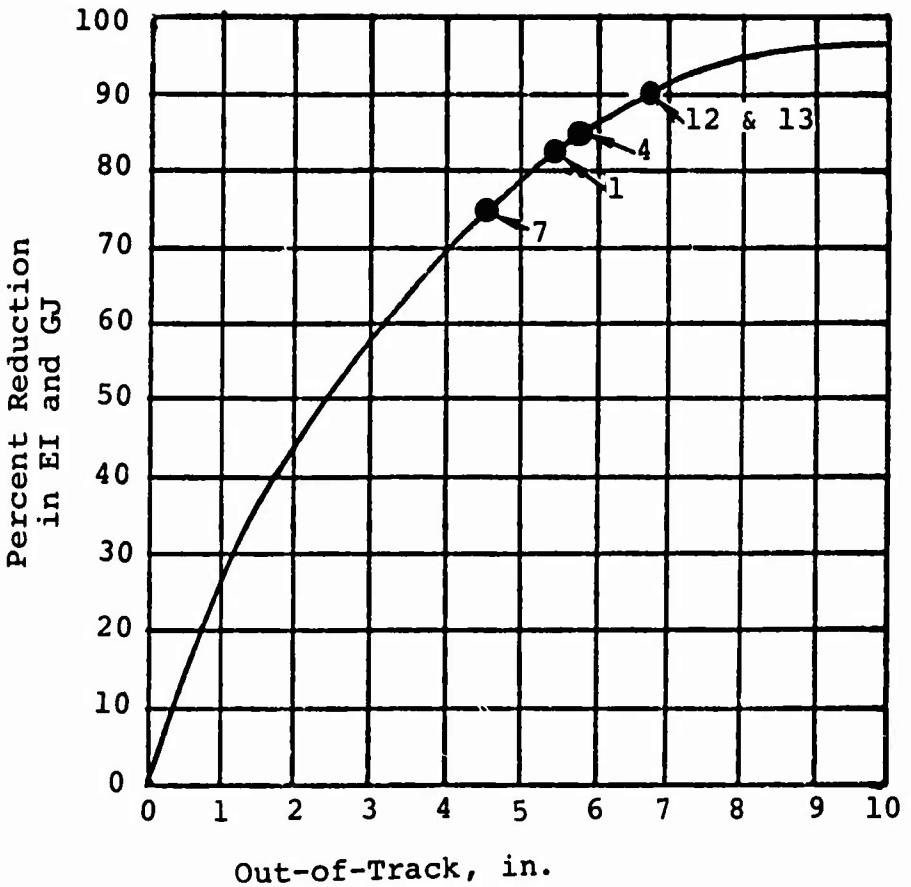

Figure 78. Blade Out-of-Track at V_{Max} After 23mm HEI Hits - Design 2.

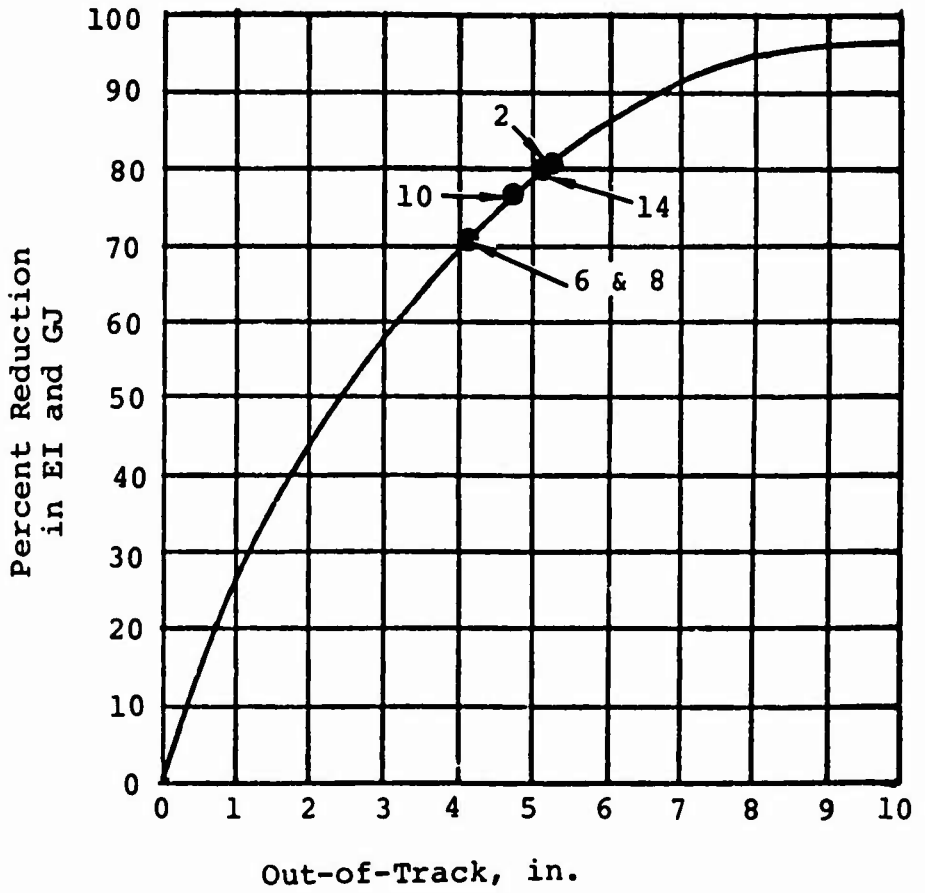

Figure 79. Blade Out-of-Track at V_{Max} After 23mm HEI Hits - Design 3.

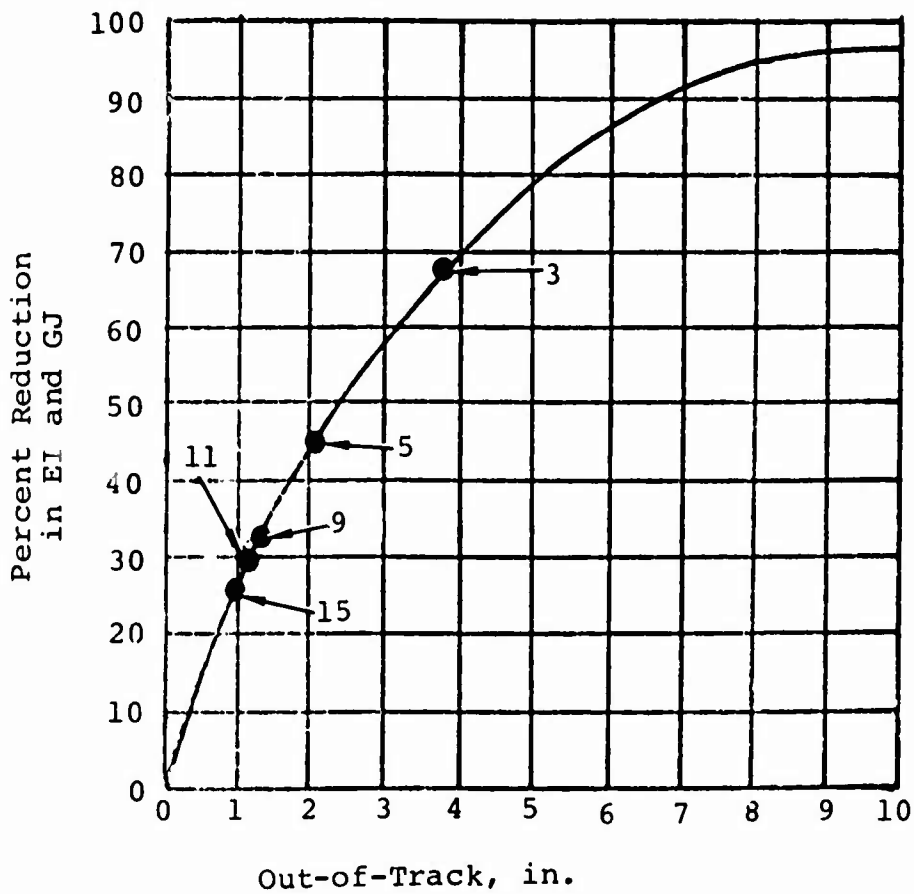

Figure 80. Blade Out-of-Track at V_{Max} After 23mm HEI Hits - Design 6A.

From the above, it may be concluded that interlaminar shear failure may, or may not, occur in a ballistically damaged blade. If the blade is well designed and the proper materials and fabrication processes are used, it is likely that an interlaminar failure would occur only after massive damage and at about the same stress level as would be calculated for a tension/bending failure. Moreover, under actual flight conditions, it could be a "soft" failure with slow progression and adequate warning through increased vibration.

Spanwise Splitting of the Spar

When detonation of the round occurs partially or totally inside the spar, the pressure tends to balloon the spar and put its walls in hoop tension. This ballooning load must be picked up by the spar inner and outer crossply fiberglass as in Designs 2 and 3 or in radially filament-wound fibers as in Design 6A. Some tendency toward spanwise splitting due to this condition was noted in some of the hits. Splitting tends to reduce the torsional stiffness of the spar.

Designs 2 and 3 could be further reinforced at the aft of the spar by alternate interleaving of the joint instead of the existing lap joint or by additional crossply across it. In the filament-wound Design 6A, sufficient radially wound fibers would be indicated.

Separation of the Aft Section from the Spar

In many of the hits, the aft section of the blade separated from the spar. This could have been due to the physical characteristics of the tested sections. They were short sections which allowed some of the damage to extend to the end of the blade. Also, each of the unloaded section had two hits, and the damage tended to overlap. Additionally, the bond material, used for expedience to fasten the aft section to the spar in Designs 2 and 3, was EC 2216. An AF126 bond, which would normally be used in an actual blade, is stronger than EC 2216 by a factor of 2:1. In Design 6A the connection was made by cure bonding the skin to the spar, which is also weaker than an AF126 bond. However, retention of the major portion of the blade aft section is essential to safe flight and, in actual flight conditions, airloads and dynamic blade bending would be present to help induce separation.

The connection between the aft section and the spar could be strengthened by wrapping the aft skin around the nose of the spar or by just making a wider bond joint. It would also be helpful to make the blade aft section noncontinuous by having spanwise sections separated or by incorporating crack stoppers.

CONCLUSIONS

This program represents the first comprehensive tests of fiberglass blades designed for increased survivability against 23mm HEI rounds. Its main thrust is to provide guidance in the design of survivable blades in the form of quantitative damage and residual strength data. It also provides visibility of additional factors affecting survivability, such as stability, out-of-track, fatigue life and the possibility of aft sections separating from spars.

The following conclusions were reached:

1. Fiberglass is a more ballistically tolerant blade material than steel, aluminum, or titanium. Because of its high ratio of ultimate strength (which prevents separation after damage) to its fatigue allowable (to which the blade is designed) and because of its low notch sensitivity, the fiberglass blade can lose more material without causing blade separation.

2. The philosophy of providing separated survivable load paths is valid. All the hits on Designs 2 and 3, which incorporated this principle, had load paths remaining which were sufficiently far apart to provide stiffness. These would have had more residual EA if more structural fiberglass had been used in the nose.

3. The alternate approach of putting most of the structural material in the nose as in Design 6A also showed up well in the tests. This design consistently had high residual strength in the nose and some remaining strength in the back of the spar. However, it would be more survivable with more spanwise unidirectional material in the back of the spar.

4. Interlaminar shear may be one of the failure modes in grossly damaged fiberglass spars. The failure of Design 6A in interlaminar shear under a load considerably lower than that calculated indicates that designing for a large residual resin shear area after damage is important. Optimum resins and cure methods, which may not have existed in this program, are also desirable. Mechanical end connections of the unidirectional fiberglass could also prevent separation. On an actual well designed blade this could be a soft failure mode with adequate warning. A finite-element analysis could be applied to this failure mode and be helpful in designing for ballistic survivability.

5. Retention of most of the blade aft section is important to survivability. Because of differences between the test specimens and actual blades in flight, it has not been shown that a real deficiency exists. However, consideration should be given to such factors as high-strength skin to spar bonds, running the skin around the spar nose and separating the aft section into sections small enough to be safely lost.

RECOMMENDATIONS

1. This program was primarily concerned with exploring the prevention of blade separation. The tendency of test sections to separate in interlaminar shear should be further explored. Variations in resin shear area, resin content, resin materials, cure pressures, stress levels, and fatigue effects should be investigated. Coupon tests and analyses of a variety of damaged sections are recommended together with finite element analyses.

2. The effects of reduction in blade stiffness due to ballistic damage were analyzed in a general way using existing analytical tools. The tendency of damaged blades toward instability and out-of-track should be further investigated by specific blade ballistic tests, measurements of actual stiffness reduction in EI flap, EI chord and GJ, wind tunnel tests of a range of blade stiffness reductions, and development of more definitive analytical tools.

3. This program considered only fiberglass reinforced composites. Future blades will probably require the use of high modulus or mixed modulus composites. The ballistic tolerance of these materials as applied to rotor blades should be investigated.